Short-term erosion pattern in the Alps-Apennines belt constrained by downstream changes of zircons morphology and U-Pb ages from the Po drainage modern sands

Marta Limoncelli

UNIVERSITÀ DEGLI STUDI DI MILANO-BICOCCA

DOTTORATO DI RICERCA IN SCIENZE DELLA TERRA

XXIV CICLO

Short-term erosion pattern in the Alps-Apennines belt

constrained by downstream changes of zircons morphology and U-Pb ages from the Po drainage modern sands

Marta Limoncelli

Esame finale di dottorato sostenuto in data 18 gennaio 2012

Tutor:

Marco G. Malusà [(1)]

Cotutors:

Andy Carter [(2)]

François Guillot [(3)]

Eduardo Garzanti [(1)]

Commissione:

Prof. Cesare Corselli [(1)]

Prof. Alessandro Gargini [(4)]

Dr. Andy Carter [(2)]

[(1)] Università degli Studi di Milano Bicocca; [(2)] Birkbeck University of London; [(3)] Laboratory CNRS-Géosystèmes, Université de Lille 1; [(4)] Università di Bologna

AUTHOR'S ADDRESS

Marta LIMONCELLI

e-mail: **marta.limoncelli@gmail.com**

Dipartimento di Scienze Geologiche e Geotecnologie
Laboratory for Provenance Studies
UNIVERSITA' DI MILANO-BICOCCA
Piazza della Scienza 4 - 20126 Milano - ITALY

This thesis has been supported by:
The Laboratory for Provenance Studies,
The Thermochronometry Laboratory, UCL-Birkbeck College
and the **Laboratory CNRS-Géosystèmes**, Université de Lille 1

"Amid all the revolutions of the globe the economy of Nature has been uniform, and her laws are the only things that have resisted the general movement. The rivers and the rocks, the seas and the continents have been changed in all their parts; but the laws which direct those changes, and the rules to which they are subject, have remained invariably the same"

CHARLES LYELL, 1830. *Principles of geology*

ABSTRACT

Downstream changes of the geochronological signature in the Po drainage allow to assess the relative sediment contributions shed from the orogenic source areas, in order to constrain the short-term (10^2-10^4 y) erosion pattern in the Alps-Apennines orogenic couple.

In this perspective, we collected modern sands in selected tributaries draining the major tectonic units exposed in the orogen, as well as along the Po River trunk and in different sites of the Po Delta. Zircon concentrates were separated according to specific quantitative procedures coupled with grain-size and grain-density analyses, which provide an evaluation of zircon content in source rocks, of hydraulic sorting effects, and related intersample/intrasample zircon variability. Our methodological approach allows to perform sediment budgets and evaluate mineral content in diverse sediment sources (mineral fertility). Budget calculations were performed by investigating geochronological signals upstream and downstream of major confluences. We employed, LA-ICPMS U-Pb geochronology on detrital zircons, because this technique allows a full control of zircon populations during separation procedures and data analysis; we found, instead, that fission track dating on detrital zircon is affected and biased by selective grain loss.

Results of U-Pb analysis performed on single grains show that all samples from the Po Delta yield similar grain-age distributions, and include grain-age populations that are rather constant both in age and size. Major peaks are found at ca. 30 Ma, ca. 280 Ma, and 400-500 Ma. Peaks in these distributions can be traced upstream up to their sources. The bulk of the geochronological signature of the Po Delta sands is displayed already upstream of the confluence of the Northern Apennines rivers, suggesting that short-term erosion rates were much lower in the Northern Apennine than in the Western and Central Alps. Age peaks typical of the eastern Lepontine dome also characterize the Apenninic tributaries, reflecting Oligo-Miocene sedimentary transfer from the Central Alps to the Adriatic foredeep, and next tectonic accretion of turbidite wedges to the Apennine belt.

U-Pb analyses were complemented by zircon typology of the whole dataset, integrated by SEM observations on selected samples. Major typological groups can be traced from entry points in the Po Plain down to the Po Delta. Euhedral zircons are largely shed from the External Massifs (Mont Blanc and Argentera) and the Periadriatic plutons. Zircon grains showing signs of chemical abrasion, possibly acquired under high-grade metamorphic conditions, were detected in tributaries draining the Lepontine area.

INDEX

INTRODUCTION

The interplay between erosion and tectonic in collisional settings is highlighted in many studies as a key process in the structural evolution and exhumation of orogenic belts (Beaumont et al., 1992; Willet et al., 1993; Zeitler et a., 2001; Burbank 2002; Konstantinovskaia and Malavieille, 2005; Reiners and Brandon, 2006; Malavieille, 2010). Erosion is the superficial removal of mass by mechanical and chemical processes, where rivers play a key role in transporting sediment of removed materials from source areas to the depositional environment (Milliman and Meade, 1983; Allen, 1998; Rahaman et al., 2009). During the last decade much attention has been focused on detrital minerals stored in recent sediments to investigate the geochronological signature of source areas by means of detrital thermochronology (Bernet et al., 2004a,b; Malusà et al., 2009) and U-Pb geochronology (Bruguier et al., 1997; Cawood et al., 2003; Amidon 2005), in order to understand erosional processes in mountain belts. Recent investigations show that on a short-term time scale, erosion is focused in space and time on small parts of the orogen where sediment budget is relative higher than in surrounding areas (Garzanti et al. 2004a; Malusà and Vezzoli, 2006; Garzanti and Malusà, 2008; Resentini and Malusà, 2011).

The aim of this study is to perform detrital zircon geochronology on modern river sands from the Po River basin in order to constrain the erosion pattern in the Alps-Apennines orogen on a short term timescale (10^2-10^4 years). The Po River Basin is a natural laboratory for such sedimentary budget calculations, because sediments shed from the Alps and the Northern Apennines are carried into the Po Plain which represents the retroforeland of the Alps and the foreland of the Apennines. Detrital zircons are very resistant to weathering and they are widely used to investigate the

geochronological signature in sediments, which provides a representative mirror of the bedrock age distributions in the drainage (Bernet et al., 2001). In Part I of this thesis, we want to give detailed instructions about our quantitative approach adopted for zircon separations, which allows an evaluation of mineral fertility in source rocks (Malusà & Garzanti, 2011), of hydraulic sorting effects, and related intersample/intrasample zircon variability (Garzanti et al., 2009). Analytical techniques include also the observation of detrital zircon morphologies, which have been performed on the basis of a simplified Pupin typological scheme complemented by analysis of SEM high resolution images. Part II of this work is aimed to discuss the choice of an efficient dating method which may be theoretically able to identify the zircon source area, by means of proper geochronological signature characterized by different peaks with specific age and size to perform reliable sedimentary budget calculations. This is vital in sediment budget studies so any possible bias which may increase the probability of missing a potential source must be carefully avoided. LA-ICPMS U-Pb geochronology on detrital zircons can be proficiently employed in this study, because it allows a full control on grain loss during analysis. The last discussion was followed by the necessity to understand how detrital zircon U-Pb ages must be treated in our analysis. For this reason, then we focus on the potential biasing during data processing in order to suggest a possible interpretation of discordant grains in our samples. In Part III of this thesis we demonstrated that downstream changes of geochronological signature can be followed along the sediment pathway in order to recognize the source areas giving the major contribution to the geochronological signature in the Po Delta. When age signatures allow discrimination of different sources, and zircon fertility and hydraulic sorting effects are calculated, we can thus determine a sedimentary budget which is aimed to constrain a relative erosion pattern in the studied area.

PART I
Methods and laboratory analysis

CHAPTER 1

Geological outline of the Po River Basin

Introduction

The Alps and the Apennines surround the Po Basin both at the north and west, as well as at the south respectively. The Alps represent a double-vergent collisional belt resulting by the Cretaceous to Eocene eastward subduction of the European continental crust beneath the Adria upper plate followed by continental collision (Coward and Dietrich, 1989; Roure et al., 1990a; Pfiffner et al., 2002). The suture zone between the two plates is marked by slices of ophiolitic materials representing the Liguria-Piedmont Ocean, which separated the European continental margin from the Adriatic margin in the Mesozoic (Marroni et al., 1992; Stampfli et al. 1998). Eastward directed Alpine subduction was gradually replaced in tertiary times by the opposite westward directed Apenninic subduction (Doglioni et al., 1998; 1999a). A foredeep formed on Adria continental crust (Menard, 1988), while Penninic and Ligurid units on both sides of the Alps-Apennines junction began to be rapidly buried under deep-water sediments (Tertiary Piedmont Basin and Epiligurid successions; Laubscher et al., 1992). Fast denudation in the Alps and huge detrital supply (Garzanti and Malusà, 2008) start soon after the climax of Periadriatic magmatism in late Oligocene associated to production of synorogenic deposit as the Macigno turbidites, which accumulated distally in the Apenninic foredeep (Di Giulio, 1999).

The Alpine belt

The Po drainage basin includes a large portion of the Alpine Axial belt, and of the Southern Alps. In the western part of the Axial belt the highest elevation of 4810 m is within the External massif of the Mont Blanc. Several mountain peaks higher than 4000 m are located in the region of the Dent Blanche and Monte Rosa nappes in the southern part of the Valais Zone. In the Southern Alps, the highest reliefs are related in the Bregaglia area. Others mountain peaks higher than 4000 m are restricted to the outer part of the belt mostly drained by the Rhone and Rhine tributaries.

The Western Alps source area- The Western Alps are located at the junction between the Adria-Africa and European plates. Tertiary-age metamorphic units are exposed in the axial part of the belt, which is flanked by the Insubric Fault and the Frontal Pennine Fault (Schmid and Kissling, 2000). Eocene Eclogite units extend from the Lepontine dome in the north to the Sestri-Voltaggio line in the south, where they are buried beneath sedimentary successions of the Tertiary Piedmont Basin and Western Po Plain (Malusà et al., 2011). Eclogite units consist of oceanic slivers (Bearth, 1967; Rubatto et al., 1998) enveloping the continental basement of the Internal Massifs (e.g. MR Monte Rosa; GP, Gran Paradiso, DM, Dora Maira, fig.1). Lower-pressure metamorphic units exposed to the west, closer to the European mainland, form a doubly-vergent accretionary wedge (Roure et al., 1996), including the Briançonnais blueschist-to-greenschist cover sequences (e.g. Combin and Lago Nero units) and basement sliver, exposed partly in the Po River basin (e.g. Ambin and Leverogne units). The European basement is exposed only in a small portion in the Po drainage, but it includes of the highest relief with the 4810 m of the Mont Blanc (MB), consisting of Upper Carboniferous granitoids intruded into amphibolite-facies metasediments and migmatites (Von Raumer et al., 1993). Their cover

sequences (Helvetic-Ultrahelvetic and Dauphinois-Ultradauphinois successions, Barbier, 1948) are scarcely exposed in the Po basin.

The Central Alps source area- this part of the Alpine belt was dominated by convergence during most of the Tertiary, initially accommodated by subduction, coupled with uppercrustal shortening on the European side of the orogen, and later by indentation of Adriatic lithosphere beneath the axial belt (Malusà et al., 2011), followed by erosional unroofing of the Lepontine dome. Exposed between the Simplon Fault in the west and the Austroalpine lid in the east, the Lepontine dome (LD fig1) consists of granitoid gneisses interleaved with Mesozoic calcschists (Berger et al., 2005), and metamorphic grade ranges from lower/middle amphibolite-facies to granulite facies to the east (Engi et al., 2004).

The South-Alpine source area- Basement and cover rocks of the Southern Alps, exposed south of the Insubric Line, are widely recognized as a complete cross section of continental crust (Handy et al. 1999). The basement consists of Variscan metamorphic rocks derived from sedimentary and igneous protoliths, later intruded by igneous bodies of Permian age.

Periadriatic intrusives - these Tertiary plutons are all exposed in the vicinity of the Periadriatic Fault System (Laubscher, 1983a). Magmatism took place during continental collision and reached a climax in the early Oligocene (Hansmann et al., 1996; Liati et al., 2000). The Periadriatic plutons (from east to west in fig.1, A, Adamello; B, Bregaglia; C, Valle del Cervo) consist of calcalkaline I-type tonalites and to a minor extent granodiorites. Gabbros, diorites and granites constitute a small fraction of most plutons. Mafic enclaves and basic synplutonic dikes are widespread in most plutons (Rosenberg, 2004).

Ligurian Alps source area- The Ligurian Alps is an E-W narrow belt composed by both ophiolitic and continental units, sealed by the Oligocene-Neogene sedimentary

deposits of the Tertiary Piedmont Basin. A general increase of the Alpine metamorphic grade can be recognized moving eastward across the belt, from the anchimetamorphic terranes of the Helmintoid Flysch units to the greenschist units of the Briançonnais domain and the eclogitic units of the Voltri Massif (VO, fig.1) (Vignaroli et al., 2008).

The Northern Apennines

The Northern Apennines are a fold-and-thrust belt developed during progressive ENE propagation of the imbricate thrust system resulting from the continental underplating of the Adria microplate below the stable European plate, during westward subduction (Boccaletti et al., 1980; Principi and Treves, 1984; Castellarin, 2001; Faccenna et al., 2001). Tectonic units in the Northern Apennines are arranged in a nappe edifice comprise several tectonic units which were derived from two main palaeogeographic domains (Treves, 1984; Principi and Treves, 1985): the Liguria-Piedmont Ocean and the Adriatic continental margin. The Ligurian units were structurally emplaced at the top of the nappe stack and consist of Jurassic ophiolites with a pelagic cover and Cretaceous to Eocene turbidite sequences (Abbate & Sagri, 1982). The continental margin units (Canetolo Complex, Tuscan and Umbrian nappes) underthrust the Ligurian units from east to west and comprise Mesozoic platform sequences overlain by Tertiary flysch formations (Marroni et al., 1992).

Ligurian Units source area- widely exposed in the Po River drainage the Ligurian Units represent the highest structural units of the Apennines. They can be subdivided on the basis of stratigraphic and structural features into two main groups (Elter 1975). The Internal Ligurian Units are ophiolitic sequences represent the remnants of the Liguria-Piedmont Ocean, including mantle ultramafics intruded by a

gabbroic camplex and covered by N-Mor basalts and sedimentary ophiolite breccias (Decandia & Elter, 1972; Abbate et al., 1980) and directly overlain by radiolarites, calpionelle limestones, and shales. The External Ligurian units are distinguished by presence of Cretaceous-Paleocene calcareous dominant sequences (the Helminthoid Flysch) associated with complexes or pre-flysch formations called “basal complexes” (Marroni et al. 1988) and they are widespread in the Taro and Trebbia valleys. They can be regarded as relicts of the former ocean-continent transition area and of the distal Adria continental margin in the Apenninic transect (Molli 1996).

Epiligurian Units source area- represented by Eocene to Pliocene sedimentary deposits which overly unconformably the Ligurian Units. These rocks were deposited in marine thrust-top piggyback basins, demonstrating that much of the northern Apennine orogenic wedge was submarine during its accretionary history until its final full emergence between the Tortonian and Messinian (Ricci Lucchi, 1986).

Foredeep Turbidites source area- widely exposed all along the Northern Apennines they are turbiditic synorogenic sediments deposited in the Oligo-Miocene Apennines foredeep (Garzanti et al., 2002). Main foredeep fills display ages younging from late Oligocene-early Miocene in the west (Macigno and Cervarola formations) to middle-late Miocene (Marnoso-Arenacea Formation) and finally latest Miocene-Pliocene in the east (Laga Formation).

They are associated to the Subligurian Units, which are represented by shaly to calcareous turbidites found tectonically sandwiched between the Macigno foredeep turbidites and the overlying Liguride thrust sheets (Canetolo Complex; Abbate and Sagri 1984), and well exposed in the Bobbio Window.

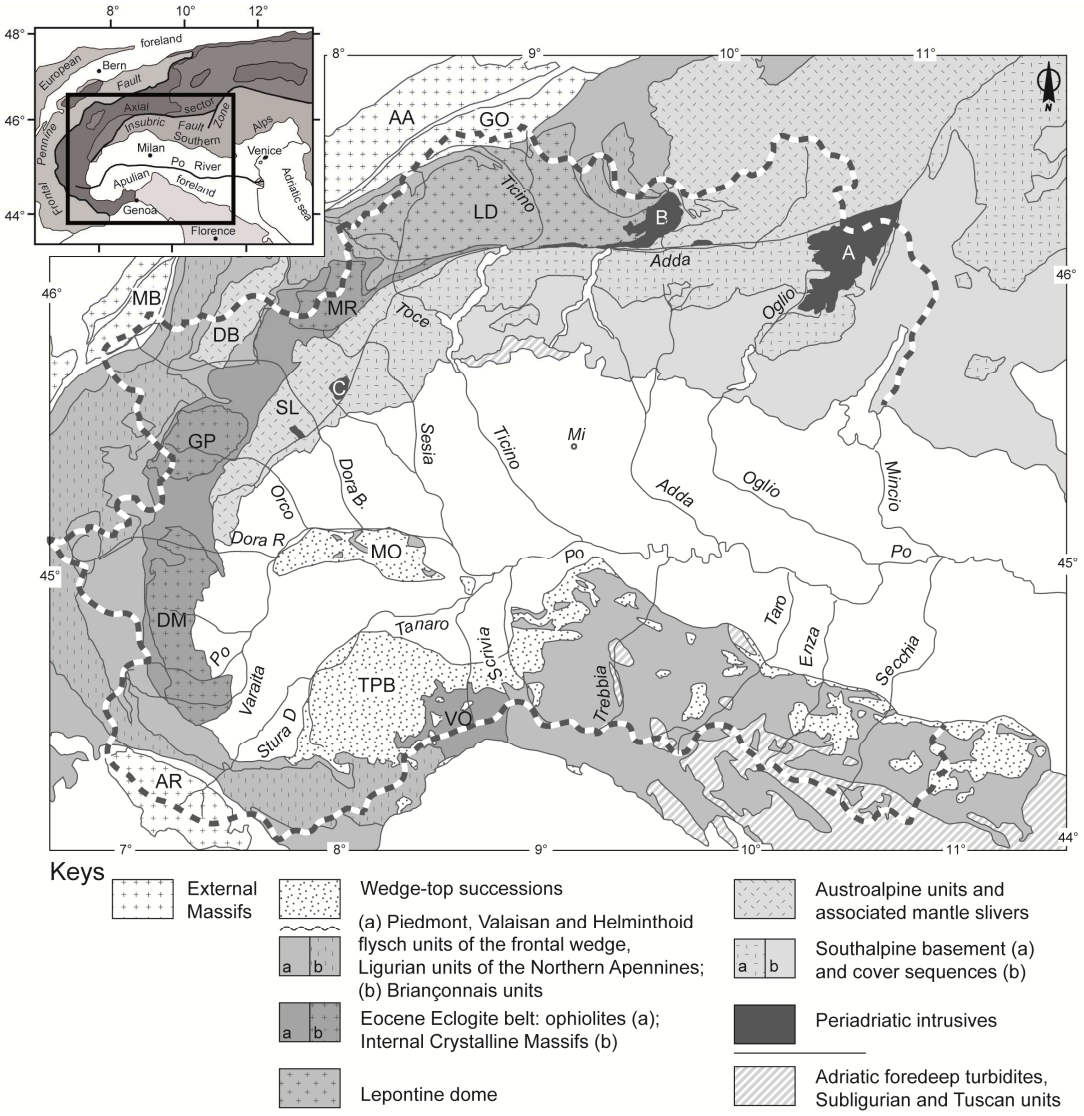

Fig.1: Tectonic map of the study area. Tectonic units are: Periadriatic intrusions A, Adamello; B, Bregaglia, C, Valle del Cervo; LD, Lepontine dome; Austroalpine Units SL, Sesia Lanzo, DB, Dent Blanche; Internal massifs MR, Monte Rosa, GP, Gran Paradiso, DM, Dora Maira; External massifs, GO, Gotthard, AA, Aar, MB, Mont Blanc, AR, Argentera; TBP, Tertiary Piedmont Basin; VO, Voltri. The thick dashed line indicates the boundary of the Po catchment. In the inset, simplified tectonic map of the Alps and Northern Apennines.

The Po River

The Po River is the most important fluvial system in Italy. It is the longest Italian river flowing from its source at 2.020 meters (Pian del Re), along 652 km and it has the larger catchment basin (74.000 Km^2) fed by 141 tributaries with a drainage area. The Po river travels eastward carrying an estimated annual sediment load of 20 million tonnes (Nelson, 1970) and it opens towards the Adriatic Sea. Most of the sediment carried by the Po River is deposited at the distributary mouths and forms a lobate delta, where some sediment is reworked by the sea and rearranged in beaches and beach ridges.

The Po River Delta

The Po River Delta experienced different phases depending on the balance between erosion and sediment deposition. The Po Delta plain occupies a broad area extending east of Ferrara and along a coastal area of ca 120 km between the Adige and Reno rivers. Most of the lower delta plain (ca. 1550 km2) is below mean sea level and half of it is deeper than 2 m below sea level (Bondesan et al., 1995a). The delta plain is poorly supplied with sediments because all of the branches of the Po River have major artificial levees (Correggiari et al., 2005). The lower delta plain includes N-S elongated topographic highs (typically less than 2 m above sea level) that correspond to ancient stranded beach ridges. The present-day delta is undergoing retreat and is evolving towards a wave-dominated, cuspate morphology (Dal Cin, 1983).

The Po Plain

The Po Plain represents both the retroforeland basin of the Alps and the foreland of the Apennines (Garzanti et al., 2011). The Po River flows parallel to the tectonic strike of both the mountain chains forming two opposite sides in the foreland basin. The northern side is formed by a gentle dipping platform merging from the Alps to the foreland basin s.s., while the southern side faces the single-vergent Apennine fold-and-thrust belt (Vezzoli and Garzanti, 2009). From a structural point of view the Po foreland basin shows a strong asymmetry in a north-south cross-section displaying homoclinal dip towards the south (Pieri and Groppi, 1981; Pieri, 1983). Each side is characterised not only by different sediment filling, but also by patterns of differential subsidence, depending on the different ratio of detrital fluxes (Ori, 1993). This because the Alps and Apennines orogens show distinct characters both in terms of geological and geophysical characters (Doglioni and Scrocca, 2004), as well as in geomorphological features.

CHAPTER 2

Methods

Introduction

This chapter provides a description of the early steps of our study from sampling strategies to zircon separation procedures.

Zircon separation techniques applied in this study were defined in the Laboratory for Provenance Studies of the Milano-Bicocca University. Zircon concentrates result from a number of progressive laboratory analyses by which determination of grain-size distribution, size-shift and HM concentration are possible and zircon fertility can be determined according to techniques proposed by Malusà and Garzanti (2011, *in press*).

Sampling strategies

Twenty-five sediment samples (fig.2) have been collected from modern fluvial bars and beaches in the Po River system:

- Fifteen modern sand samples were taken from the main Po River tributaries at the end of major valleys before they entered the Po Plain.
- Five samples were collected in selected sites along the Po river trunk, downstream the confluence of major rivers.
- Four samples were collected in different sites of the Po Delta at the closure of the depositional system.

Collected samples range in size from coarse to medium sand. This because zircon has a density of ~4.55-4.65 g/cm^3 (Deer et al. 1992) and is typically deposited in the finer tail of coarser grained material. This process of size-density sorting, prescribe by the settling equivalence principle (Rubey 1933; Garzanti, 2008), states that detrital grains with the same settling velocity are deposited together. Size shift of zircon in equilibrium with quartz is 1 φ (Garzanti et al., 2008). The suitable size window for zircon separation analysis, is thus 1 φ smaller than the average diameter (Dm) of quartz grains, assumed to corresponds to Dm in most of the cases (Malusà and Garzanti, 2011).

Additionally, we can combine granulometric data with petrographic and heavy minerals data, to estimate the amount of zircon lost outside the analyzed grain-size window.

Grain density measurement

Density of bulk sediment can be calculated by measuring the sediment weight on air and after immersion in a fluid of known density (e.g. water) Results are corrected for a control factor depending on temperature. Liquid can varies in fact between 0.1 and 1 ‰ for each ℃ increment (handbook of chemistry an d physics", 66th Ed.1985-1986, F4-F5).

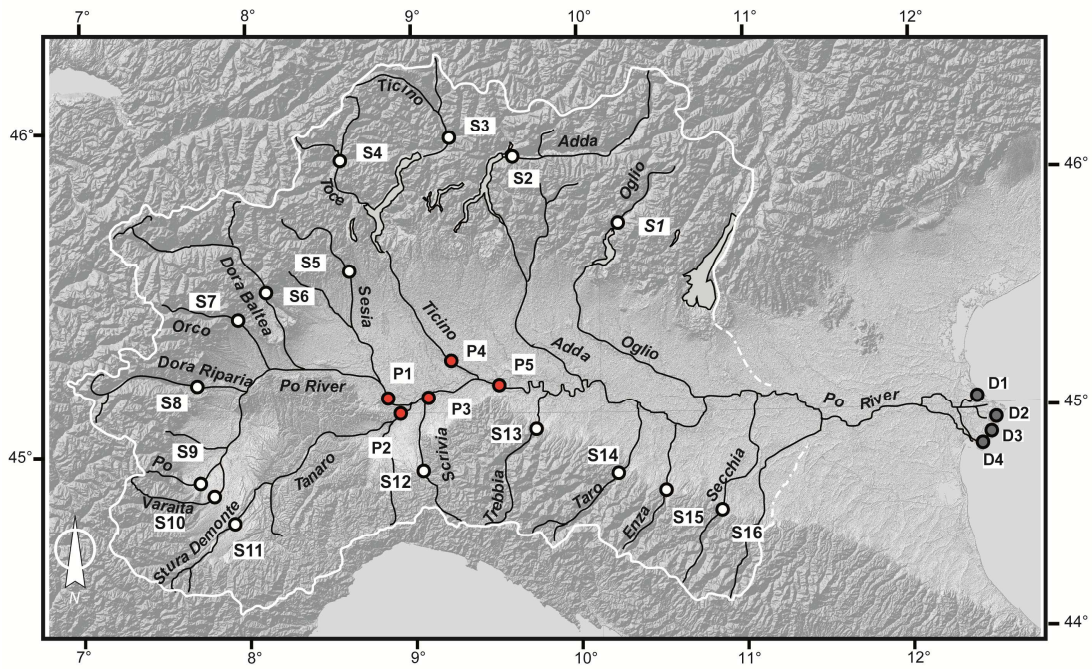

Fig.2: Samples Location. Grey dots show the Po Delta samples were collected from beaches close to the main channel of the modern Po River. Red dots indicate sampling location along the Po River trunk to allow partitioning of geochronological signal. White dots show tributaries samples collected at the end of major valleys to detect the geochronological signal and assess fertility of single source area.

Techniques for zircon separation

Avoid sample contamination

Contamination of samples during separation has to be carefully avoided. We employed compressed air for blowing sieves before they are cleaned in an ultrasonic washing machine. When sieves are dried they are inspected carefully to the light before use to ensure that no grains from previous samples are trapped inside the mesh. If there is contamination, it is removed with a wire brush and compressed air. Compressed air is also employed for cleaning the Franz Magnetic Barrier Laboratory Separator. The chute and the aluminium collectors are blown thoroughly to ensure all remaining residual grains from previous samples are removed.

Gravimetric separation

Sieving

About 2-3 kg of sediment samples were processed by sieving using a sieves column with a diameter of 60 cm (fig.3.A2). Each sample is separated by sieving at 1 φ sieve intervals. This procedure is organised as follow:

- Before sieving the bulk sediment has been carefully dried, then a sample splitter is employed to obtain significantly smaller representative portions of the sample.
- A representative portion of the bulk sample is stored in a bottle
- Ca 300 g of the partitioned sample were sieved in a column between 2000-63 µm
- Resulting grain subclasses are weighted separately and single fractions were stored in plastic bottles. Residual material could potentially be used for other analysis.
- Grain-size distribution was plotted graphically on a logarithmic size scale to get sorting, skewness and mean diameter of the analyzed sediment. We thus chose the size window for further separation steps, usually 63-250 µm.

Hydrodynamic separation by Gemini Shaking Table

Separation principle of the Gemini table is based on the difference of specific gravity of minerals contained in sediments (fig.3.A3). A water film flows on the inclined table surface producing a symmetrical flux of sediment material. Minerals flow according to their density being forced to enter into some defined lanes, so that heavier minerals concentrate in the internal lanes while the lighter minerals in the external ones. The density mechanical separation is always associated to a contemporaneous shape mechanical separation. In fact light mineral obtained from the shaking table separation techniques includes bright-coloured minerals (quartz, feldspar, and carbonates) but also includes biotite and muscovite. Their density is higher than 2,9 g/cm^3, they are normally classified as heavy minerals. Because of platy habit, the micas tend to float and thus to be forced into the external lanes of the table, together with lighter minerals. The Gemini shaking table works automatically for hours:

- At first connect electrically the shaking table and the vibrating funnel, then connect the water pipe to the faucet.
- Let the water flows on the shaking table so that a thin water veil starts to form on the surface of the shaking table, then switch on the engine.
- Once the Gemini table starts to shake, regulate the water flow so that the shock waves forming at the top of the table are not under than ca 10 cm (fig.3.A3)
- The finer fraction between 63-125 µm has to be poured into the vibrating funnel, set at 50-60 pulse/sec, and switch on
- Wait that the first fraction start to flow on the shaking table, then when the funnel is empty pour the last coarser fraction into the funnel and let the table working
- The table is working efficiently when the water veil and the constant shaking of the table, force the grain particles to flow as they forms two distinct trails, the dark-coloured is associated to heavier minerals which are forced to enter in the internal lanes, while a brighter-coloured trail flow into the external lanes
- The minerals falling off from the vibrating table are kept in trays. The lighter and flatter minerals “TSL” (including micas and biotite) are collected in the lateral tray while the heavier and rounded minerals “TSP” (e.g. amphibole, garnet, zircon, apatite, epidote, rutile, tourmaline, kyanite, and sphene) in the central trays.

Heavy Liquids

Zircon has a density in the range 4.6-4.7 g/cm^3, while its density is subject to changes with metamictization up to a saturation level at ~ 3.9 g/cm3 or a density decrease of ~ 17% (Murakami et al., 1991). Other common minerals in sands are quartz with a density of 2.65 g/cm^3, and feldspars, which have a density in the range 2.55-2.76 g/cm^3. Magnetite has a density of 5.2 g/cm^3 (Deer et al. 1992), apatite has a density of 3.1-3.35 g/cm^3 (Deer et al. 1992). Quartz and feldspars can be separated from heavier minerals such as kyanite, apatite, zircon and magnetite in an initial gravity separation stage by Na-metatungstate (density of 2.9 g/cm^3). This allows to separate denser minerals from minerals lighter than 2.9 g/cm3:

- A solution of Na-metatungstate is calibrated to produce the required density of 2.9 g/cm3, by addition of distilled water or evaporation.
- Place the solution on a hot plate under a cupboard overnight. Secondly we use to perform a set constituted by ten funnels for light minerals as much as heavy minerals recovering (fig.3.A4).
- Place the sample in a graduate test tube and add carefully the heavy liquid since a standard weight that should be approximately the same for all the other test-tube.
- Once the graduate test tube is filled with the sample and the Na-metatungstate, they have to be carefully shaked before using the centrifuge.
- The centrifuge works efficiently only if the weights of all the graduate test tubes are equivalent (fig.3.A4). The centrifuge works for 50 revolutions per min
- The separation by centrifugation is effective when sample shows floating and sinking material in the liquid (fig.3.A4).
- To separate the sink from the floating material, we use to refrigerate the sinking pouring the liquid nitrogen (see risk of use in the appendix) in proper Becker of polystyrene since the sink sediment is completely recovered. Then dive the test tube into the liquid nitrogen and wait few second since the sink is frozen.
- Pour the floating sample in a filter paper applied in a funnel. The undiluted Na-metatungstate will pass into the collection beaker with the density unchanged.

- When the heavy liquid is settled out as much as possible, exchange the collection beaker with the wash-beaker and wash the sample with demineralised water. Remove the sample, which will be labelled as TSP<2.9, when it is well cleaned and put in a low temperature oven until it is dried.
- The denser separate labelled as TSP>2.9 is now de-frost and still in the test-tube. It has to be handled in the same way.
- In this manner the Na-metatungstate retains the set density and is ready for another run. The wash solution can be air dried or dried on a hot plate (~100℃) until it is once again at the desired density

Magnetic separation

Magnetic susceptibility is the measure of the ease a material is magnetized by application of a magnetic field. This value can be considered in terms of volume magnetic susceptibility (Xv) or mass magnetic susceptibility (Xg), which is derived by dividing volume magnetic susceptibility by the density of the material being examined (4.6–4.7 g/cm3 for zircon; Deer et al., 1992). Diamagnetic materials have negative magnetic susceptibilities and are weakly repelled by a magnetic field. Paramagnetic materials have positive magnetic susceptibilities and are moderately attracted by a magnetic field. Ferromagnetic materials, such as iron and many iron compounds have high positive magnetic susceptibilities and are strongly attracted by a magnetic field. The following basic settings are used initially:

- Magnetite is removed with a hand magnet to avoid blockage of the chute (fig.3.A5).
- Separation chute set to 10° inclination with a mode rate vibration.
- Magnetic field is gradually increased by setting the amperage in three steps, in order to remove efficiently the ferromagnetic minerals. If necessary, one step at very low electromagnetic field (0.2 Amps) is applied to remove the finer Magnetite. After that the step at 0.3 Amps is applied, which is followed by two other steps at 0.6 amps, and to 1.2 Amps so that zircon and apatite (usually non-magnetic) crystals are separated from more magnetic particles such as garnet, amphiboles (fig.3.A5).

- The magnetic grains are attracted by the electromagnet and fall into the black aluminium sample collector along the chute channel.
- The non-magnetic grains are not attracted by the electromagnet, so they fall into the upper channel in the chute and flow into the gray aluminium sample collector.
- The aluminium sample collectors are removed from the equipment. Usually there is a distinct difference in colour between the magnetic and non-magnetic grains. The magnetic grains are darker and sometimes they show a marked red-to-dark-pink color which depends on the abundance of garnet. Magnetic grains are stored in a plastic can marked with the sample number and annotated “M>2.9”.
- Non-magnetic grains are removed from the gray aluminium sample collector and marked as D>2.9. Usually zircon, apatite, sphene, rutile and other heavy minerals are present.
- Replace empty aluminium sample collectors in equipment and switch off electromagnetic field. Residual magnetic grains caught on the electromagnetic poles will fall down the chute into the aluminium collector. Increase chute vibration to maximum to enhance all residual magnetic grains to flow into collector.
- Clean the chute and aluminium collectors thoroughly with compressed air between poles to remove all traces of sample from the equipment.

Gravity separation using Diiodomethane

Under the fumehood, pour non-magnetic grains into a separation funnel containing Diiodomethane in order to separate zircon from apatite (fig.3.A6). The gravity separation could work great, if Diiodomethane is stirred every 15 minutes allowing the lighter grains to come off from the heavier grains which settle to the bottom.

- The heavier grains at the bottom are then carefully drained into filter paper. Once the ‘D>3.3’ are removed, uncontaminated Diiodomethane is recovered into the storage bottle.
- The funnel containing the filter paper with the ‘D>3.3’ is transferred to a flask for Diiodomethane residuals and flushed with acetone to remove Diiodomethane from filter paper and grains.
- The filter paper with the ‘D>3.3’ is removed from the funnel and placed in a clean bowl and allowed to dry in the fume cupboard.

- The flask for diiodomethane residuals is placed under the separation funnel containing the remaining Diiodomethane with the ‘D<3.3’. This is drained through a clean filter paper, flushing the separation funnel and filter paper to remove as much Diiodomethane into the “washings” flask as possible and also to ensure no grains are left sticking to the inside of the separation funnel.
- The filter paper with the ‘D<3.3’ is removed from the funnel and placed in another bowl to dry in the fume cupboard.
- Once the separation is successful, a small quantity of the ‘D>3.3’ containing a concentration of zircon are mounted on a glass slide with Canada balsam and observed on a petrographic microscope in order to evaluate the quality of zircon concentrates.

Techniques for refining the zircon concentrates

A zircon concentrate could still contain a lot of larger grains (e.g. kyanite). If they are larger than zircons, they could be separated by sieving in order to obtain a good grain mount for an efficient analysis; otherwise we can apply a higher intensity magnetic separation to remove grains containing ferromagnetic inclusion. We use to create a thin film of water on the sieve surface which is stroked gently by hands so that the smaller grains can pass through the sieve meshes. After the extract is filtered through the mesh, the larger grains are examined under a microscope to ensure there are no zircons.

A more powerful magnetic separation is useful when the zircon concentrate is plenty of kyanite and sphene showing abundant ferromagnetic inclusions. These grains with weak ferromagnetic properties are picked up by using a strong electromagnetic field increased to a maximum of 2.0 DC Amps, with a chute inclination at a shallower gradient, for example 5° instead of 10°, reducing t he speed at which the grains flow down the chute. The chute could be set to vibrate more gently. However by increasing the magnetic field some zircon grains containing Fe inclusion and thus

slightly magnetic and may be separated from other zircons into the magnetic grain concentrate. This is undesirable even if there are sufficient zircons in the non-magnetic concentrate as it causes bias in the evaluation of zircon content in the analysed sample. Therefore it is essential to examine magnetic and non-magnetic concentrates to assess efficiency of separation and ensure that significant numbers of zircon grains are not being separated into the magnetic concentrate.

Samples preparation for U-Pb dating

When a good zircon concentrate is obtained from the separation techniques previous described, we proceed to mount this sample in hard resin on a glass slide. Once the zircon slides are ready, out of 100-200 microphotographs were joined together in order to obtain a map of the sample where all the zircons grains are selected for further dating analysis.

Mounted samples and hand polishing

Samples preparation steps have been performed in the laboratory for provenance studies at University of Milano Bicocca, according to the following procedures:

- Preheat a laboratory hotplate on a temperature around 130°C.
- The resin is prepared by mixing 10 parts of epoxy resin with 1 part of hardener with the help of a syringe. Ensure the good quality of the mixing dropping a small quantity of resin on a blank slide which is then placed on the hotplate to cure it.
- Pour a small quantity of zircon concentrate in a clean piece of white paper and write the number of the sample on it then scratch the sample number on the glass slides for identification,
- Place the glass on the hotplate and put on it 2-3 drops of resin, then carefully pour the sample of concentrated zircon grains onto the centre of the slide.
- Working with the slide on the hotplate, stir the grains in the resin to spread them evenly into an area of resin approximately 1-2 cm square on the slide.
- Leave the slide on the hotplate for approximately 5 minutes to allow the resin to cure. Then let stand the resin for 24 hours.

- The slide is polished using a silicon carbide abrasive disc grade P100C which is placed face up on a glass plate previous wet copiously with water.
- Wet the slide to be polished with water and place it in a metal holder which ensures the surface of the resin is kept flat against the abrasive disc during polishing.
- Polish with a circular motion, applying even pressure, and inspect the slide periodically under a binocular microscope to monitor the progress in exposing the zircon grains.
- A margin of unabraded resin around the edge of the mount is an indication of evenness of the polishing and the thickness of resin left on the mount.
- As the resin gets thinner, grains will start to appear with translucent surface when viewed through the microscope. At this point, continue polishing without the metal holder and using less pressure which will produce slower abrasion and allow more control of the reduction in thickness of the resin.
- Polishing by hand in this way continues until zircons break the scratches on the surface of the resin.

Finishing the grain mounts by polishing machine

Polishing step was performed at the Thermochronology Laboratory of the Birkbeck College of London at UCL, by means of Struers Planopol-V polishing machine.

- The rotating grinding wheel of the machine is covered by a paper disc greased with diamond paste of 0.3 micron to provide an even polishing surface.
- The hand-polished slides are placed in cylindrical metal holders and loaded into the motorised rotating mechanism on the machine which uses weights to produce a constant and gradual polishing action.
- After about 10 minutes of polishing remove the slides from their metal holders, and examine them under the reflected light microscope to monitor progress in exposing cross-sections of zircon grains.
- Slides will probably require more polishing to expose different grain sizes to avoid bias and provide that all zircons in the samples will be analysed.

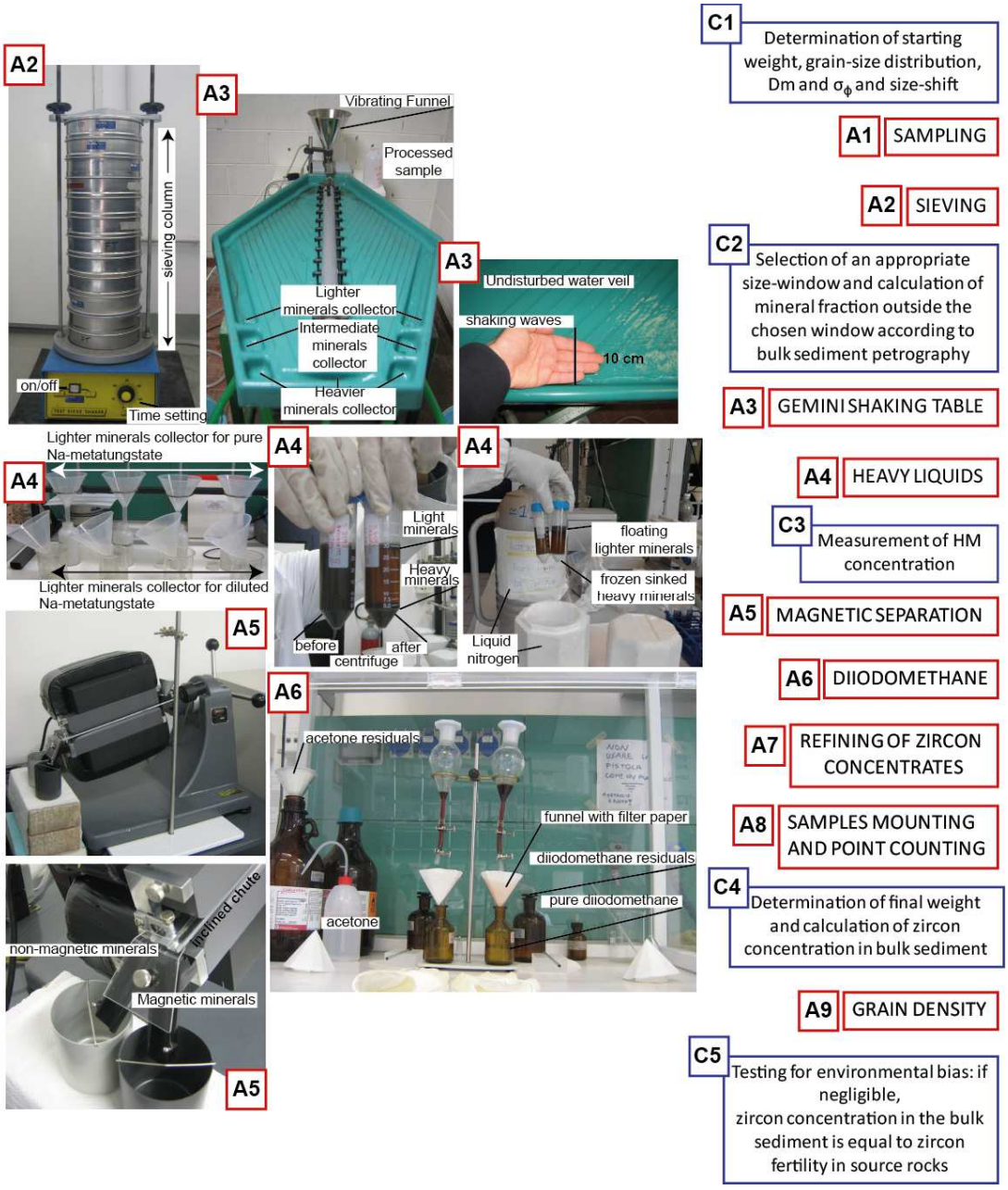

Fig. 3: Equipments in use in the Laboratory for Provenance study and geochronology of the Milano-Bicocca University for zircons and heavy minerals separation. In the column on the right, red squares indicate progressive steps of laboratory analysis which are associated to quantitative measurements (blue squares) of grain-size distribution, size-shift, Dm, σϕ (C1) and selection of an appropriate size window (C2), HM concentration (C3), and assessment of zircon fertility (C4) and testing for environmental bias (C5). Sampling procedures (A1) are followed by sieving sand samples (A2). Then they are processed with the Gemini shaking Table (A3) prior calibration of efficient water flux by measuring shocking waves length on the edge of the table which force grain particles to enter in some defined lanes. Heavy liquids separation set up (A4) and heavy liquids separation techniques (A4) Frantz magnetic separator (A5) and Diiodomethane separation set up (A6)

Recording of zircon grains for further analysis

Once zircon concentrates are mounted on the polished slide, a photomicrograph is taken which will act as a “map” of the slide in the perspective of further geochronological analysis. This task records the position of each grain providing a useful tool in order to match results provided by morphology of zircon grains and all possible following analysis. Furthermore this allows generation of large and complete dataset for each zircon grain in each sample. Making maps for each sample requires lots of pictures taken under a petrographic microscope -ca 100-200 photomicrographs depending on the slide’s size- which have been arranged together in a sort of mosaic. While the larger visual field of binocular microscopes provide easier and faster way to create sample maps, the result obtained by the mosaic work, offers the ideal resolution to avoid bias in selection of grains during analyses.

Sample preparation for Fission Track analysis

Early works describe sample preparation, etching using cleaved (split) crystals immersed in boiling phosphoric acid to reveal tracks (Fleischer et al., 1964). Then the introduction of mounting zircon in Teflon® and etching with a strong base (eutectic solution of KOH:NaOH, NaOH and water, or KOH:NaOH:LiOH), made the basic methodology for handling zircon more suitable for routine FT analysis (Gleadow et al., 1976; Naeser, 1976, Garver 2003). Many problems related to detrital zircon fission tracks methodology are usually due to etching procedure rather than sample mounting, this is because of the sample-to-sample variation in the response of zircon to chemical etching, as a consequence of different U content and α damage accumulation (Gleadow et al., 1976; Rahn et al., 2004). Sample preparation procedures described below, derives from observations and training in

different laboratories that routinely date zircon by fission track method (at the CNR of Pisa, University of Bologna, Union College of London) .

Sample mounting

In detrital zircon fission track is important that each zircon population is detected during analysis, for this reason selection of large clear crystals (e.g. equant grains, prismatic stubby or prismatic euhedral-needles grains) is not adequate to our purpose. We are more likely, instead, to drop zircon concentrate with no previous picking of zircons grain, on three or more mounts for each sample, in order to use a large number of grains during analyses:

- The sample code is written with a needle pen on the backside of the Teflon mount
- Drop enough of zircon concentrates, prior refined, on a silica glass slide.
- The silica slide is now shifted onto a hot plate at a temperature of 315 ℃.
- A second silica glass plate of the same size is also pre-heated on the same plate.
- A sheet of 0.50 mm thick PFA Teflon® is cut to the size of 1.5x1.5 cm2.
- The Teflon sheet is tilted to allow falling down on the glass and cover completely the zircon grains on the hot silica slide,
- Then the second preheated silica slide is put on the Teflon sheet and pressed gently until its bottom ends melt slightly, so that the grains are fixed into the sheet slide.
- Teflon sheet having zircon grains is removed from the hot plate, then pressed between two silica slides and put in the oven at 100℃ for flattening.
- Handling in the same way so that three or more mounts for samples are provided

Grinding and polishing

Flat internal surfaces of the mineral grains are exposed by grinding and polishing procedures. In order to stabilize the mount during grinding and polishing a metallic support is fixed together with the mount by using a double-coated tape. For using

internal surface of zircons it is essential to remove half of the thickness of the zircon grains by progressive steps to avoid the lost of zircon grains for too much polishing:

- The mount with zircons is ground gently several times in one direction perpendicular to the c-axis on the wet grinding paper of 1000 mesh size and observed under an optical microscope for the grinding scratches. This procedure continues until the grinding scratches are observable on most of the grains
- After the grinding, the mount is polished with 15 µ and 3 µm diamond paste on polishing clothes.
- The Struers Planopol-V polishing machine is equipped with a mover device and an extension head system. The mover device can rotate and weight itself on a polishing depending on the hardness of mineral grains.
- After finishing grinding and polishing the mount is cleaned with alcohol and it is ready for etching

Etching of spontaneous fission-tracks in detrital zircons

Detrital suites typically have a large variation in single-grain radiation damage, which is generally attributed to α-recoil damage from the decay of uranium and thorium (Garver and Kamp 2002). Accumulated α-damage increases the chemical reactivity of zircon, so that highly damaged grains (generally older grains all else being equal) are much easier to etch than grains with little damage. To ensure that none of the major age groups was excluded from detection,"*multi-mount technique*" (Naeser et al., 1987), was used (fig.4).

Fission tracks in zircon grains can be enlarged and made visible in an optical microscope by chemical etching. For etching of zircon mounts, we used an appropriate oven where we kept Teflon beaker containing the eutectic NaOH:KOH (1:1) etchant. The temperature of the heater in the oven is controlled by a precise temperature controller. The required temperature of the etchant is 224 ℃ for the FT dating. Approximately a half day is necessary time to achieve a proposed

temperature of the etchant. When the etchant is ready, three or four zircon mounts are put into each beaker for etching. Short etch times were selected as 6 hours, while long and vey long etch times ranged between 12 hours and 24 hours respectively. The ideal situation would have been to have a short etch with no over-etched grains and a long etch with no under-etched grains, arranged so that the differently etched mounts would overlap in their grain-age distributions. We used this as a general target when etching was done, but a perfect balance is almost impossible to achieve because there always seem to be grains with exceptionally high or low uranium contents that are not etched right, while the majority of grains is etched reasonably well.

Packing samples for irradiation

In the external detector method (Fleischer and Hart, 1972) a mica external detector is placed over the grain mount during the thermal neutron irradiation:

- The sample code is written with a needle pen on the back of the mica, then the mica detector is put on the mount
- The mica detector and the mount are coupled and wrapped up with tape of size slightly larger than the mica sheet, then the sample code is written on it.
- The dosimeter glass for monitoring thermal neutron fluence is also attached to the mica sheet as well as the zircon mount.

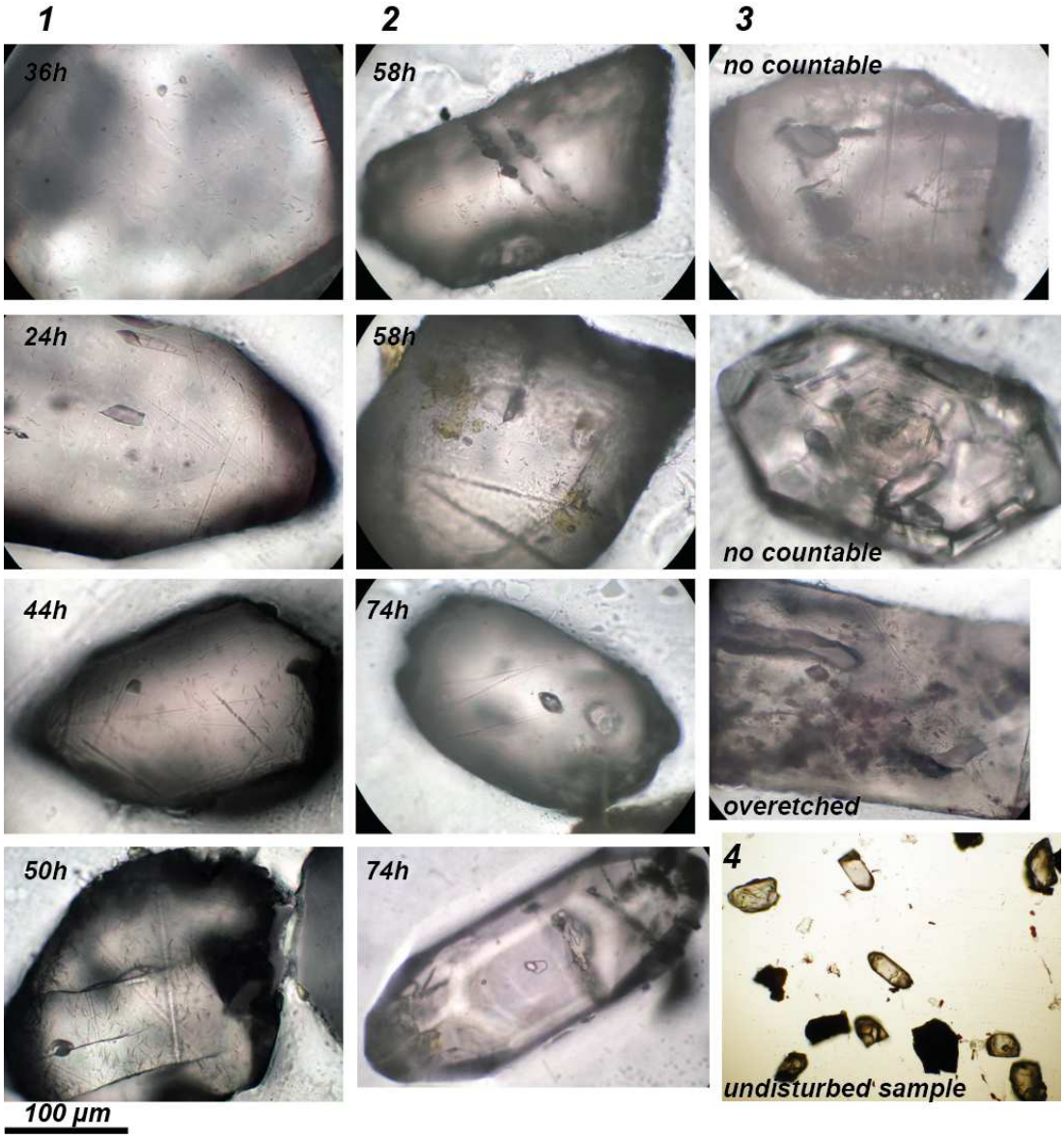

Fig. 4: Effects of different etching time on detrital zircon grains from the same sample D2, h-hours of etching time. In the first row progressive steps of increasing etching times for achieving a number of zircon grains suitable for counting, so that tracks look like in the last picture of the same row. In the second row zircons not suitable for counting because no tracks were appeared also after e very long etching time (74 hours), probably for the very low uranium content. In the last row, zircons not suitable for counting because over-etched or zoned or disturbed by many fluid inclusions. Last picture shows the state of sample before etching

CHAPTER 3

Zircon morphology

Introduction

Zircon ($ZrSiO_4$) is a common accessory mineral in various igneous sedimentary and metamorphic rocks, and shows extremely variable external morphology and internal textures. Zircon is tetragonal and most commonly grows as doubly terminated prismatic crystals with elongation (length to width) ratios ranging from 1 to 5 which could give information on the crystallization velocity (Corfu et al., 2003). Morphological features reflect the geological history of the mineral and of its host rock and represent a widely used tool to characterise different magmatic metamorphic and sedimentary sources (Muller et al., 1995; Wang et al., 2002; Guillot et al., 2002). Its ability to survive many cycles of melting, metamorphism, sedimentation and erosional processes that destroy most other common minerals, makes zircon a widely used mineral in studies of detrital systems. Zircon is also suitable as a geochronometer, from its measurable U, Th and Pb contents. Many studies combined detrital zircon geochronology and typology, providing important information to distinguish between different sources of sediment (Dunkl et al., 2001; Garver and Kamp, 2002; Moser et al., 1996). The aim of this section is to describe how we performed zircon morphology observations on analyzed samples. Zircon morphology have been performed on the basis of a simplified Pupin typological scheme applied of grains observed under an optical microscope and complemented by analysis of SEM high resolution images.

Analytical methods

In common rocks zircon ranges in size from about 20 to 200 µm (Silver and Deutsch, 1963). Morphology of zircon grains from a sand sample can be observed under a binocular microscope that allows us to observe macroscopic properties, such as colour, degree of transparency or opacity, external morphology and development of faces. The presence of fluid inclusions, fractures and alteration is best appreciated under a higher magnification microscope (AXIOPLAN) using transmitted light. Microscopic examination is useful to reveal features such as growth zoning and metamictic zones, which display different interference colours when viewed in crossed polarized light (Chakoumakos et al. 1987, Murakami et al. 1991). Zircon of typical size has a fourth order birefringence according to the Michel-Lévy interference colour chart, hence interference colours are in the high-order white, whitish-yellow or pink in thicker grains (Mange and Maurer, 1992). Even if zircon presents many peculiar features (strong relief, strong birefringence, and typical form) which can help to distinguish it from other minerals, in rounded and abraded grains, this task is not always easy. The difficulty of distinguish zircon from monazite during zircon grains sampling is overcame using a pocket spectroscope, to apply directly on the microscope in place of the standard ocular. The device shows the absorption spectrum for lanthanum as a black band in the orange colour scale when the objective is pointed on a monazite crystal. Monazite ($Ce,La,ThPO_4$) contains lanthanum as an essential constituent while it generally only at trace level in zircon. However the main problem in the observation of zircon morphology is usually the small size of zircon that challenges the power of resolution of petrography microscopes. Observations on zircon grains are organised in a specifically designed form where both internal textures and morphology have been annotated (see in appendix table 5).

External morphology

Because grain size is a frequent consideration in conventional zircon analysis (Silver, 1963b; Silver and Deutsch, 1963) and a potential provenance feature (Morton et al., 1996), the size of analysed grains was routinely measured under the microscope. Additionally five morphologic categories were distinguished (fig.5):

1) Euhedral grains, prism and pyramids are easy to observe and typological classification could be applied with good degree of confidence.
2) Sub-rounded grains, prism and pyramids are not always detectable, but a shape could be recognizable and the typological classification may be applied considering a certain degree of potential bias
3) Rounded egg-shaped and rounded spherical grains, showing length/ width ratio around 1, and acicular prismatic (Miller et al., 2006) grains characterized by high length/width ratio.
4) Grain fragments with sharp edges and occasionally euhedral prism or pyramids may be recognized.

Comparison between grain-age and grain-size could be helpful to understand if hydraulic effects have affected the grain-age distribution.

Internal textures

Colour- Zircon occurs in many colours including colourless varieties (fig6 A,B,C,D,E). Most zircons fall into two general colour series. A common pink series that ranges between pink (fig.6.3), rose, red, purple (‘‘hyacinth’’, fig. 6.E4), and a less common yellow series (fig.6.5) that ranges between pale yellow, honey, brown. Colours are related to trace element composition and increasing radiation damage and time elapsed since cooling; concentration of uranium and thorium; and heavy

rare earth element (HREE) content (Garver and Kamp, 2002). While colourless varieties in zircon occur in young crystals (< 60 Ma) or in metamorphic rocks, according to Gastil et al. (1967) and Kodymova (1977), indicating that colour removal occurs in a number of crustal sections that show progressive metamorphism of rocks between ~350 and 400℃. Metamictic zircons also have been observed, as milky and opaque crystals (fig.6.2) characterised by significant change in colour, density and optical properties (Deer et al., 1982; Speer, 1980). The amorphous and isotropic metamictic form is caused by the radioactive decay of U and Th in zircons which induce strong damage to the crystalline structure (Ewing, 1993).

Growth Zoning- Well developed in mainly in magmatic zircons (fig.7). The origin of growth zoning results from the interplay between different factors during the stage of crystal growth, as the nature of the crystal liquid interface, the degree of super-saturation of the melt, the rates of diffusion, and the state of oxidation (Mattinson et al., 1996). The composition of the zones tends to vary between two end members, one of which is very low in trace elements, approaching the composition of pure zircon, and the other a zircon component highly enriched in trace elements with up to several wt % of the impurity element (Speer 1982).

Cores- Other very common feature in zircon is the occurrence of cores. These are visible under a microscope if distinct differences in U content between a core and rim are highlight by differences in colour (fig.8). Differential metamictization expands the high U part and transforms the original colourless domains into pink to brown, or even opaque, zircon. In the opposite case, with a low U core surrounded by a high U rim, the rim will become much darker than the core. In some cases the only visible sign of cores is a trail of small bubbles at the core rim boundary (ghost core, fig.8).

Fractures- Differential metamictization of zircon causes volume expansion of the U rich domains with consequent fracturing of the more resistant and brittle low U

domains (Lee and Tromp, 1995). Typically the fractures start at the interface with the more metamictic domains and develop radially outward across the low U bands (fig.8.4).

Alteration- Chemical alteration is generally related to fracturing which allows fluids to penetrate into the structure, mostly in zircon grains that are extensively metamictized (fig.8.4). The alteration process has been shown to hydrate zircon, leaching some elements such as Pb and depositing others such as Fe and Ca (and possibly common Pb), hence making the mineral unsuitable for isotopic analysis (Medenbach 1976, Krogh 1982).

Fluid Inclusions- Zircon can include minerals and fluids from the crystallization environment (fig.9). Even if inclusions in zircons are widely used to provide important clues concerning crystallization conditions and paragenetic associations, this is not the aim of our study. However fluid inclusions have been observed in terms of their abundance and location in the zircon crystals, because these features may be critical in the interpretation of U-Pb discordant ages.

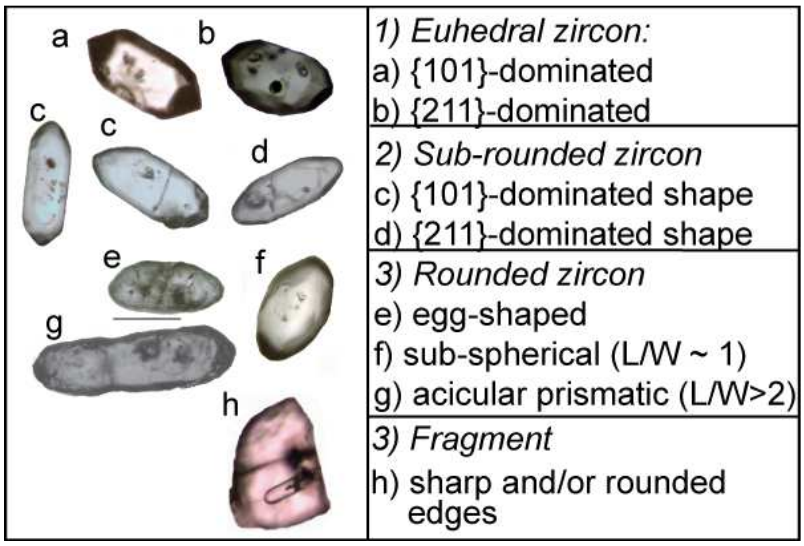

Fig. 5: Categories of zircon morphologies defined according to the relative proportion of length (L) and width (W) of zircon grains (from a selection of some observed zircon grains).

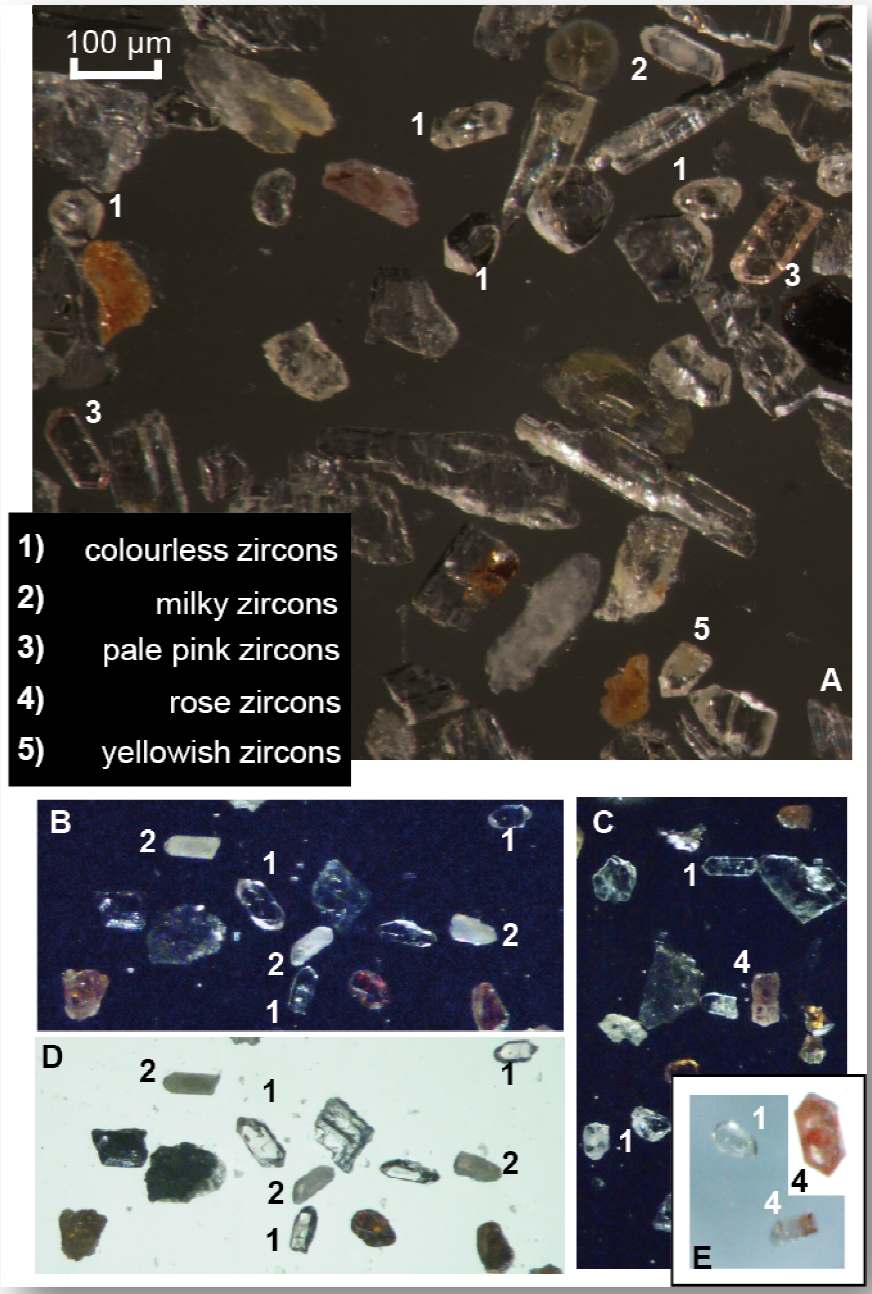

Fig. 6: Suite of detrital zircons from samples of the Po River Delta, show a wide range of colour categories. In all photographs zircons imaged with a binocular microscope using reflected light (dark background) and polarized light (white background), all grains are between 63-250 µm.

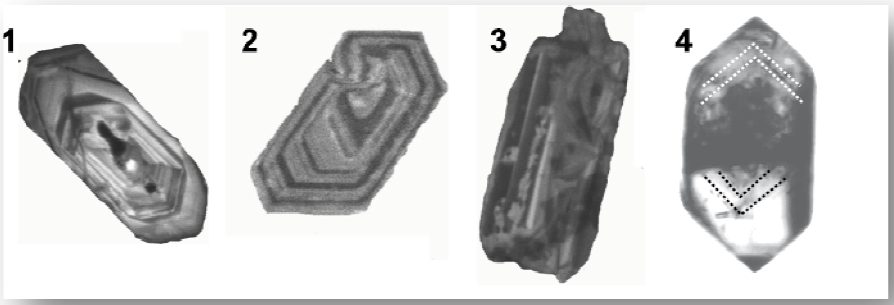

Fig. 7: Complex and other types of zoning in zircons from sand sediment sample. All grains are between 63-250 µm. From 1 to 3 zircons imaged with BSE.1 (from S8 sample) and 2 (from S6 sample)- complex growth zoning with local intermediate resorption (e.g. Zheng-Xiang Li et al., 2002), 3 (from S8 sample)- Patchy zoning, the bright band seams indicate altered fractures disrupting original zoning (e.g. Vavra and Hansen, 1991). In 4 zircon imaged with AXIOPLAN microscope, 4 (from S6 sample)- zoning marked by different colour bands

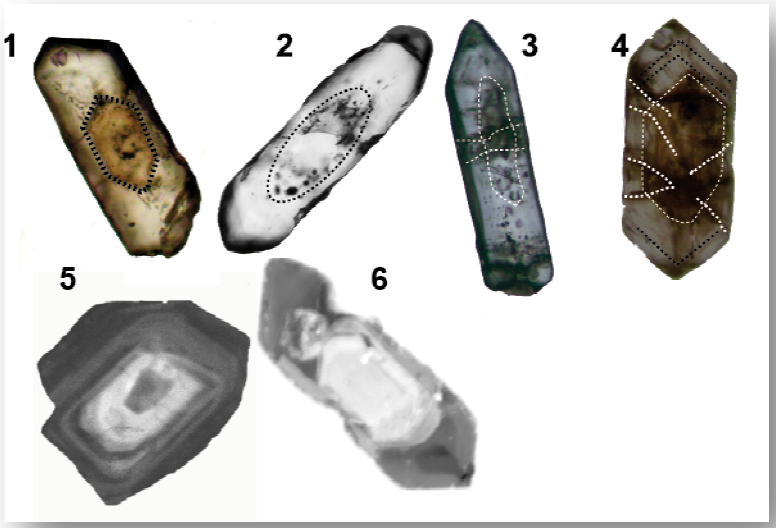

Fig. 8: Variable appearance of cores in detrital zircons from sand sediment. All grains are between 63-250 µm. From 1 to 4 zircons imaged with AXIOPLAN microscope. 1 (from D3 sample)- euhedral shape core darker than the surrounding crystal. 2 (from D3 sample) and 3 (from S3 sample)- ghost cores. 4 (from S11 sample)- zoning zircon with metamictic core and radial fractures pattern with possible alteration. 5 (from S6 sample) and 6 (from P3 sample) zircons imaged with BSE where respectively sub-rounded and euhedral older cores are shown.

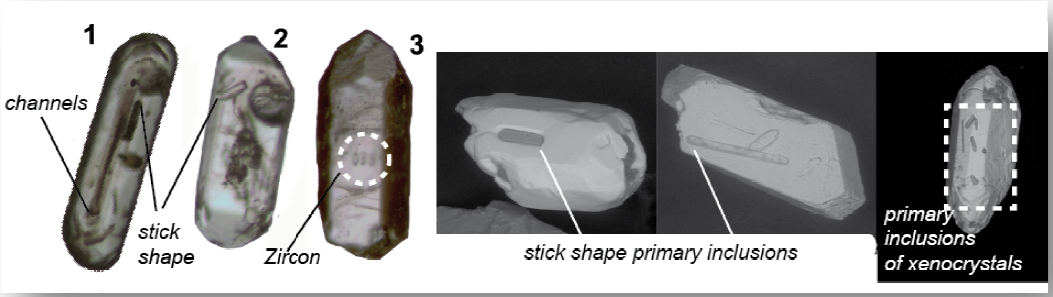

Fig. 9: Inclusions in detrital zircons from sand sediment. All grains are between 63-250 µm. Zircons imaged with AXIOPLAN microscope. 1 (from S8 sample)- inclusion in central position with channel shape, and stick shape inclusions. 2 (from S16 sample)- stick shape inclusion and opaque minerals in central position. 3 (from S11 sample)- possible zircon inclusions with euhedral shape. Last three zircons from sample S6 are imaged with SEM, to highlight stick shaped inclusions

Zircon typology

Systematic examination of zircon typology has led to the widely employed Pupin classification scheme (1976). The method of Pupin is based on the relative development of pyramidal and prismatic faces that is described by two indices. The vertical index (IT) of the typological diagram describes the relative development of prismatic faces: high IT-indices indicate the dominance of the {100} face, low IT indicates the dominance of the {110} face. The horizontal index (IA) instead describes the relative development of the main pyramidal faces: high A-indices indicate the dominance of the {101} face, whereas low A-indices indicate the dominance of the {211} face. In this study euhedral zircon grains are classified on the basis of the relative development of pyramidal faces (A-indices), since they are still recognizable also in sub-rounded grains, where prismatic faces are usually round. Observation of zircon typology is a progressive steps process which led to group zircon grains into two different classes:

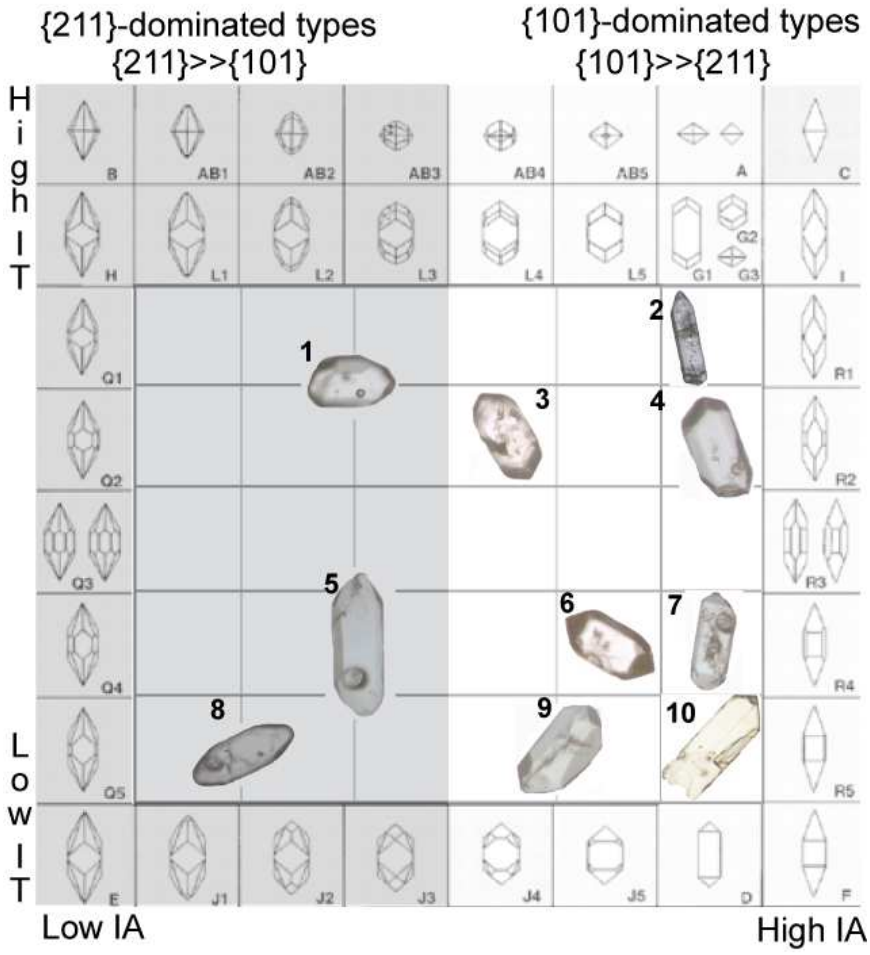

Fig. 10: Pupin diagram (1980), in which zircon crystals are classified according to the relative development of the {100} vs. {110} prismatic forms and the {211} vs. {101} pyramidal form. On the right side in white, {101}-dominated zircons are shown where 2 is P1 (sample S3), 3 is S9 and 6 is P2 (both from sample S2), 7 is S20 and 9 is P4 (both from sample S16), then 10 is P5/D (sample D3). On the left side in grey {211}-dominated zircons are shown where 1 is S3/S7 (sample S12), 5 is S17 (sample S16) and 8 is S21 (sample S3)

- Zircons are observed on a polished section with a high-magnitude microscope
- Pyramids of zircon grains are observed by focusing in and out from the polishing surface of the mineral, when possible, also prisms are considered.
- Then pyramidal faces {101} and {211} are identified by considering their typical shape and by measuring angles between the crystals faces
- "butterfly" shape discriminates the {211} pyramidal faces, while a "chevron" shape is typical of {101} pyramidal faces

Morphological types are organised in a rectangular grid where different pyramidal proportions are arranged in columns and different prism proportions in rows (fig.10).
It is worth noting that our aim is trace the zircon provenance, not the rock forming processes. We are interested in using the typology and textural features of zircon grains as independent parameters to test partitioning based on zircon U-Pb ages.

Typological analysis by SEM

Although the typological method proposed by Pupin is become widespread, its application to detrital zircon studies is controversial because in sedimentary deposits euhedral zircons could be rare and sub-rounded grains, where original crystal faces are not totally reliable, may be of difficult interpretation. The methodology is affected by a certain degree of bias that imposes strong limitations in its reproducibility restraining its application to geochronological methods. The bias of this method has been challenged by different techniques (e.g. Vavra, 1993; Benisek and Finger, 1993), which applies high resolution imagines in catodoluminescence, electron microprobe and back-scattered electron. In our study, we complemented microscope analysis with high resolution images of zircons surface carried out in the Laboratory of Scanning Electron Microscopy (SEM) according to the procedures proposed by Guillot (2007):

- Zircons grains were dropped randomly on a slide of double face tape
- Then zircons grains are examined in 3 dimensions, to better identify the angles between faces in euhedral and sub-euhedral grains.
- This method allows statistical counting that can take into account the euhedral zircons as well as sub-rounded crystals, providing a complete typological dataset of all zircons population represented in detrital samples (fig.11).
- At least an Excel spreadsheet is used to make statistical analyses of all zircons contained on a slide (Guillot, 2007).

In our work the Pupin methodology is used at first and always combined with other geochronological methods (U-Pb and/or Fission tracks, in the following chapters), while typology on high resolution SEM images provided a useful test of reproducibility of typological observations performed with the Pupin method. For this reason, typological observations with SEM have been applied on selected samples representative of the Central and the Western Alps.

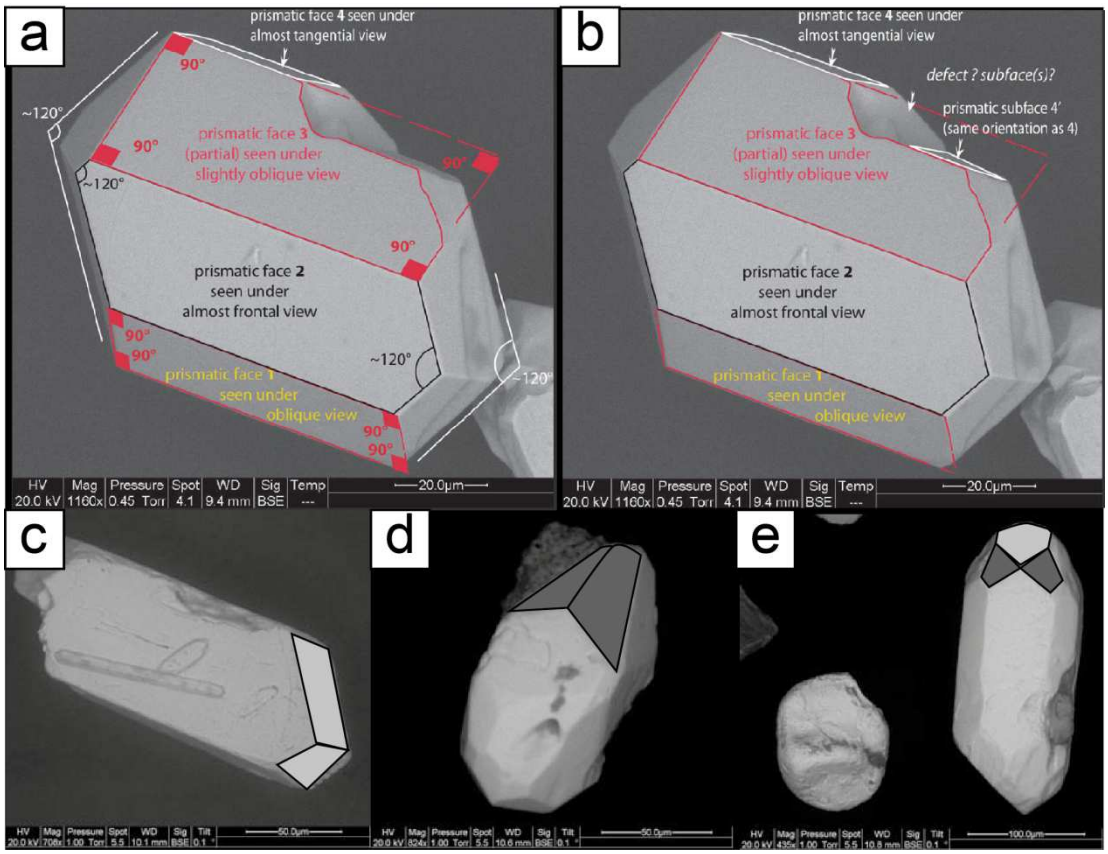

Fig. 11: Zircons imaged with SEM. Pyramidal faces are identified according to the angles measured between faces, a-b-c in euhedral grains, and d-e in sub-rounded grains. a-b after Guillot 2007, only {101} pyramids are shown, c- (sample S6), typical "chevron" shape of {101} pyramids (in clear grey), d- (sample S3), typical "butterfly" shape of {211} pyramids (in dark grey), e- both {101} and {211} pyramids are shown.

PART II
Dating methods

CHAPTER 4

Grain-loss estimation and choice of a suitable dating method

Introduction

Any geochronological method applied to detrital zircons may be theoretically able to identify the source area of sediments they produce. Therefore age and size of each peak representing zircon grain populations should be properly detected. This is important since we are interested to discriminate between potentially sources exposed in the Alps-Apennine orogen, which give the major contribution to the geochronological signature of the Po Delta. In this kind of study geochronological methods should permit to follow sediment along its pathway from source area to depositional environment, in order to quantify the relative contribution of each source area by combining together geochronological signals upstream and downstream of major confluences. In this perspective, the suitable dating methods has to allow a full control on zircon grain-age populations since the early separation steps to final delivery and any loss of zircon grains must be avoided.

In this work we want to discuss critically the choice of the dating method, by comparing the pros and cons related to the application of the most widely used dating strategies in this kind of studies, the U-Pb geochronology and the fission tracks dating of detrital zircons. We are interested in comparing both methods in order to answer to the following questions:

1) What is the geochronological method which provides a truly control on zircon grains populations?
2) What are the potential effects of the grains-loss on sediment budget calculations?

Problems related to Fission Track analysis of detrital zircon in sediment budget calculations

The major problem related to detrital zircon fission track dating is beyond any doubt the zircon loss during etching, just before dating analyses, when lost zircons sometimes reach 70% of total mounted grains. Observation under an optical microscope of the state of grain mounts at the end of etching procedures (described in detail in Chap.2) reveals the occurrence of a large number of holes into the Teflon where zircons grains were previously attached. Moreover a large number of zircon grains are not suitable for counting because over-etched. In order to understand if the grain-loss affects specific populations of zircon or not, we have analysed the possible relations between grains morphologies and grain-loss during etching.

Typology and other morphological features of 16 mounts from 5 different samples have been recorded before and after etching. Point counting more than 100 zircon grains (when possible), was applied in order to not select particular grains. Between the observed zircon grains, we annotated which of them were suitable for counting. After etching the morphological characteristics that are still recognizable is only the external shape. For this reason we discriminated between:

- Rounded/sub-rounded grains even with different shapes (ovoid, acicular prismatic, spherical),

- Angular grains including fragments and the euhedral grains belonging to {211}-dominated or {101}-dominated types (see description in Ch.3)

Our results show that, in all analysed samples, euhedral grains and fragments are enriched with respect to rounded-sub-rounded grains after etching, which implies that rounded/sub-rounded grains are lost easily. This result may be explained at first with a shape controlling factors: edges in angular grains have a best fit with the Teflon with respect to the rounded-grains which tend to come off the Teflon and fall into the etchant. However microscopic observation of samples after etching show that loss of rounded/sub-rounded zircon grains could be also caused by over-etching, because they are often polycyclic, hence they represent very old grains with high α-damage. Resulting graphs show that morphology of zircon grains is a factor controlling the grain-loss more than etching time. This may be supported by the following observations. In the Po Delta samples (fig.12.A), in fact, we can estimate an important grain-loss in spite of small increments of etching time. The difference of 6 hours between the two etching steps was required to better highlight tracks shown by a specific zircon grain-age population abundant in the total amount of grains. However, the increment in etching time aimed at increasing the number of grains suitable to counting, had the inverse effect, decreasing in fact this number. This can be explained by the loss of a large number of rounded and sub-rounded grains as a consequence of the heating and cooling of Teflon mounts each time it is removed from the etchant to control the state of etching procedures. However, such a differences in increasing etching time not affect the grain loss in sample P3 (fig12.B) probably because in this sample there are a lot of large and clear grains making easier to recognized countable grains. This may support our idea that the factor controlling the grain-loss should be the morphological characteristic of zircon grains. Therefore the decreasing number of countable zircons by increasing the etching time

in sample P1 shows (fig. 12.C), may suggest that the majority of zircons in the analysed mounts are rounded and polycyclic, so that they have the tendency to be over-etched and no suitable to be counted. Preferred grains-loss of specific population is directly reflected on the age distribution, with an important discrepancy of the peaks in terms of ages and size observed in samples located at the same site where we expect to find the same age signature (e.g. Bernet et al., 2004, fig 12D).

With the last discussion we have answered to the first question, and indirectly we addressed also to the choice of the right dating strategies. LA-ICPMS U-Pb geochronology on detrital zircons results the more suitable dating method in this kind of study, because it allows a full control during separation procedures and data analysis; fission track dating on detrital zircon is, instead, biased by selective grain loss.

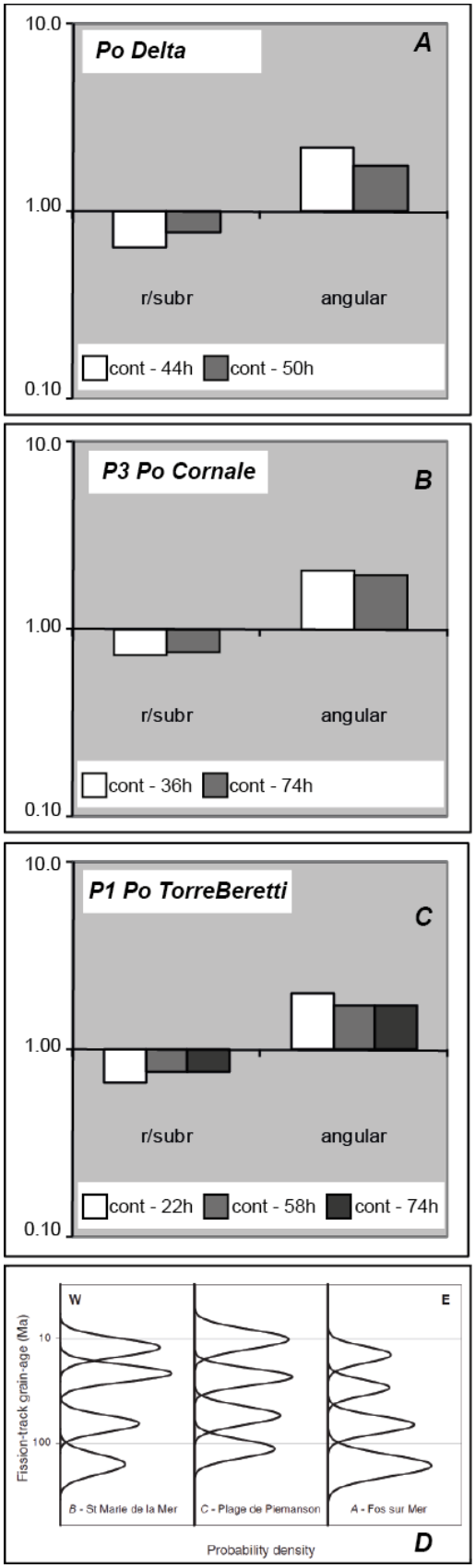

Fig. 12: Plots A, B, C show distributions of zircon morphologies after etching vs. distributions of zircon morphologies in the unetched sample. The horizontal line marks the distribution of zircon morphology of the unetched sample, so that values above this line represent an enrichment of grains with respect to values below the line. D- (from Bernet et al., 2004). Probability density plots of three samples from the Rhône delta, showing an important discrepancy in terms of grain-age populations and size of the peaks, in spite of the three distributions should represent the same sample from the delta.

Detrital zircon U-Pb geochronology

Introduction

Zircon ($ZrSiO_4$) is one of the most important minerals in geochronology. Zircon incorporates among a number of other trace elements, U and Th, which can substitute Zr^{4+}. Over geological period of time, U and Th decay to form stable Pb isotopes. Since Pb^{2+} is mostly excluded during crystallization, Pb in natural zircon is mainly radiogenic whereas initial or common Pb is mostly insignificant. This is the underlying assumption for U-Pb dating of zircon.

The U-Pb single grain ages, record the time of zircon formation in igneous or high grade metamorphic environments. The U-Th-Pb isotopic system in zircons typically has a closure temperature higher than 900° C, which explains why zircon is apparently such a robust geochronometer and is capable of remaining isotopically closed through extended periods of high-grade metamorphism and partial melting of the host rock (Lee et al., 1997). This significant high resistance to thermal overprinting of the U-Pb dating system applied in detrital systems lies in its high resistance to resetting and ability to “see through” lateral thermal events (Carter & Bristow, 2000; Carter & Moss, 2009).

Today our current ability for accurate determination of the U and Pb isotopic compositions of smaller and smaller quantities of zircon, results of progress in U-Pb geochronology. Many techniques (e.g. SHRIMPS and LA-ICPMS) have the ability to select and analyze those parts of single zircon grains that are concordant and record single or successive growth events.

In situ U-Pb geochronology was born some two decades ago with the introduction and development of high-resolution secondary ion mass spectrometry: the SIMS or

SHRIMP (Sensitive High Mass Resolution Ion MicroProbe), described and improved by many authors (Compston et al. 1984, Williams 1998, Compston 1999, Davis et al.,2003).

This technique evidenced for the first time the existence of age heterogeneities within the single crystals of zircon and other accessory phases and therefore the need for high-spatial resolution (tens to hundreds of cubic micrometers) geochronological data.

The SIMS or SHRIMP give error margins about 20times larger than conventional dilution analyses (Pin and Rodriguez, 2009), but show many advantages upon the conventional isotope dilution-thermal ionization mass spectrometry (ID-TIMS) dating technique, because the more readily identifying concordant portions of grains, does not require chemical treatment of samples prior to the analysis, and is essentially non-destructive. A major obstacle to the wider use of ion probe dating has always been the high cost of instrumentation and the long time required to obtain a large dataset.

Laser ablation inductively coupled plasma mass spectrometry (LA-ICPMS, Ireland, 1999) emerged in 1985 and rapidly became an important analytical tool for trace element determinations in geological samples (Jackson et al., 1992). It was soon realized that the large variations in radiogenic Pb and Pb-U isotopic ratios found in nature could be resolved by ICPMS techniques and, when coupled to a laser, ICPMS could be used as a dating tool similar to the ion probe. The potential usefulness of laser sampling for in situ dating by ICPMS was illustrated in many pioneering work of Jinying (1982), Yaoling, (1985), Feng et al. (1993), Fryer et al. (1993), Hirata and Nesbitt (1995) and Jackson et al. (1996).

U-Pb dating equations

U-Pb geochronology is based on the decay of U to Pb (Faure, 1986):

$^{238}U \rightarrow {}^{206}Pb$	$t1/2 = 4.47 * 10^{9}$ years	decay constant $\lambda = 1.55125^{*}10^{-10}$
$^{235}U \rightarrow {}^{207}Pb$	$t1/2 = 0.704 * 10^{9}$ years	decay constant $\lambda = 9.8485^{*}10^{-10}$
$^{232}Th \rightarrow {}^{208}Pb$	$t1/2 = 14.01 * 10^{9}$ years	decay constant $\lambda = 0.49475 \times 10^{-10}$

The age equation for any of the U-Th-Pb decay systems takes the form

$$T = (1/\lambda) * \ln(1 + D/P) \qquad (1)$$

Where T is the age, λ the constant decay for etheir ^{238}U, ^{235}U or ^{232}Th, and D/P the daughter-parent atomic ratio of the respective parent: $^{206}Pb/^{238}U$, $^{207}Pb/^{235}U$ or $^{208}Pb/^{232}Th$. The D/P ratio for any given T can be calculated by

$$D/P = e\lambda^{T} - 1 \qquad (2)$$

By taking equation (2) for each of the two U/Pb systems and dividing, the following equation can be iteratively solved for T if the $^{207}Pb/^{206}Pb$ (here related to radiogenic lead) is measured, noting that the present day $^{238}U/^{235}U$ is 137.88,

$$\frac{^{207}Pb*/^{235}U}{^{206}Pb*/^{238}U} = \frac{e^{\lambda 235T} - 1}{e^{\lambda 238T} - 1} \qquad \frac{^{207}Pb*}{^{206}Pb*} \times (1/137.88) = \frac{e^{\lambda 235T} - 1}{e^{\lambda 238T} - 1}$$

or (3)

These equations form the basis for all U-Pb age calculations and the construction of all relevant diagrams. Minerals that have remained closed for U and Pb give identical values for *t* using both the $^{206}Pb/^{238}U$- and the $^{207}Pb/^{235}U$ systems. In this case *concordant* ages are obtained, which are commonly represented on a conventional or "Wetherill" concordia diagram, that is the locus of all concordant U-Pb systems. Whenever the U-Pb system of a mineral is disturbed and the mineral looses or gains Pb and/or U in a later event, non-concordant or discordant ages are obtained. Analyses of these minerals will plot off the Concordia curve. The effect of the Pb loss on U-Pb ages can be minimized by calculating an age based on the $^{207}Pb/^{206}Pb$ ratio (Faure, 1986). The $^{207}Pb/^{206}Pb$ age is a better estimate for minerals with possible Pb loss because it is assumed that any Pb loss will mobilize equally ^{206}Pb and ^{207}Pb, thus not changing their ratio. The relationship between the $^{207}Pb/^{206}Pb$ ratio and the time results from the difference in the half-lives of their respective parents. The ($^{207}Pb/^{206}Pb$) ratio is the ratio of the radiogenic ^{207}Pb to radiogenic ^{206}Pb.

In each dataset we need to distinguish between the main population of grains preserving a "primary" age (Nemchin & Cawood, 2005) against those related to inheritance or Pb-loss or "discordant".

The Concordia diagram defines the meaning of concordant and discordant point. The concordant point represents a point when the two Pb/U ratios correspond to a given age. A discordant point is instead a point that has different calculated ages for the two Pb/U measured ratios. If one plots out all concordant points for all times in the past, the result is a curve termed the Concordia (Wetherill, 1956a,b). Isotopic composition of zircon should generally lie on this curve where such analyses that fall below the Concordia curve are termed "normally" discordant, whereas analyses that plot above or to the left of the Concordia curve are "reversely" discordant.

LA-ICPMS system

The equipment U-Pb dating was carried out using a New Wave aperture-imaged, frequency-quintupled, laser ablation system (213 nm) coupled to an Agilent 7500a quadrupole-based, inductively coupled plasma mass spectrometer (ICP-MS, Yokogawa Analytical Systems, Inc., Japan) following the methods described in Jackson et al. (2004). Ablated material is transported toward the detecting system by an argon/helium mixture which is more efficient than air and reduces background signals (Jackson et al., 2004). The laser ablation software provides set-up of laser properties (e.g. output, repetition rate, spot size), control of sample stage movement and laser focussing, a live image of the sample for accurate positioning of the spot and monitoring during ablation. The Agilent software provides control of ICP-MS parameters and data acquisition. GLITTER software (developed by the ARC National Key Centre for Geochemical Evolution and Metallogeny of Continents [GEMOC] at Macquarie University and Commonwealth Scientific and Industrial Research Organization [CSIRO] Exploration and Mining) provides a graphical presentation of isotope counts and ratios from a laser ablation run, calculation of ages of samples and standards, and, most importantly, a time-resolved signal selection allowing unstable signals to be excluded from age analysis.

Laser ablation settings

Standard laser settings for all analyses of sample and standards were as follows:

- Output 55%
- Repetition rate 5 Hz
- Spot size 55μm

However, we preferably used the laser spot size at 40μm in order to be able to analyse relatively small or thin grains without too much ablation of surrounding resin.

It is important to analyse all grain sizes in a sample in order reduce bias in the distribution of ages measured for a sample.

The disadvantage of a smaller spot size is a reduced laser ablation sample rate, which means less data acquired per grain analysis. The advantage is reduced risk of Pb contamination resulting from ablation of the resin surrounding a grain. Each ablation run was set up as follows:

- Initial laser warm up without ablation to establish a measurement for the background signal, (timing required: 30 sec.)
- Laser ablation of grain: 30 sec.
- Before opening the sample cell and drawing the stage, remember to set the laser ablation system to "bypass" to avoid air being drawn into the system
- Place the glass slide into the sample cell and turn off the cell
- Every time the sample cell is opened to change sample it is necessary to purge the cell in order to enhance the argon plasma out of the ICPMS

Calibration

The LA-ICP-MS requires ‘tuning’ before a session to correct for mass fractionation.

This is done by continuously ablating the glass whilst fine-tuning ICP-MS parameters and measuring the U, Th and Pb isotope ratios, which are known with some accuracy in the glass. The aim is to setting measurements close to the known isotopic ratio values and minimizing standard deviation of the measurements.

Prior to laser ablation of the zircons grains in the sample itself, 2 or 3 ablation results of the zircon standard are obtained and transferred into GLITTER software which should produce $^{206}Pb/^{238}U$ ages around 337 Ma (Sláma J. et al. 2008). In addition, 2 or 3 spot analyses of the glass are obtained at the beginning and end of the session and these will be used to calculate U ppm and Th ppm and the U/Th ratio for each grain analysis.

Sample analysis

Sample maps provide a record of the actual grains selected for ablation and allows the progress of the analyses in a mount to be monitored which may help to avoid bias in selection of grains.

- The laser ablation spot is set up after focusing the image of the slide by the video linked to the laser ablation system. Zircon grains are usually easily identified because they shine brilliant white while other minerals, except for pyrite and oxides which are shine clear white, are dull. In such case when pyrite and oxides grains look similar to zircons, seeing on the sample maps could be helpful because pyrite and oxides are opaque.
- Prior to each ablation, each grain dating is set up with a specific file number related to sample number and a sequential number of analyses.
- An ablation spot should target a grain in order to avoid resin, fractures, and inclusions as they are a source of discordant ages (see discussion in ch.5).
- Ensure system has been purged for 30 seconds and start laser ablation.
- The ablation is monitored in real time by viewing the laser directly on screen and checking the signal received by the ICP-MS. The signal should ideally rise sharply and flatten out within a few seconds for the remainder of the ablation. Occasionally a poor signal is received, maybe because a grain has not been properly exposed by polishing.
- After ablation, the file containing the data is imported into the GLITTER software which enables the signal (counts per second and isotope ratios) to be analyzed as a function of time, and hence also as a function of progressive ablation depth (Jackson et al. 2004). If possible, the flat stable part of the signal should be selected (Jeffries et al. 2003)
- During an ICP-MS session, it is necessary to periodically ablate the standard zircon and use the measurement to monitor and correct for drift in ICPMS results during a session. In this study, the practice was to run three or four analyses of the standard zircon after every 30 or 40 analyses of zircon grains always checking the age of the standard zircon to assess the calibration ICP-MS

Data handling

All analyses of zircon grains in the sample, the standard zircon, and the NIST 612 glass were imported into GLITTER for time-resolved signal selection, after which the counts per second and isotope ratios of the entire session were saved in text format for being processed in an excel spreadsheet:

- The raw data file for each sample containing the results of each ablation is copied to a Microsoft Excel® spreadsheet which uses the Isoplot add-in (Ludwig 2003) to calculate concordant ages, isotope ratios and Pb corrections and produce relative probability plots.
- Isoplot produces a table of uncorrected ratios, uncorrected ages and ^{208}Pb corrected ages based on $^{206}Pb/^{238}U$, $^{207}Pb/^{235}U$ and $^{207}Pb/^{206}Pb$ and percentage discordance between the $^{206}Pb/^{238}U$ and $^{207}Pb/^{235}U$ ages for each analysis (see Table 6 in appendix).

Common Pb correction and limits for rejection of discordant ages

Partial correction for common lead has already done by selection of the time-resolved signal in GLITTER. However, the additional ^{208}Pb common lead correction provided by Isoplot (Ludwig 2003), can be also used because it is easily incorporated into spreadsheets, even though its assumption of ideal concordance may not always be justified (Anderson 2002).

The common approach to reject discordant ages is to set percentage limits. Although rejection of discordant ages is a problematic step of U-Pb ages analyses of detrital zircons, and it cannot be settle only by choosing a cut-off value. For this reason the aim of next chapter is to discuss the problem of rejection of discordant ages.

Switching from $^{206}Pb/^{238}U$ ages to $^{207}Pb/^{206}Pb$ ages for older grains

For younger grains, the $^{206}Pb/^{238}U$ age is more precise than the $^{207}Pb/^{206}Pb$ age because ^{207}Pb counts are too low to be accurately measured (Nemchin and Cawood 2005). Many workers use $^{206}Pb/^{238}U$ ages for young grains and $^{207}Pb/^{206}Pb$ ages for older grains but there is no agreement on the age at which this switch takes place (e.g. Clift et al. 2006b and Cawood & Nemchin 2000 use $^{207}Pb/^{206}Pb$ ages for grains >1200Ma; for Campbell et al. 2005 the limit is > 1100Ma; for Enkelmann et al. 2007 the limit is >1000-800Ma).

U-Pb ages from detrital zircon of Po River Basin are quite young which are better suited to 207 corrections, and we opted to not report older ages than 900 Ma uncorrected for common Pb using the ^{208}Pb methods. This is because the very old analysed grains (>1Ga) only account for a small percentage of detrital zircons and does not seem to be significant of a source area. They could represent, instead, detrital zircons from the Pan-African basement with Proterozoic to Archean inheritance (e.g. Schaltegger, 1993), being representative of the Pre-Alpine events which are behind the interest of our study.

CHAPTER 5

Discordance in detrital zircon U-Pb analysis

Introduction

The U-Pb system is characterised by a high resistance to thermal overprinting (>700-900℃, Mezger & Krogstad, 1997), without completely resetting or loosing age information (e.g. Carter & Bristow, 2002; Williams, 1992; Lanyon et al., 1993). Although zircons used for U-Pb geochronology may experience partial resetting for Pb-loss or contamination of common lead during its initial formation or in some later events. Several publications examined the possible causes of bias in zircon U-Pb ages as a result of several thermal overprinting (e.g. Aleinikoff et al., 1989; Kröner et al., 1994), fluid circulation linked to a low grade metamorphism and even weathering (Stern et al. 1966; Gebauer & Grünenfelder, 1976; Black, 1987), as well as possibly leaching within laboratory handling (e.g. Naylor et al., 1970; Davis et al., 1982). Either incorporation or loss of lead is very common in zircons, so as to be considered as the factors which control and potentially bias U-Pb analyses leading to the identification of one or more zircon populations preserving discordant ages. Also weathering and diagenesis provide discordant age in zircon grains because the contamination of the isotope La^{139} in sub-aereal environment (Fleischer & Altschuler, 1969). Presence of discordant ages in U-Pb detrital zircon ages could be a characteristic that zircons acquired during subsequent geological process (Carter & Moss, 1999). In detrital zircon dataset is often difficult to establish if discordant ages may produce meaningless peaks which have to be rejected or if they may reflect a characteristic of the source areas and, in this case, the problem with the rejection of

such discordant data is to increase the probability of missing a potential source. As a consequence the interpretation of discordant U-Pb ages from detrital zircons populations could be extremely difficult and special care should be taken to reject some of the most discordant data. The necessity to understand how discordant ages have to be treated is important in interpretation when using age dataset to constrain every provenance component in the source areas.

In this chapter we focus on the treatment of discordant data from detrital zircons in those samples where discordant ages affected rather an half of the total analysed grains. We not claim to address the problem of analysis of detrital zircon discordant data. Our aim is, instead, to highlight potential biasing during data processing and provide a possible interpretation of discordant grains in our samples. We used a qualitative approach to data treatment; which is applied to all the analysed samples, making possible a comparison between different dataset.

Bias in LA ICPMS analysis of detrital zircon

In our detrital samples, each zircon grain was observed for typology before laser ablation. This provides a first order understanding of the possible source of bias in zircon analysis. In addition this should avoid the difficulty to distinguish zircon from other heavy minerals during LA-ICPMS sampling. In this study, it is reasonably to believe that among the resulting discordant ages, only a small part are clearly meaningless because related to a wrong sampling of other minerals grains. While discordance in ablated zircons may be dependent on their internal structures, or else, on the related thermal history. Frequently among discordant zircons we are able to identify those characterized by a severe pattern of fractures or rich in fluid inclusions. Anyway an ablation spot should target a grain to avoid fractures,

inclusions as well as resin as far as possible. Zircons displaying discordant ages can be recognized in two phases of analysis:

- During sample ablation with LA ICPMS, we are able to check when the signal is proper of a zircon grain by the typical shape rising sharply and flatten out within a few seconds after the ablation. Once data where imported into GLITTER software, the signal is translated in isotope ratio (Jackson et al., 2004). Change in the isotopic composition in a zircon grain may be resulting from Pb-loss or inheritance.
- During data processing with Isoplot (Ludwig, 2003), some of the analyzed zircons may display discordant ages, expressed as a positive value of the Pb^{206}/U^{238} ratio. The range of tolerance is defined between 0 and 5 % above the Concordia diagram (Wetherill, 1956). In our analyses discordant zircons may display a narrow range of 1% up to 9 % common lead caused by lead loss after crystallization or contamination by no radiogenic lead at the time of initial crystallization. In addition we found discordant ages with lower values of common lead because the lead contained in the U-Pb system is entirely radiogenic.

Approach

During processing data in GLITTER, we can directly appreciate what is causing a variation in the isotopic composition of zircon grain. This is because the software is able to estimate among the Si and Zr isotopes, also the amount of the isotope La^{139}. The lanthanum isotope is mainly common in weathered zircons, which are very abundant in detrital samples. Consequently enrichment of this isotope could characterize a sedimentary rocks source. Resulting discordant ages from lanthanum

contamination are usually meaningless, so they can be used just to identify the source area and eventually trace its sediment pathway, but they cannot be considered in further analysis in the same manner than good ages. Other possible causes of changing in the isotope composition are the abundance of fractures, inclusions or inherited cores which may be encountered as the laser drills down into the zircon grain. It is often difficult to avoid this source of error mainly when a grain is small or thin, and ablation of resin seems inevitable. Also the mounting resin which was partially ablated in many analyses could be a source of discordance. When inclusions and fractures exposed by ablation are invisible in transmitted light as well as under the microscope they cannot be avoided during ablation. This source of bias could result only after processing data with Isoplot as this leads to discordant ages. In detrital zircon dataset is often difficult to establish if such discordant ages may produce meaningless peaks which have to be rejected, or if they may reflect a characteristic of the source areas. In this last case the problem with the rejection of such discordant data is that this increases the probability of missing a potential source. However the decision to apply a certain degree of filtering to reject discordant data is subjective and can also vary from case to case. Before rejecting discordant ages as meaningless, we choose to investigate the possible source of bias looking into the internal structures of zircons as a mirror of the complex thermal history as a source of common lead or Pb-loss.

Methods

The best resolution of internal textures is provided by cathodoluminescence (CL) or back scattered electron (BSE) imaging. Both techniques have been performed on selected grains in two different laboratories at UCL and Universitée de Lille 2.

The CL emission is usually attributed to the electronic transitions of 5d electron transition elements, of 4f electron electronic transitions of the trivalent rare earth elements (REEs), vibrational luminescence of the uranyl ion, or defect related phenomena (Marshall 1988). Back scattered electron imaging reveals contrasts in average atomic number of regions of a phase; the higher the number, the more electrons an area will “reflect” and the brighter it will appear in the resulting image (Corfu et al., 2004). The element primarily responsible for these BSE intensity variations in crustal zircon is Hf, with U having a secondary effect (Hanchar and Miller 1993). Both techniques reveal similar features in investigating zircons; however, usually the bright areas in CL are dark in BSE and vice versa (Hanchar and Miller, 1993; Koschek, 1993; Nasdala et al., 2001).

Application to discordant zircons from selected samples

Five examples for investigating the possible causes of discordant zircons are given below:

DETRITAL ZIRCONS FROM TICINO RIVER (S3)

Detrital zircons from the Ticino River, draining the eastern part of the Lepontine dome, show a variety of morphologies and internal features, which are assigned to the geological processes experienced by the source area. Most U-Pb detrital zircon ages scatter around 450-550 Ma with other minor peaks between 280 Ma, 100 Ma and a small young peak around 40 Ma. Discordant ages are spread in the entire age distribution but some zircon populations used to be characterized by strong discordance. This is always the case for zircon populations ranging between 100 and 140 Ma. Zircons from this population show dull surface and marked zoning, as the effect of polycyclic history and a developing degree of metamictization which induces

to Pb-loss (plate 1, n.83). A younger zircon population is represented by a small peak around 40 Ma and presents some discordant ages. Because this population includes only few grains essentially discordant, the decision to reject them may increase the probability to miss their source. This population results discordant usually because the low amount of radiogenic lead in young zircon is not always detectable by the LA-ICPMS resolution (plate 1, n.33, 34, 74). In older zircons the most common reason for discordance is the growth zoning or the growth of new zircon around old cores. This may cause discordant ages when zoning is very tight with metamictic bands or large old cores may occur in small zircon grains.

In discordant zircon it is quite commonly observed that regular growth zoning is interrupted by textural discontinuities and succeeded by the growth of a new zircon characterised by a different zoning pattern (plate 1, n.8, 9, 14). Zircon shown in plate 1, n.52 is characterized by an irregular sub-rounded external appearance, an almost uniform internal texture, and evidence of marginal resorption and reprecipitation (e.g. Hanchar unpublished data/ Corfu, 2004). In some cases discordant zircons not show clear internal textures and their resolution results very complicated (plate 1, n.20, 68). Strong discordance in zircon grains may derive by overgrown or complex intergrowths of xenotime, showing shine white area around or inside zircon (plate 1, n.53,113). Xenotime crystals could be formed during diagenesis and can thus be used to constrain the age of sedimentation (e.g., Fletcher et al. 2000), because of their structural affinity (i.e., isostructural), zircon and xenotime could be locally found in association with each other.

DETRITAL ZIRCONS FROM DORA BALTEA RIVER (S6)

Detrital zircons from the Dora Baltea River, draining the northern Western Alps, are evidenced by a mixture of morphologies and internal features, related to the thermal

history of the source area. Most U-Pb detrital zircon ages scatter around 280-320 Ma with many minor peaks spreading constantly between 120 Ma and 650.

Discordant ages lie mostly within the main zircon population where observations in BSE and CL put in evidence marked zoned zircons and inherited cores. In these cases the simplest reason for discordance is the occurrence of different U and Th content and trace elements composition between zircon zones (plate 2, n.45). Overgrowth and old cores of xenotime are frequent in strongly discordant metamictic zircon (plate 2, n.86, 110), and Archean zircons (plate 2, n.18, 35, 41).

In figure 15 grain n. 55 is a discordant zircon with large fluid inclusion of primary or secondary generation. This means that the system zircon is not remained closed and the lead contained in the system could be not of radiogenic origin. In this case no radiogenic lead may be incorporated into the mineral at the time of initial crystallization or in some later event. When no radiogenic lead is incorporated into the system, known as common lead, then discordant ages leading to an increasing in the apparent age of U-Pb system are expected (Andersen, 2002). Analysis of main elements on the BSE has revealed that composition of larger inclusion contains high amount of Si, probably deriving by quartz filling (fig.15).

It could be interesting to note that zoning, cores and occasionally complex internal textures could characterized also zircons with concordant ages (plate 2, n.6, 96, 113) and not such big differences are observable between concordant and discordant grains (plate 2, n.1, 45, 81, 98) in terms of internal structures. This means that CL and BSE cannot always address the problem of discordance, because the point is in the diverse degree of radiation damage between zones and different part within a zircon. For this reason investigating the phenomenon of annealing of radiation damage generated in α-decay events in zircon, may be very useful. Raman spectroscopy provides high resolution in estimating metamictization and it may

represent a useful tool in such investigation (e.g. Nasdala, 2001). Raman image can use to correlate the intensity patterns in BSE and CL images with radiation damage phenomena and to document in detail the internal structures of heterogeneously metamictic zircons.

DETRITAL ZIRCONS FROM DORA RIPARIA RIVER (S8)

Detrital zircons from the Dora Riparia River typically contain old inherited zircon cores. Most U-Pb detrital zircon ages scatter around two major peaks the dominant at 280-320 Ma and a prominent at 520-580 with many minor peaks spreading constantly between 120 Ma and 800.

Images in BSE and CL show complex internal textures that may induce to discordant ages in most of zircon populations. Internal pattern revealed that the possible reason for discordance is ablation of zoning patterns with metamictic bands (plate 3, n.5, 35, 140, 142). Although in n.140 and n.142, a similar pattern is observed, and both zircons display concordant age, because the laser drilled in an area inside the zircon characterised by a more homogeneous composition. This may also explain how discordant age of zircon in plate 3, n.37, is turned into concordant when the second spot drilled a more uniform area. Difference in trace element and U composition may become very small yielding only slightly visible zoning pattern (plate 3, n.16,35a) and in some cases there is no visible zoning at all (plate 3, n.1, 3). Intergrowth of xenotime characterised discordant Archean zircon (plate 3, n.60, 63, 66).

DETRITAL ZIRCONS FROM THE PO RIVER AT TORRE BERETTI (P1)

This detrital zircons suite comes from the Po River trunk, in the sample location after the confluence of rivers draining the Western Alps.

U-Pb detrital zircon ages are represented by an important population around 280-320 Ma following by older minor peaks older. Discordant ages are mostly

concentrated in this last population with ages between 360-520 Ma, mainly characterised by high rounding degree and small size, so that the ablation spot can hardly avoid such areas within a zircon grain related to its older history (plate 4, n.10, 31, 73). Although the occurrence of complex internal patter related to strong difference in uranium content inside the same zircon grain is counted as the first cause of discordance, it must be specified that complex internal structures are not always accompanied by discordance (plate 4, n.002, 22, 28, 49, 50, 51).

DETRITAL ZIRCONS FROM THE PO RIVER AT CORNALE (P3)

This detrital zircons suite comes from the Po River trunk, downstream sample P1 and before the Central Alps rivers confluences.

Most U-Pb detrital zircon ages scatter around 280-320 Ma with other minor peaks between 280 Ma, 100Ma and a small young peak around 40 Ma. Discordant ages are mostly concentrated in the younger population (30-40 Ma) where zircons are characterised by high values of common lead and as a consequence strong discordance. This zircon population not necessarily shows particular internal textures which may be the cause of discordance. This is because very young population like that, contain high content of uranium with respect to the accumulated radiogenic lead which cannot be solved by the LA-ICPMS resolution (plate 4, n.36, 44). The decision to reject this population may increase the probability to miss their source.

In older zircons the most common reason for discordance is the growth zoning or the growth of new zircon around old cores (plate 4, n.38, 56). This may cause discordant ages when regular growth zoning is interrupted by textural discontinuities and succeeded by the growth of a new zircon characterised by a different zoning pattern (plate 4, n. 6, 75, 71, 112,).

Strong discordance in zircon grains may derive by overgrown or complex intergrowths of xenotime, showing shine white area around or inside zircon (plate 4, n. 52, 113).

Conclusions

In samples where discordant data are very consistent we preferred to check each analysis line by line (almost 150 analyses are carried out for each sample) and manually rejecting discordant analyses, instead using the automatic procedures to select concordant dates using a pre-defined parameter. The strategies to display both concordant and discordant data, is to include both together within the probability density plot diagram (e.g. Roback and Walker, 1995; Morton et al., 1996) to illustrate that discordant data exists and has been considered. Probability density distributions obtained for analysed samples display both concordant and discordant ages as well as only concordant ages. Concordant ages are obtained applying a filter of 5% of discordance. Our results show that the general trend of both probability density distributions is similar, as a consequence discordant ages spread on the whole zircon grain-ages distribution and not affect only a particular populations as shown in probability density plot indicated in the following chapters.

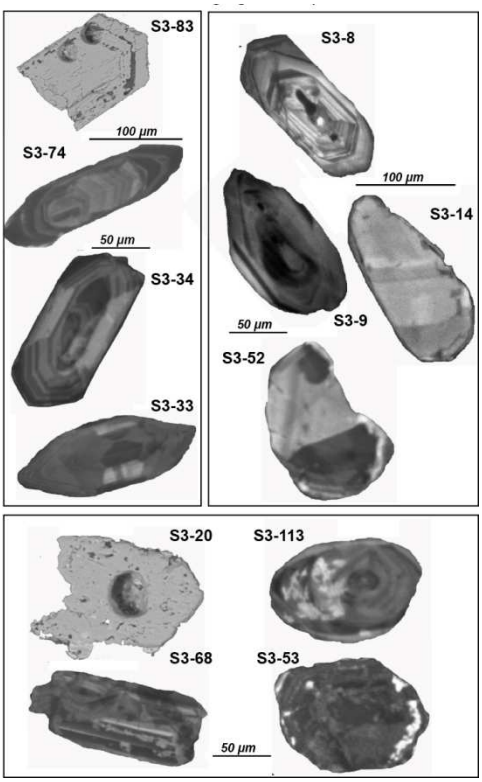

Fig. 13: Plate 1, Sample S3. CL-images of detrital zircons from Ticino River draining the Lepontine dome in the Central Alps. The left block shows euhedral morphology and well defined zoning. The right block shows rounded or sub-rounded zircons with patchy zoning. The following row shows rounded or uneven grains where internal pattern is not easy recognizable

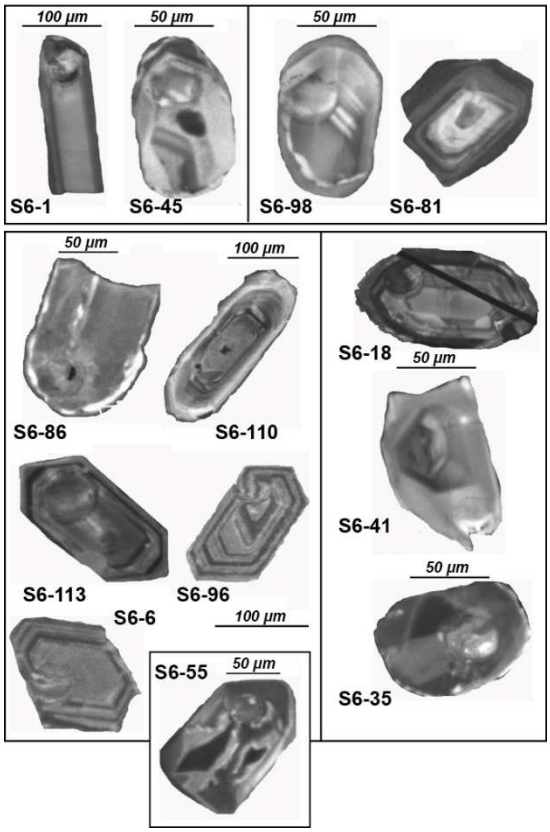

Fig. 14: Plate 2, Sample S6. CL-images of detrital zircons from Dora Baltea River draining the North-Western Alps and the Mont Blanc massif. Note that many of the zircons are rounded with older cores, but also euhedral grains are common with zoning patter probably of magmatic origin.

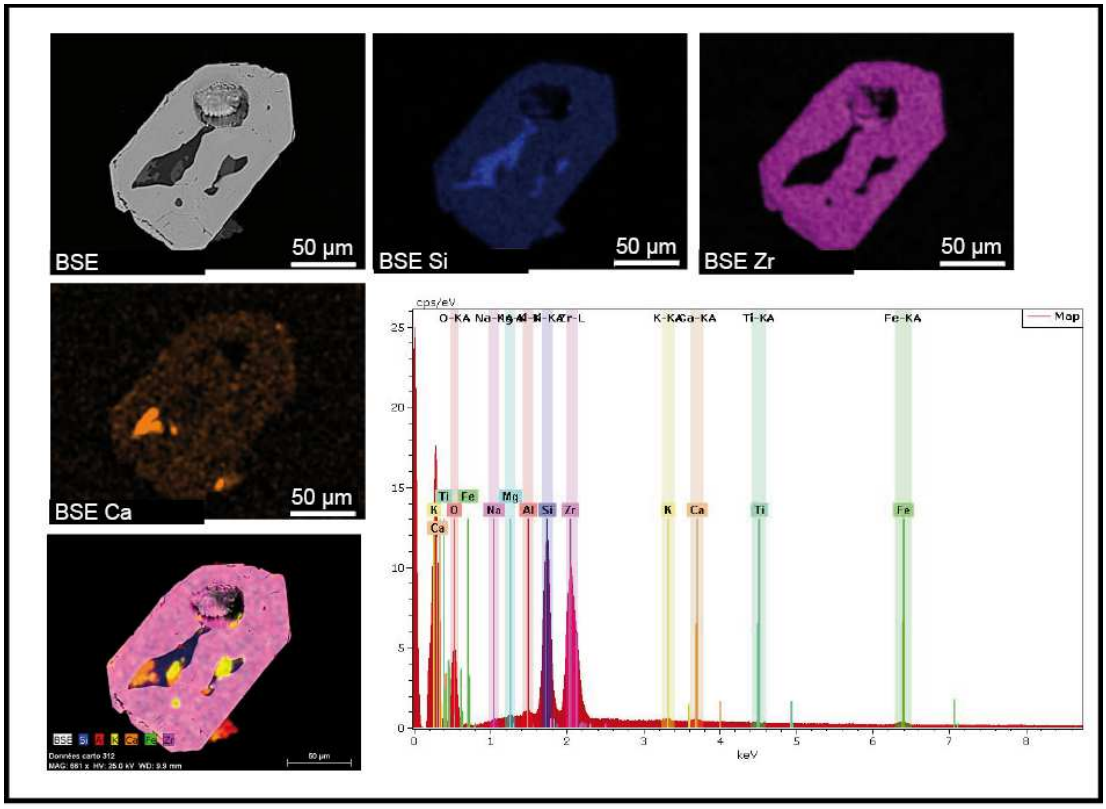

Cartho Ph 55: MAG 661X HV:25.0 kV WD: 9.9 mm

Fig. 15: X-rays of zircon grain n.55 of sample S6. X-rays produced by the interaction of electrons with the sample, are detected in the SEM equipped to determine major elements in large inclusions

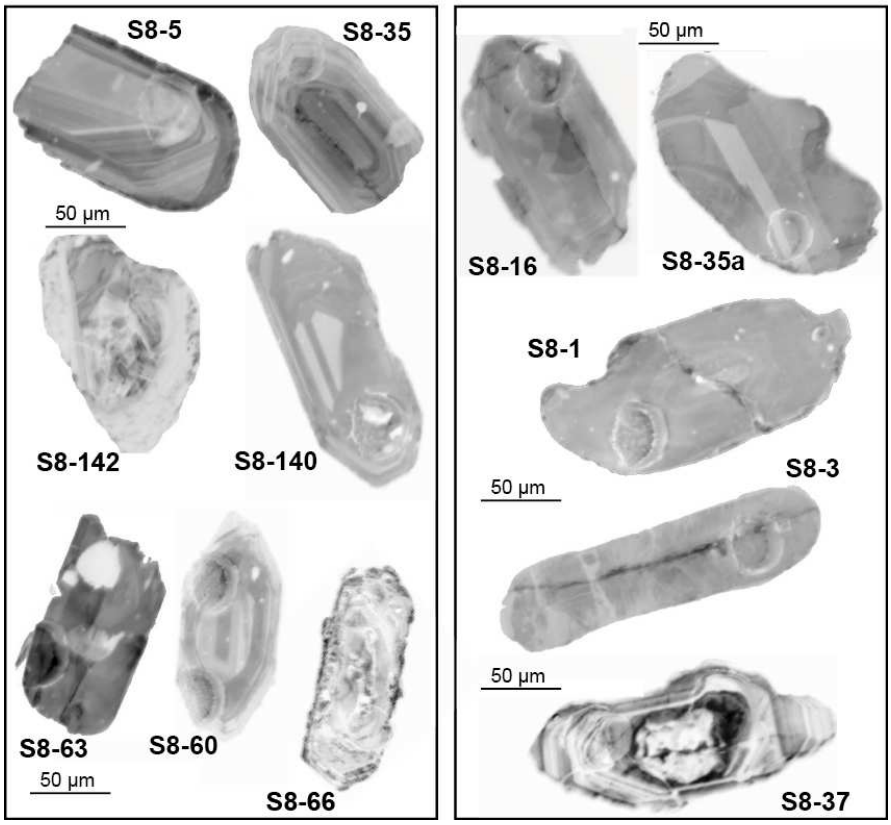

Fig. 16: Plate 3, sample S8. CL-images of detrital zircons from Dora Riparia River draining the Dora Maira Internal massif. Many of the zircons have complex internal structures more complicated by the high rounding degree. The presence of ghost zoning in zircons from the right block suggests a possibly magmatic resorption

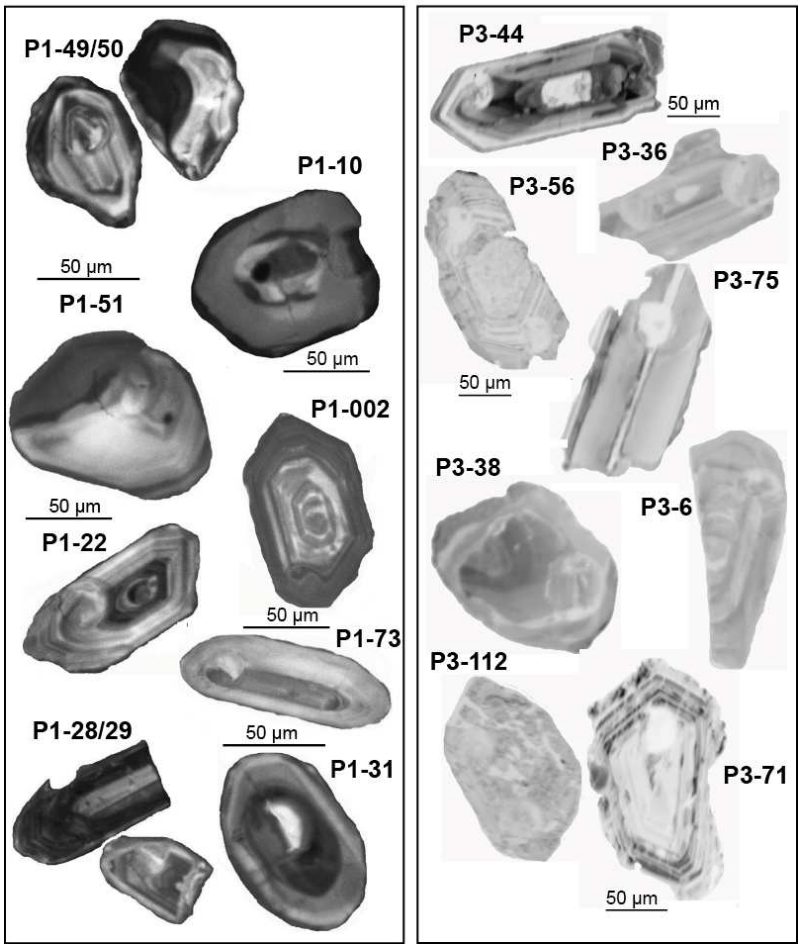

Fig. 17: Plate 4, sample P1 (left) and P3 (right). CL-images of detrital zircons from two collecting sites of the Po river trunk. The left block show morphology and zoning of zircons which are mostly concordant. Note that rounded zircons are mainly discordant. The right block shows zoning and cores in uneven zircon grains suggesting a possibly reworking in the crustal source.

Part III
Analysis of detrital zircons

CHAPTER 6

Samples description

Introduction

Fourteen major tributaries were sampled in order to characterize the zircon contribution of the major source areas, including the Austroalpine and Southalpine basements and Bregaglia and Adamello intrusives (samples S1, S2), the Lepontine Dome (samples S3, S4), the Monte Rosa and Sesia Lanzo units (sample S5), the Mont Blanc Massif (sample S6), the Gran Paradiso and Dora Maira units (samples S7,S8, S9), the Argentera Massif (sample S10) the Tertiary Piedmont Basin and underlying units of Ligurian Alps (samples S12, S13, S14), then the Ligurian Units and the foredeep turbidites of the Northern Apennines (samples S15, S16). Four samples have been collected in different sites of the Po Delta (sample D1, in the northern side of deltaic body, samples D2, D3 in the southern deltaic body, and sample D4 on the outer part of Bocca di Goro channel.

In this chapter samples are grouped for source areas and for each of them we have evidenced their grain-size distribution calculated after separation procedures (see table 1 in appendix) and the state of zircon concentrates in terms of abundance of zircon grains with respect to other heavy minerals. Identifying characteristics of detrital minerals found in our samples were also described (see table 2 in appendix) according to reference works of Devismes, (1978), Parfenoff, et al. (1970) and Mange and Maurer (1992). Morphology of zircon grains and typology of euhedral grains have been recorded (see table 5 in the appendix) and interpreted according to the Pupin diagram (see discussion in Ch.3) for sub-types classification (fig.18).

The same zircon grains were sampled for U-Pb dating and morphological observations in order to match results from both techniques and assessing the robustness of geochronological signature with respect to hydraulic sorting effects. In order to exploit the possible correlations between grain-ages populations and morphologies of zircon grains, U-Pb dating results were plotted against quantitative morphological observations.

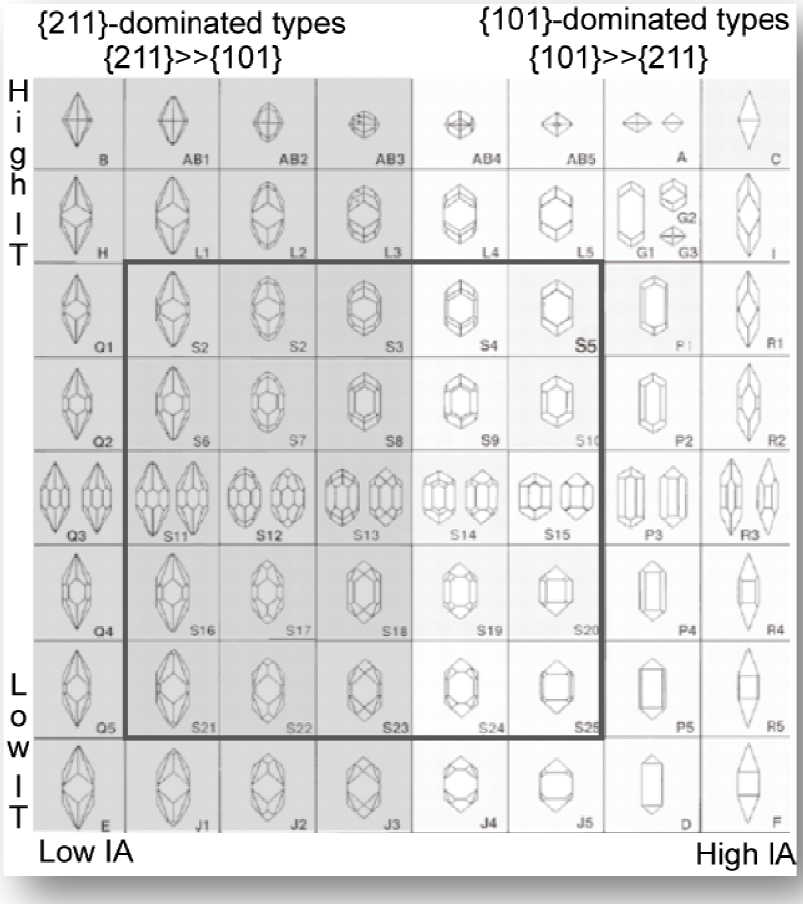

Fig. 18: Morphological classification of zircon crystals according to Pupin (1980). Subclasses are determined according to the ratio of different prisms and pyramids, so that the insect indicates the S-fields while the outer part the P-fields. White colouring indicates the field of {101}-dominated zircons, in grey the field of {211}-dominated zircons

Po River Delta

Length/width ratio (and average volume) vs. U-Pb grain ages plots, show that none of the samples collected in the Po Delta show any correlation (R^2=0.009) between age and crystal size, thus minimizing the effects of size-sorting on single grain age distribution. Resulting graphs of all combined Po Delta samples are reported in figure 19, showing that there is no linear correlation between U-Pb ages and L/W ratio or volume, in any samples, testifying to the lack of hydraulic sorting effect on single grain age distribution.

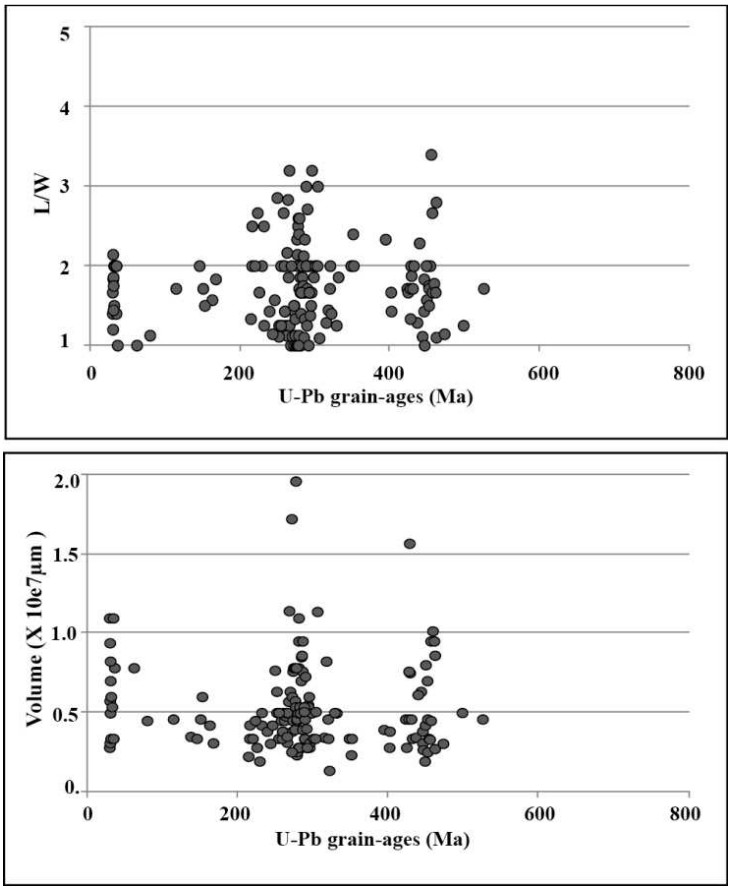

Fig. 19: Diagrams of L/W vs. U-Pb grain-ages and average volume vs. U-Pb grain ages for all the Po Delta samples

SAMPLE D1

General

Sample D1 was collected from beach sand in locality Boccasette.

According to the granulometric distribution for sample D1 calculated during zircon separation procedures (table 1, appendix) grain-size of zircon grains is between very fine-to-fine sand with a few silt grains. State of zircon concentrate at the end of separation procedures show high concentration of zircon grains, so that no further separation was required. Zircon concentrate was observed on a polished slide for morphological analysis prior to geochronological dating.

Zircon concentrate (density >3.3 g/cm^3) contains other diamagnetic minerals where the kyanite was the most abundant with grain-size considerably larger than zircon (table 2 , appendix).

Morphology of zircon populations

In sample D1 the majority of zircons show rounded and sub-rounded morphologies, where the 49 % is represented by sub-rounded grains, in which euhedral shape is often recognizable, and the 38% of rounded shaped groups the acicular prismatic (according to Miller et al., 2006), egg-shaped and spherical grains. Euhedral types represent only the 14%, with a slightly difference between the {101}-dominated (5%) and the {211}-dominated zircons (9%).

Examination of euhedral zircons according to Pupin, 1980 shows different typology:

- There are acicular prismatic needle shaped zircons with as in Plate 5, 1.1, possibly P1/P2 type
- Some S24/S14 or S20/P4 type zircons as in Plate 5,1.5
- Moderate amount of S10/S15 types in Plate 5, 1.3

- Moderate amount of S11/S21 types

Examination of colour series in zircon grains (according to Gastil et al., 1967), groups a dominant colourless series of zircon grains are associated with a less common pale pink series, usually in euhedral and acicular prismatic grains. Rounded zircons are always colourless, but colourless zircons could present different morphologies. A less common series showing milky zircons is often associated with different degree of metamictization:

- Many colourless zircons are widely diffused (Plate 5)
- Some pale pink zircons are observed (Plate 5, 1.4)
- Rose zircons tend to show a certain degree of opacity narrow to the rims, localized in the core of zircon grain, or distributed in the crystal as in Plate 5, 1.2
- Few milky zircons showing different colour shade from white-to-rose, see Plate 5, 1.1, 1.5, 1.6.

Morphological observation by SEM

Zircon grains occur as sharp irregular fragments (from 1 to 15 first three rows, plate 6), sub-rounded to rounded grains (from 16 to 30, middle rows, plate 6), and euhedral crystals (last 2 rows from 31 to 40, plate 6). Uneven or conchoidal breakage patterns are often exhibited which is possibly related or to fracturation during sample handling in laboratory, or else this fracture pattern could be acquired during diagenesis or during transport of grains.

- Plate 6, rows 1, 2, 3 from 1 to 15: zircons grains appear as irregular fragments where faces are sometime preserved (1), showing conchoidal fracturation or abraded surface (2,4,5,10), ricrystallization inside fractures is common (7,8,9)

- Plate 6, rows 4,5,6 from 16 to 30: zircon grains are well rounded usually characterised by smooth surface, where no evidence of abrasion are shown, but some relicts of prismatic faces can be observed
- Plate 6, rows 7,8 from 31 to 40: euhedral zircon type are highlight by the SEM, so that it is possible to note the slightly sub-rounded surfaces characterising the {211}-dominated zircons (from 31 to 35), while the {101}-dominated zircons is well represented by euhedral type corresponding to P1/S5 or P2/S9 types (from 36 to 40) according to Pupin diagram (fig18).

SAMPLE D2

General

Sample D2 was collected from beach sand in locality Barricata.

According to the granulometric distribution for sample D2 calculated during zircon separation procedures grain-size of zircon grains is between very fine-to-fine sand. State of zircon concentrate at the end of separation procedures show few zircon grains much smaller than other heavy minerals and high amount of large crystals of kyanite, so that refining of zircon concentrate by means of further separation was required. We applied a stronger magnetic separation but the concentrate was much improved only after sieving with finer mesh (see ch.2 for details). Photomicrographs 7.2.1a and 7.2.1c want to show the state of zircon concentrate respectively before and after refining. The high quality resolution in both pictures, used as sample map for morphological and dating analysis of sample D2, allows to assess such difference, by counting the same number of minerals, zircon grains are around the 3 % in 7.2.1b vs. the 6 % in 7.2.d after further separations.

Diamagnetic minerals in zircon concentrate (density >3.3 g/cm^3) are given in table 2 (appendix) where kyanite, zoisite and rutile were the most abundant having grain-size considerably larger than zircon.

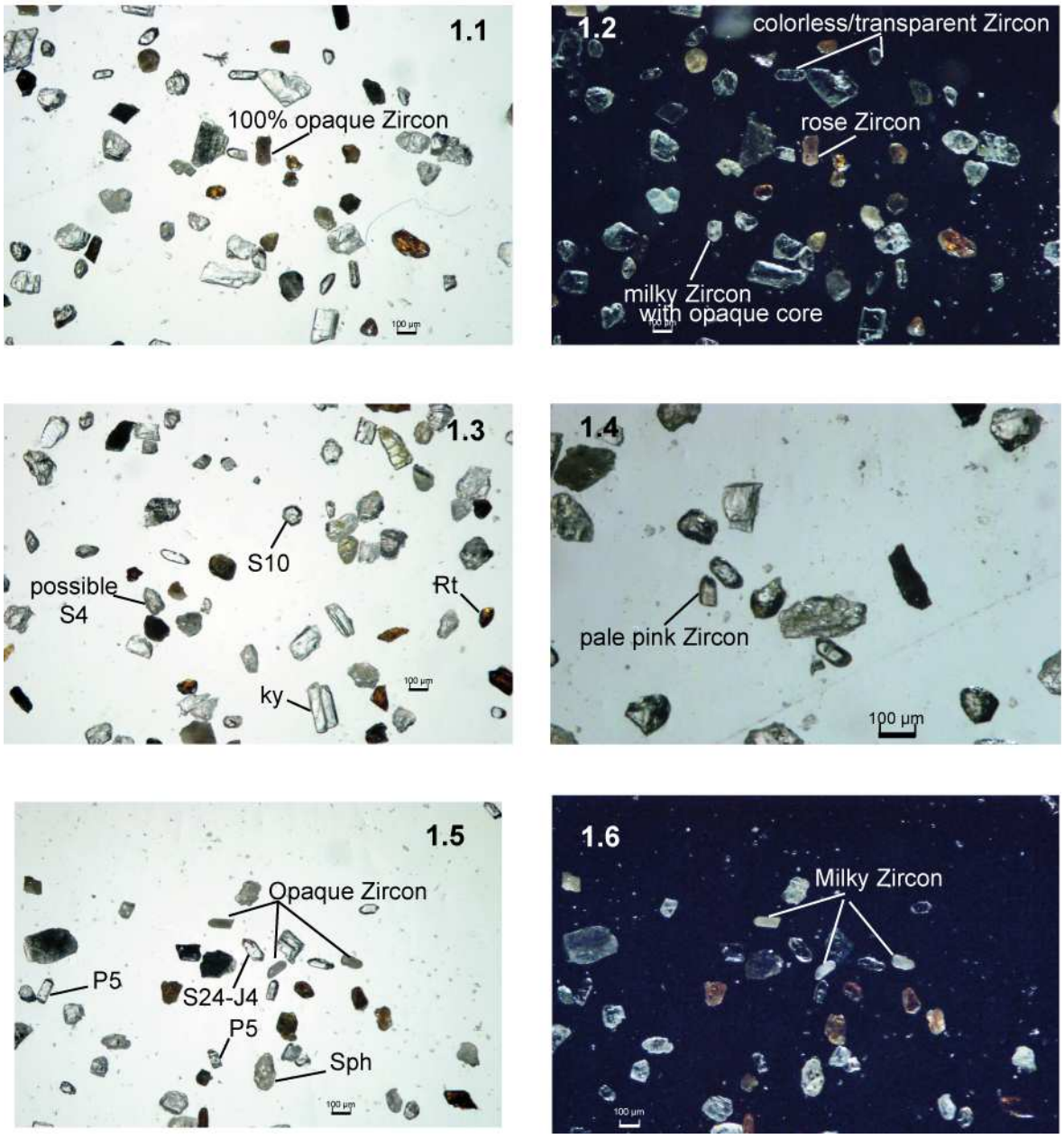

Fig. 20: Plate 5. Photomicrographs of sample D1. 1.1, completely opaque zircon, 1.2

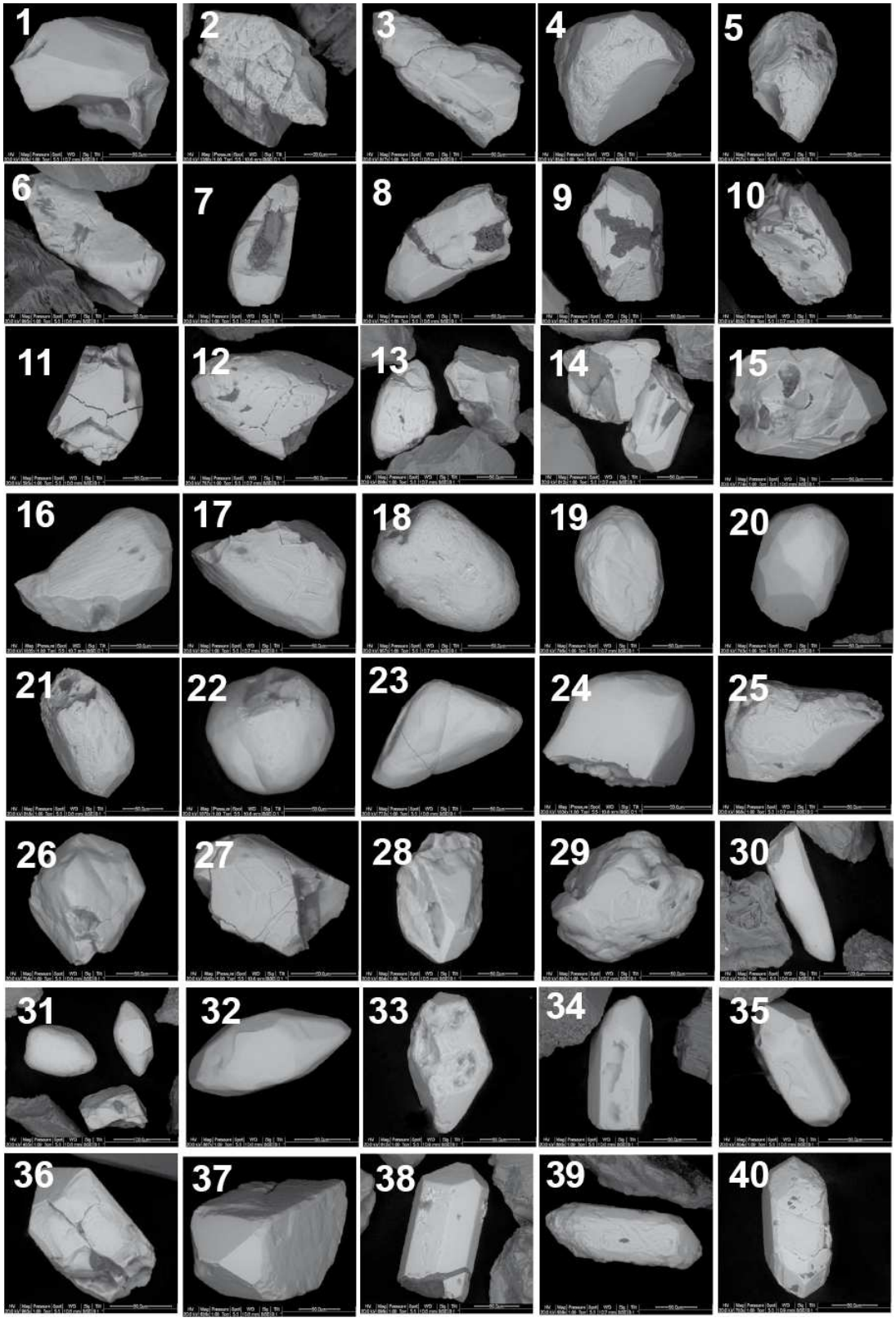

Fig. 21: Plate 6. SEM images of sample D1

Then zircon concentrate was observed on a polished slide for morphological analysis prior to geochronological dating.

Zircon concentrate (density >3.3 g/cm^3) contains other diamagnetic minerals where the kyanite was the most abundant with grain-size considerably larger than zircon (see table 2).

Morphology of zircon populations

In sample D2 the majority of zircons show rounded and sub-rounded morphologies, with 73% of rounded/sub-rounded grains. Euhedral types represent only the 26%, with a marked dominance of {101}-dominated zircons (18%) with respect to the {211}-dominated (8%).

Examination of euhedral zircons according to Pupin, 1980 shows different typology, where the {101}-dominated zircons are largely dominant with acicular prismatic and acicular prismatic grains as shown in plate 7.2.3. Dominant colourless series of zircon grains are associated with a quite common pale pink series, which have been emphasized in reflected light and dark background in plate 7.2.4. A less common series of milky zircons is often observed.

Examination of colour series in zircon grains, show different groups:

- Many colourless zircons are widely diffuse in plate 7
- Some pale pink zircons and few milky zircons are also observed (plate 7.2.4)

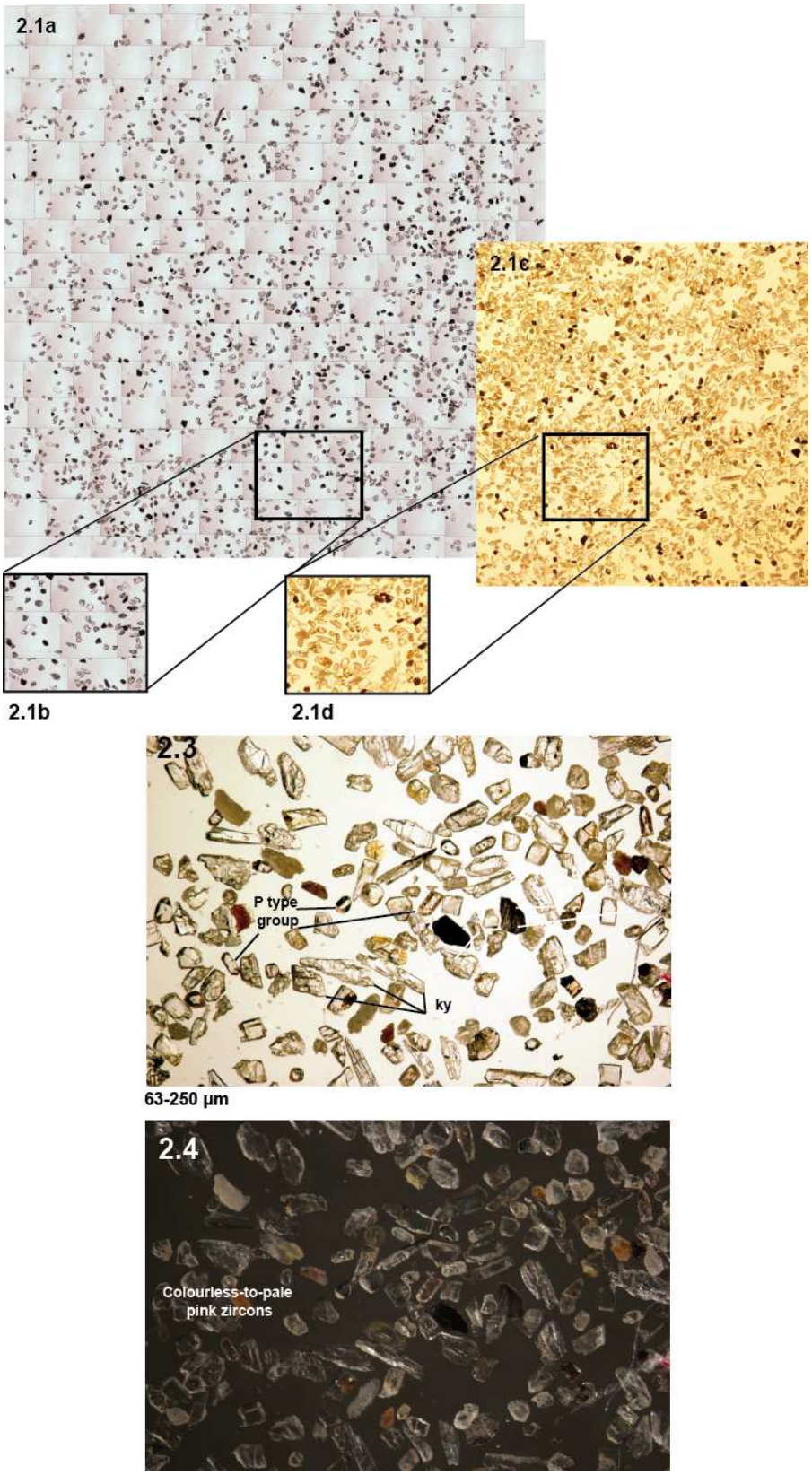

Fig. 22: Plate 7. Photomicrographs of sample D2

Morphological observation by SEM

Rounded zircon grains show pitted and frosted surfaces, *sensu* Mange and Maurer, 1992 (from 1 to 6 first row, plate 8), composite structures (second row from 7 to 10, plate 8) and smoothed faces in some sub-euhedral crystals (from 11 to 15 third row, plate 8). Euhedral types are characteristic and they are still recognizable whether smoothing of pyramidal and prismatic faces:

- Plate 8, row 4, number 16, 17, 18: euhedral zircons {211}-dominated, the same is true for sub-euhedral zircons number 13 and 10 in upper rows.
- Plate 8, rows 5, number 19, 20, 21: zircon grains seen normal to the c-axis, so that the four faces of the summit pyramid is emphasised, as well as the prismatic habit of zircon crystals.
- Plate 8, row 5, number 22, 23, 24, 25 : euhedral zircon {101}-dominated where type P1/S5 or P2/S9 are dominant. In these pictures there are more neighbours zircon grains showing different morphological features because the zircon concentrate is dropped randomly on the slide used for SEM analyses, hence the occurrence of more {101}-dominated zircons with respect to {211}-dominated zircons support the microscopic observations prior discussed.

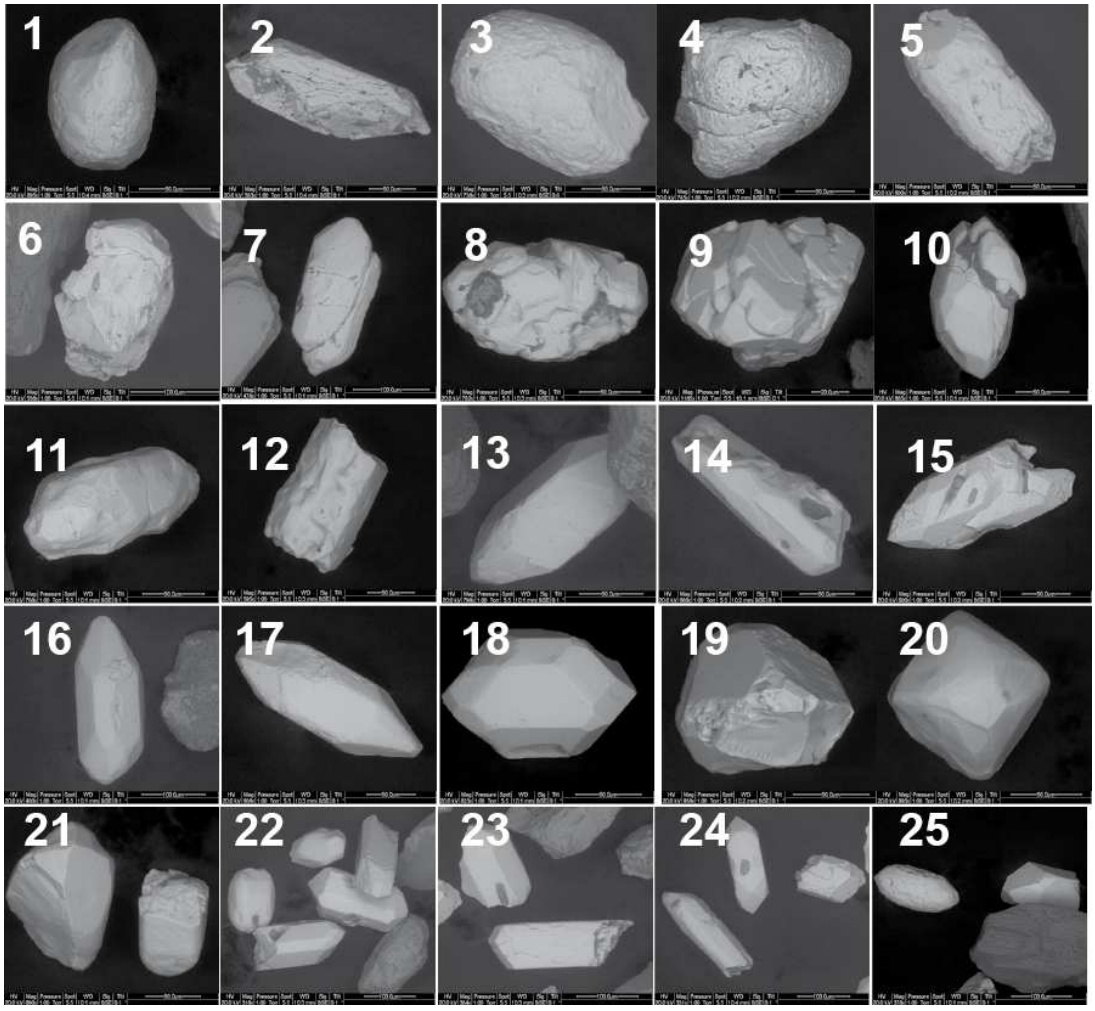

Fig. 23: Plate 8. SEM images of sample D2

SAMPLE D3

General

Sample D3 was collected from beach sand in locality Bonelli.

According to the granulometric distribution for sample D3 calculated during zircon separation procedures grain-size of zircon grains is very fine sand with a few silt grains. State of zircon concentrate at the end of separation procedures show high concentration of zircon grains because large crystals or other heavy minerals are

scarce, so that no further separation was required. Zircon concentrate were observed on a polished slide for morphological analysis prior to geochronological dating. Heavy minerals observed in the zircon concentrate are given in table 2 (appendix)

Morphology of zircon populations

In sample D3 the majority of zircons show rounded and sub-rounded morphologies, where acicular prismatic, egg-shaped and spherical grains are well represented. Plate 9 show a wide range of different features:

- Xenocrystic cores could show different colour as a consequence of the different degree of metamictization, and a sub-euhedral shape possibly the relict of a polycyclic zircon which worked as nucleation point during crystallization of the surrounding zircons as in plate 9, 3.2b
- Ghost cores can occur in rounded zircons as a delimited area marked by small inclusions as in plate 9, 3.2e
- Rounded grains can show a patterns of smooth edges and humpbacked surface (3.2c), or uneven breakage and irregular shape (3.2d)

Euhedral types show a dominance of {101}-dominated respect to {211}-dominated grains. Examination of euhedral zircons according to Pupin, 1980 shows different typology:

- There are many zircons with acicular prismatic habit as in Plate 9, 3.1
- Some P5/D type are observed with long and thin inclusion probably with melt origin, as in Plate 9 3.2a

Colourless series of zircon grains are the most common, but few yellowish grains locally occur (plate 9.3.2c)

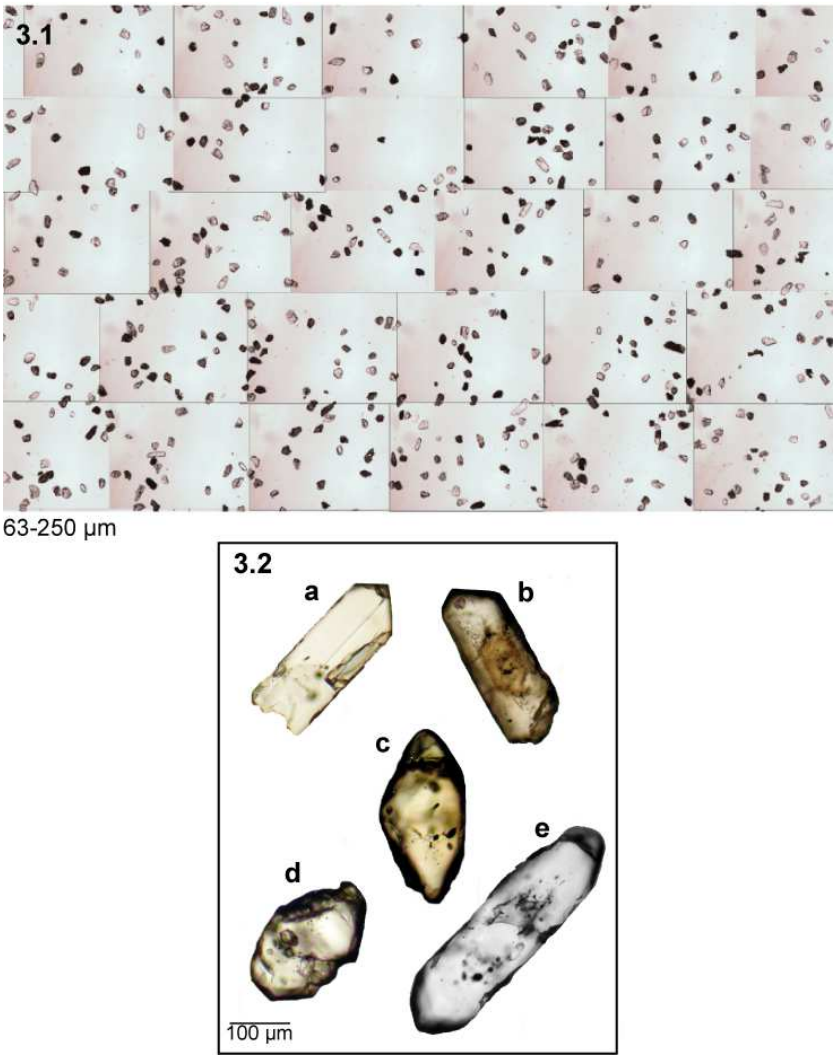

Fig. 24. Plate 9. Photomicrographs of sample D3

SAMPLE D4

General

Sample S4 was collected at the southern side of the Po Delta from a beach sand on Isola dei gabbiani near the Bacucco lighthouse. According to the granulometric distribution for sample D4 calculated during zircon separation procedures grain-size of zircon grains is between very fine-to-fine sand. State of zircon concentrate at the end of separation shows zircon grains not larger than 125 µm. Zircon concentrate

(density >3.3 g/cm^3) contains diamagnetic heavy minerals similar to other Po Delta samples as the most common are kynite, zoisite and rutile (see table 2 in appendix for details).

Morphology of zircon populations

There are almost only fragment of zircon grains in sample D4 (95%) probably related to the high energy depositional environment. Only colourless zircons have been observed.

Central and Southern Alps

Morphological analysis performed on zircon concentrates after mounting on a polished slides were plotted against geochronological data. Resulting graphs (fig.25) show that no linear correlation occurs between grain-age populations and L/W ratio or average volume of grains, thus minimizing the effects of size-sorting on single grain age distribution.

SAMPLE S1

General

Sample S1 was collected at the end of major valley of the Oglio River before the confluence into the Iseo Lake, at Rogno.

According to the granulometric distribution for sample S1 calculated during zircon separation procedures grain-size of zircon grains is between fine-to-medium sand. State of zircon concentrate at the end of separation shows few zircon grains with some other heavy minerals (see table 2). We found this concentrate difficult to refine

because of the small quantity of zircon grains which may reduce further after separations. Some apatite grains were also found, indicating that possible troubles occur during separation.

Zircon concentrate (density >3.3 g/cm^3) contains other diamagnetic minerals where carbonates are clearly distinguished, and few grains of andalusite were also found (table 2 in appendix for details).

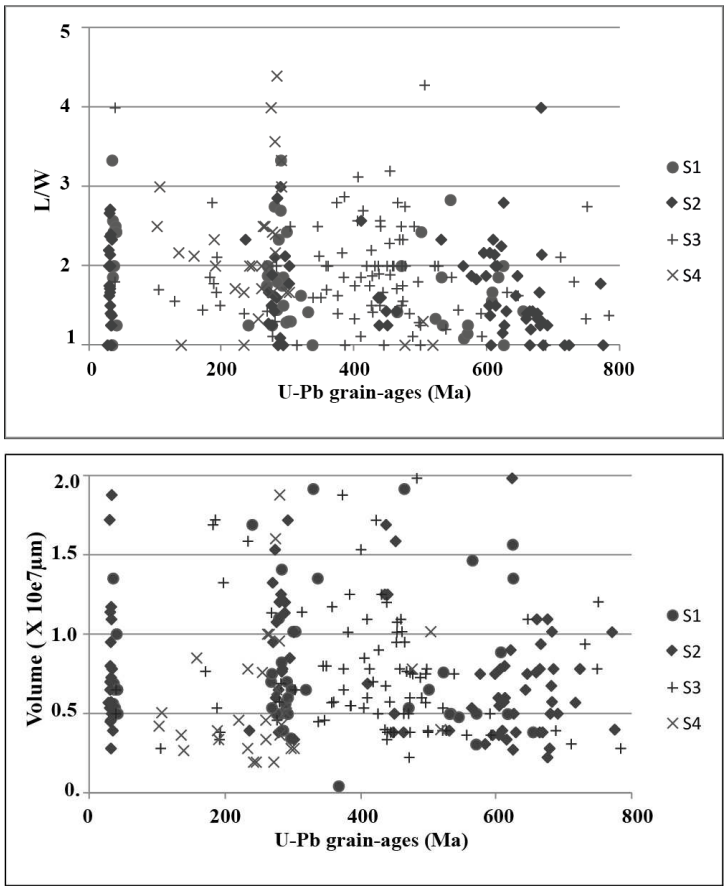

Fig. 25: First diagram shows no linear correlation between L/W vs. U-Pb grain-ages, as also demonstrated by the coefficient of linear correlation R^2, calculated for each sample: R^2S1=0.036; R^2S2=0.023; R^2S3=0.09; R^2S4= 0.097.Second diagram shows that there is no linear correlation between Average Volume vs. U-Pb grain ages, that support a negligible effect of hydraulic sorting on analysed sample; coefficient of linear correlation R^2 shows very low values: R^2S1=0.017; R^2S2=0.022; R^2S3=0.013; R^2S4=0.032

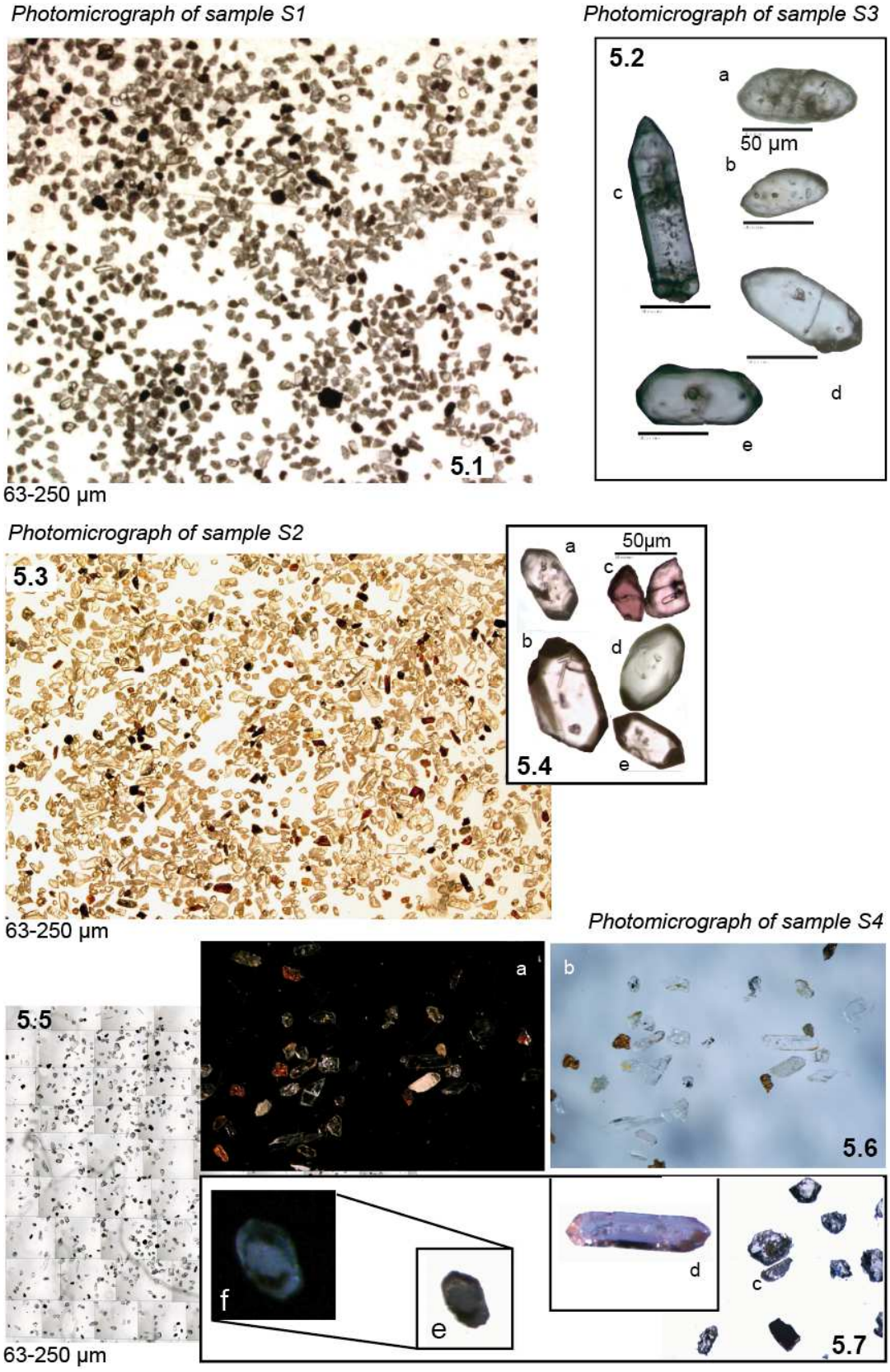

Fig. 26: Plate 10. Photomicrographs of detritus shed from the Southern Alps (samples S1 and S2) and the Central Alps (samples S3 and S4).

Morphology of zircon populations

In sample S1 the majority of zircons show rounded (75%), with many egg-shaped and acicular prismatic grains. Few euhedral grains are the 26% of the total, where the 16% are {211}-dominated zircons and the 10% are the {101}-dominated zircons. The former is represented mainly by S16/S17 and S21 types, while the latter usually correspond to the S19/P4 types. Only colourless zircons have been observed.

SAMPLE S2

General

Sample S2 was collected from the Adda River before the confluence into the Como Lake, near Dubino.

According to the granulometric distribution for sample S2 calculated during zircon separation procedures grain-size of zircon grains is between fine-to-medium sand, with enough grains larger than 125 µm, which is quite rare in our samples. Therefore state of zircon concentrate at the end of separation show a good concentration of zircon grains

Zircon concentrate (density >3.3 g/cm^3) contains other diamagnetic minerals where zircon grains can be represented by very large (table 2, appendix).

Morphology of Zircon populations

Sample S2 is dominated by zircon grains irregular or rounded with a tendency to sphericity (Plate 10, 5.4d), representing the 86% of the total amount of zircon. Euhedral types are the 18%, where the {101}-dominated grains represents the 11% and the {211}-dominated, instead, the 7%. Majority of euhedral grains are younger

than 35 Ma and they are identified as {211}-dominated. In Sample S2 the following features have been observed:

- {211}-dominated zircons are represented mainly by egg-shaped crystals like S12 types but also S21/S16 and S13 types have been observed.
- {101}-dominated zircons show prismatic habit, usually referable to P4 and D/P5 types, as shown in Plate 10, 5.3a and 5.3b,e, respectively

Colourless zircons are the most common, however there are also few grains showing pink-to-rose shades as shown in Plate 10, 5.3, usually belonging to the younger grain-age population (20-40 Ma).

SAMPLE S3

General

Sample S3 was collected at Bellinzona along the Ticino River, draining the eastern part of the Lepontine Dome, before the Maggiore Lake.

According to the granulometric distribution for sample S3 calculated during zircon separation procedures grain-size of zircon grains is between fine-to-medium sand.

State of zircon concentrate at the end of separation procedures show few zircon grains much smaller than other heavy minerals, and high amount of large crystals of kyanite, so that refining of zircon concentrate was required (see ch.2 for details). Then zircon concentrate was observed on a polished slide for morphological analysis prior to geochronological dating.

Morphology of zircon populations

In sample S3 rounded and sub-rounded zircons are widely diffuse representing the 84 % of the total zircon amount. Few euhedral grains are characterised by {211}-dominated zircons with the 10%, and few {101}-dominated zircons (7%).

Examination of euhedral and sub-rounded forms show the following features:

- Rounded large zircon grains have apparent abraded and frosted surfaces Etch-pits, facets and grooves (sensu Mange and Maurer, 1992) on the surface as shown in plate 10, 5.2a,b.
- Few {211}-dominated zircons can present acicular prismatic shape referable to S6/S11 type, as in plate 10, 5.2c
- {211}-dominated zircons are mainly represented by lower L/W ratios associated to S11/S21 and S12/S2 (plate 10, 5.2d,e), possibly with almost rounded outline that could make difficult the typological interpretation.

Abundant fluid inclusions and the occurrence of pitted surfaces (plate 10, 5.2 a,b,c), are usually found in old zircon populations (>360 Ma). Only colourless series of zircon grains have been observed associated with a less common milky series.

Morphological observation by SEM

Analysis by SEM on sample S3 revealed rounded zircon grains with abraded and frosted surfaces (from 1 to 15, plate 11) or high rounding degree (from 16 to 20, plate 11), as well as sub-rounded (from 16 to 25, plate 11) and sub-euhedral grains (from 26 to 30, plate 11), which have been described in detail below:

- Plate 11, Rows 1,2 numbers 1 to 7: well-rounded zircons with abraded surface
- Plate 11, Rows 2 numbers 8,9,10: frosted surface and breakage pattern normal to C axis are often exhibited

- Plate 11, Rows 3, numbers 11 to 15 : some rounded detrital zircons exhibit abraded and pitted surfaces (*sensu* Mange and Maurer, 1992) possibly due to metamorphic dehydration reactions typically generated during amphibolite to granulite facies as suggested by analogue textures observed in different context (e.g Sinha et al., 1992; Williams, 2001). Observation under the microscope reveals that these zircons are mostly milky or opaque (plate 10, 5.2a,b)
- Plate 11, Rows 4 numbers 16 to 25: the high rounding degree is regarded as a criterion of magmatic resorption or of metamorphic origin (e.g. Corfu et al., 2003).
- Plate 11, Rows 5 and 6 numbers 21 to 30: many sub-rounded grains where the shape of euhedral types has been identified as {211}-dominated, in particular S16 and S13 types are revealed. {101}-dominated zircons are represented mainly by P3 morphology.

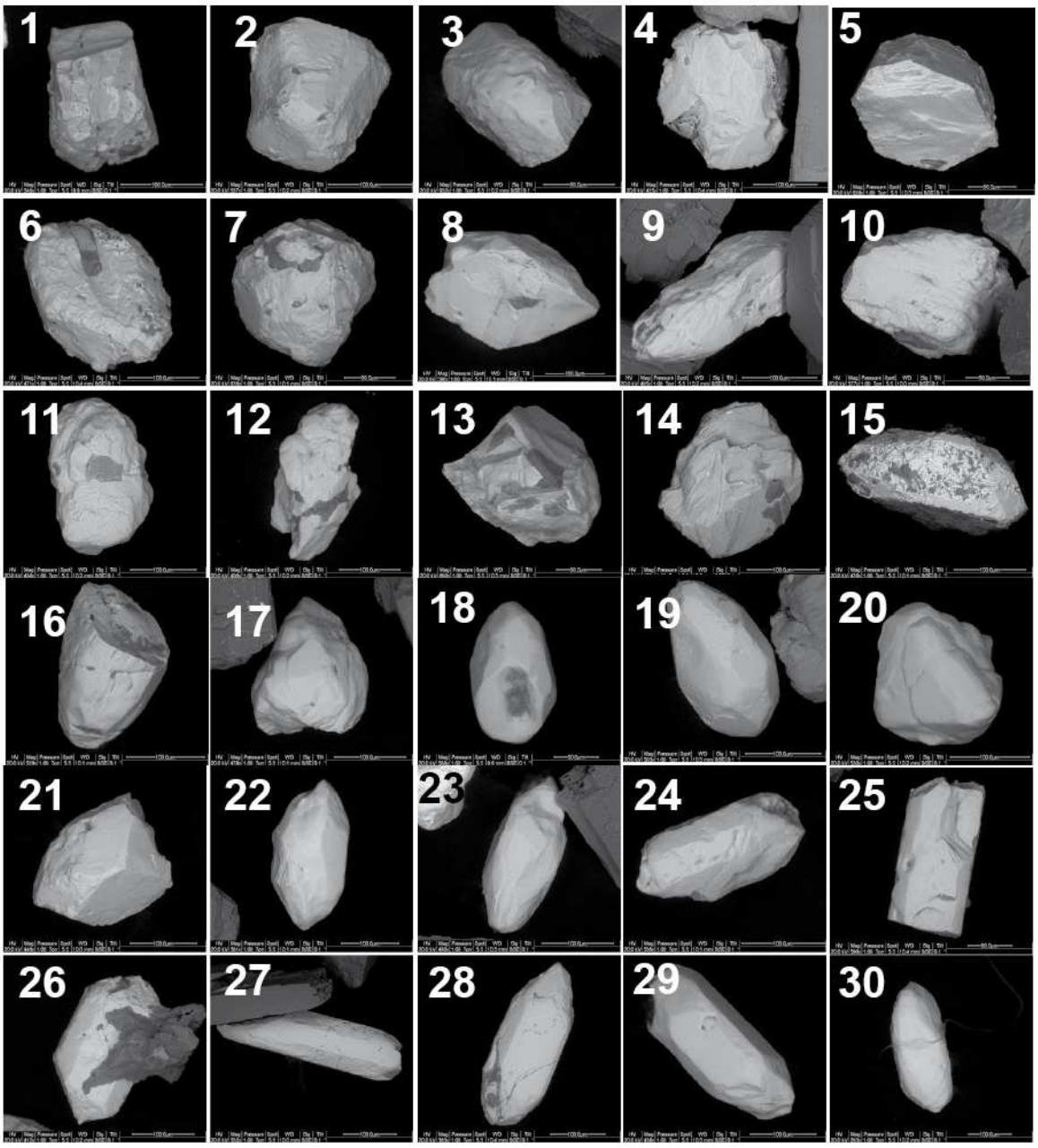

Fig. 27: Plate 11. SEM images of sample S3

SAMPLE S4

General

Sample S4 was collected along the Toce River, draining the western side of the Lepontine Dome, before its confluence into the Maggiore Lake.

According to the granulometric distribution for sample S3 calculated during zircon separation procedures, grain-size of zircon grains is between fine-to-medium sand.

State of zircon concentrate at the end of separation procedures show the same features of previous sample S3, probably because both samples comes from different sides of the same source areas, so that refining of zircon concentrate by means of further separation was required.

Zircon concentrate (density >3.3 g/cm^3) contains other diamagnetic minerals which are given in table 2, in appendix.

Morphology of Zircon populations

In sample S4 the majority of zircon grains are rounded and sub-rounded (85%), with a dominance of acicular prismatic form. Euhedral types are really scarce only the 3% are {101}-dominated while the 6% is {211}-dominated as S12 and S17 types.

Colourless zircons are the most common, however there are also few grains which show a marked pink-to-rose shade, and in particular:

- Few euhedral {211}-dominated zircons are transparent with a typical pink colour, otherwise the same nuance can be found in opaque/milky zircons that register ages ranging between 100 and 240 Ma.
- Almost opaque core occur mainly in sub-rounded grains

Western Alps

None of samples collected from Po River's tributaries draining the Western Alps show any linear correlation between grain-age populations and L/W ratio or average volume of grains (fig.28). Resulting graphs of samples are reported below showing that there is no linear correlation between U-Pb ages and L/W ratio or volume, in any samples, supporting the idea that detected grain-age populations are not concentrated by the hydraulic sorting effect and the proportions with which they occur in a sediment sample mirror the importance with which they occur in the source area.

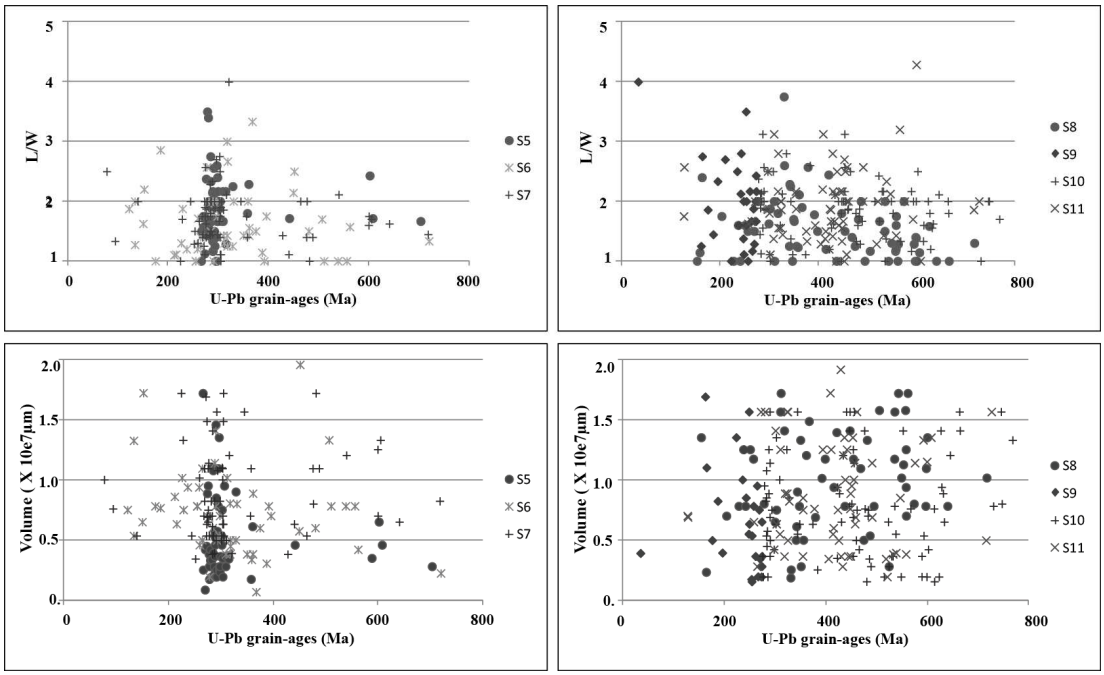

Fig. 28: Diagrams of L/W vs. U-Pb grain-ages of samples from the northern Western Alps (left) and southern Western Alps (right) show no linear correlation between L/W vs. U-Pb grain-ages, as also demonstrated by the coefficient of linear correlation R^2, calculated for each sample: R^2S5=0.003; R^2S6=0.006; R^2S7=0.012; R^2S8= 0.083; R^2S9=0.02; R^2S10=0.02; R^2S11=0.003. the same is true for diagrams of average volume vs. U-Pb grain ages which show no linear correlation between Average volume vs. U-Pb grain ages, that support a negligible effect of hydraulic sorting on analysed samples; coefficient of linear correlation R^2 shows very low values: R^2S5=0.006; R^2S6=0.004; R^2S7=0; R^2S8= 0.03; R^2S9=0.03; R^2S10=0.0; R^2S11= 0.003

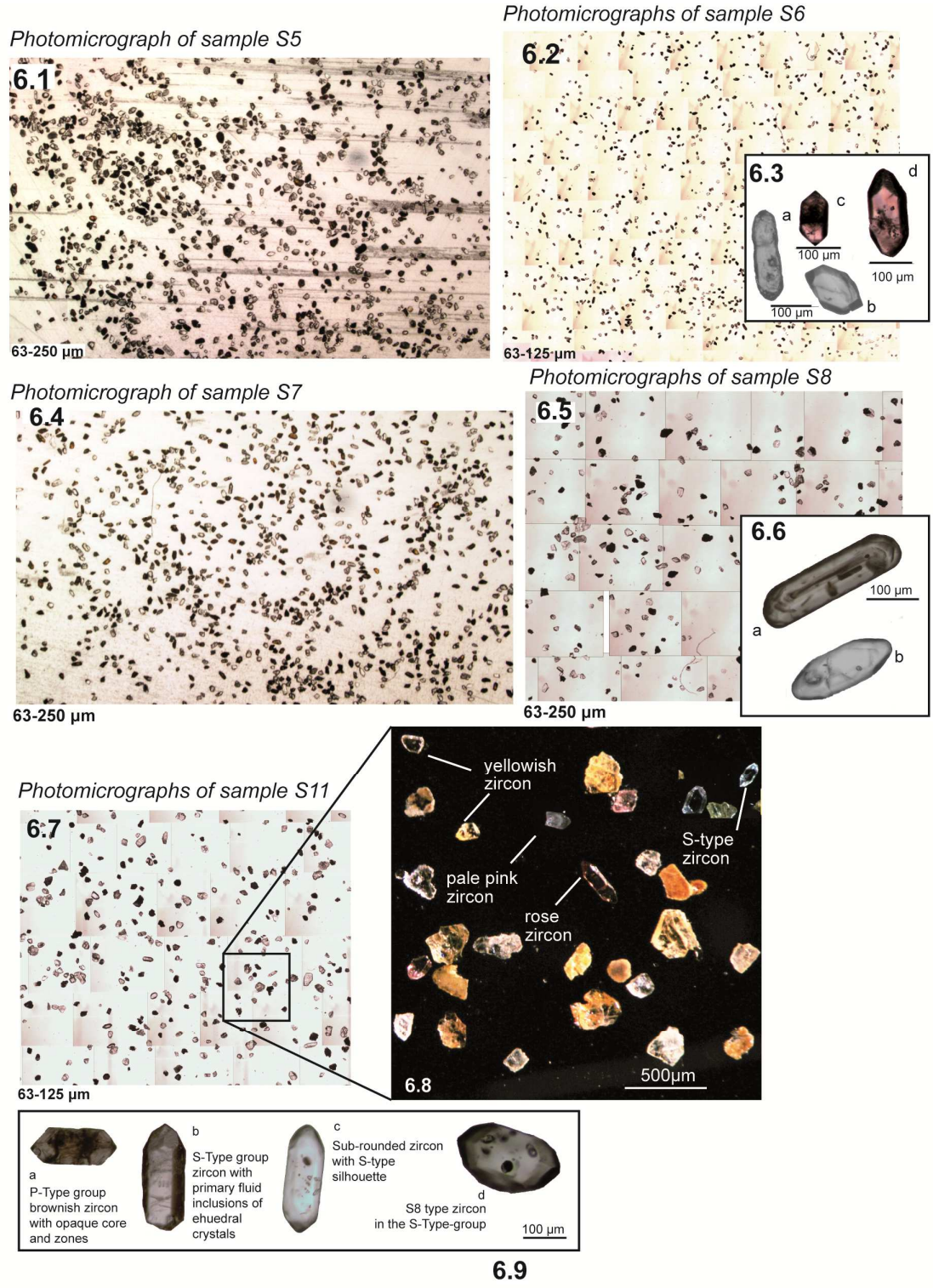

Fig. 29: Plate 12. Photomicrographs of samples from the Western Alps

SAMPLE S5

General

Sample S5 was collected at the end of major valley of the Sesia river at Romagnano. According to the granulometric distribution for sample S1 calculated during zircon separation procedures, grain-size of zircon grains is between fine-to-medium sand. State of zircon concentrate at the end of separation show an excellent concentration of large zircon grains between 63-200 µm. Zircon concentrate (density >3.3 g/cm^3) contains other diamagnetic minerals where kyanite, rutile and sphene are the most abundant (see table 2 in the appendix for details).

Morphology of zircon populations

In sample S5 the majority of zircons are rounded (75%), with many acicular prismatic grains. Euhedral grains are the 25% of the total, with a clear dominance of the {101}-dominated (23%) and few {211}-dominated zircons (2%). {101}-dominated zircons are represented mainly by many P5/P2 types as well as S25/S15 and S24/S14. Only colourless zircons have been observed.

SAMPLE S6

General

Sample S6 was collected at Quassolo at the end of major valley of the Dora Baltea River, draining the External Massif of the Mont Blanc.

According to the granulometric distribution for sample S6 calculated during zircon separation procedures (see table 1), grain-size of zircon grains is between fine-to-medium sand.

State of zircon concentrate at the end of separation procedures show few zircon grains much smaller than other heavy minerals and high amount of large crystals of rutile, so that refining of zircon concentrate by means of further sieving was required. We pass the sample through a finer sieve to concentrate zircon grains between 63-125 µm and remove larger grains. Stronger magnetic separation was applied to remove minerals with eventually ferromagnetic inclusions.

Then zircon concentrate was observed on a polished slide for morphological analysis prior to geochronological dating.

Zircon concentrate (density >3.3 g/cm^3) contains other diamagnetic minerals where the kyanite and zoisite were the most abundant with grain-size considerably larger than zircon (see table 2 in appendix).

Morphology of zircon populations

In sample S6 rounded and sub-rounded zircons are widely diffuse representing the 75 % of the total zircon amount, well represented by the egg-shaped and acicular prismatic form (plate 12, 6.3a). Euhedral zircon {101}-dominated are the 21% mainly represented by P1/P4 types (plate 12, 6.3c), S5/S15 and few S25 (plate 12, 6.3b). The {211}-dominated zircons instead are only the 4% with some S22 types (plate 12, 6.3d) or usually recognizable by the typical shape of sub-rounded grains.

A most common colourless series (56%), of zircon grains is associated with a some pink-to-rose series (plate 12, 6.3 c,d) which represents the 30% of total. Majority of red series zircons cluster around 65-200 Ma in age.

Morphological observation by SEM

Analysis by SEM on sample S6 revealed rounded zircon grains with high rounding degree (from 1 to 20, plate 13) where less common abraded and frosted surfaces can be recognized (*sensu* Mange and Maurer, 1992). Sub-rounded grains are

usually associated to {211}-dominated shape (from 21 to 28, plate 13). Detailed description is provided below:

- Plate 13, Rows 1,2 numbers 1 to 10: the high rounding degree is regarded as a criterion of magmatic corrosion (e.g. Mange and Maurer, 1982).
- Plate 13, Rows 3,4 number 11 to 18: well-rounded zircons with slightly abraded surfaces and composite reabsorbed zircons (17,18).
- Plate 13, Rows 5 and 6 numbers 21 to 28: between sub-rounded grains with {211}-dominated shape, some quite recognizable morphologies can be identify as in the view of prismatic face 100<<110 so that n.21 could be labelled as S4, while others grain typologies are not usually evident (number 24 to 28). Probably S11 (n.22) or S7 (n.23)
- Plate 13, Rows 7, 8 numbers 29 to 40: the {101}-dominated zircons are the most common morphology as shown in numbers 29 to 34, or S25 with small {211}-pyramidal faces (35,38), usually easier to be recognized thanks to their tendency to lean on the slide offering a perfect view orthogonal to the C axis (39).

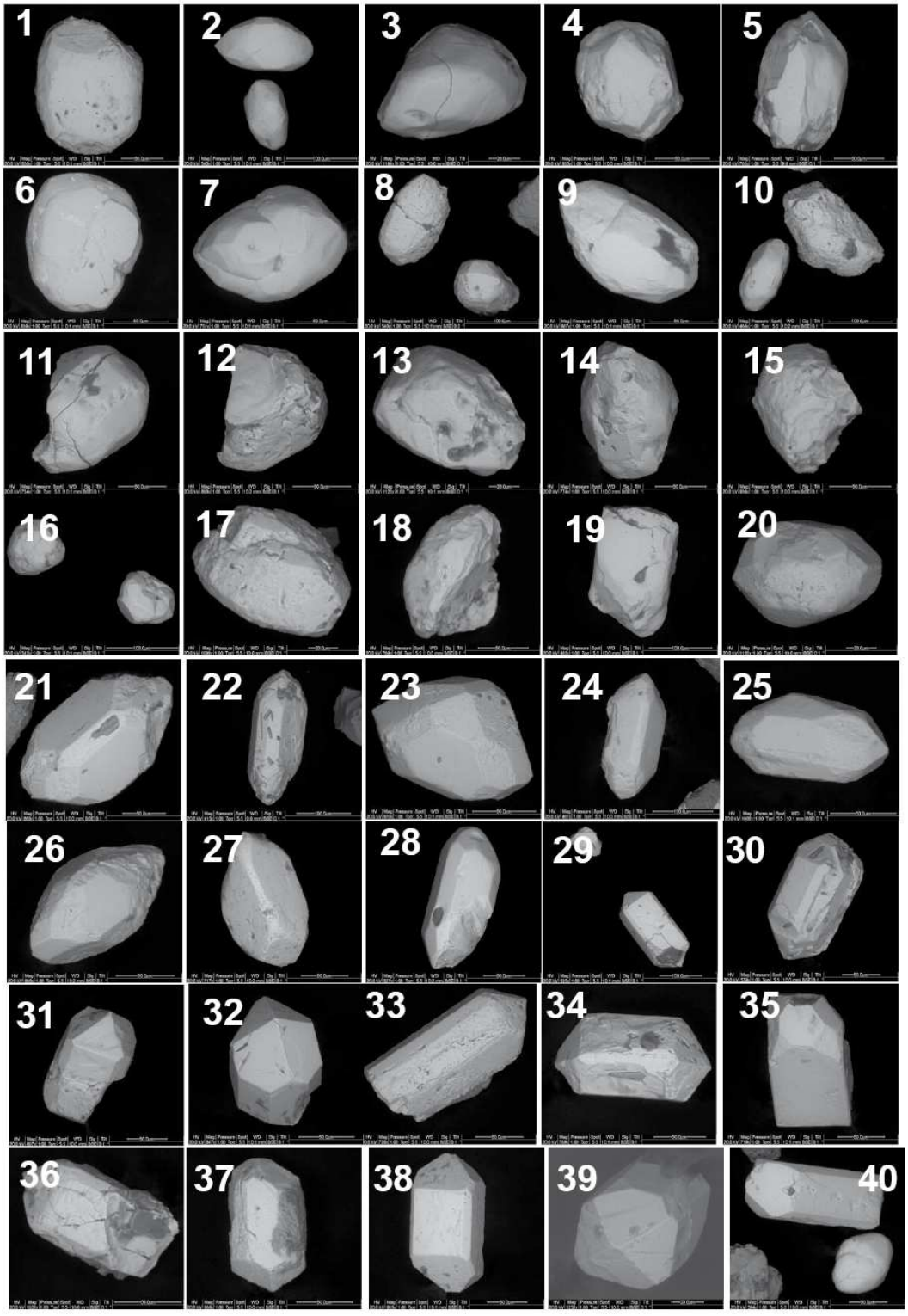

Fig. 30: Plate 13. SEM images of sample S6

SAMPLE S7

General

Sample S7 was collected from the Orco River at Visignano.

According to the granulometric distribution for sample S7 calculated during zircon separation procedures (table 1, appendix) grain-size of zircon grains is between medium-to-coarse sand. State of zircon concentrate at the end of separation shows a quite good concentration of zircon grains representing the smaller grains in the whole concentrate. We tried to improve the state of concentrate being careful to lose no zircon grains during finer sieving, at the end of which a slightly better zircon concentrate was observed.

Morphology of zircon populations

In sample S7 the majority of zircons are rounded (75%), with many egg-shaped grains. Euhedral grains are the 26% of the total, where {101}-dominated zircons are the 12% and {211}-dominated zircons are the 14% are quite equivalent. {101}-dominated zircons are mostly represented by P5/P4 and P1 types as well as S19/S20 and few S4, while the {211}-dominated zircons are characterised however by a quite equivalent size between {101} and {211} pyramidal forms, where the most common typological combinations are represented by the couples S17-S18, S22-S23 and S13-S14 with also few S11 types.

SAMPLE S8

General

Sample S8 was collected along the Dora Riparia River at Avigliana. According to the granulometric distribution for sample S8, grain-size of zircon grains is medium sand. State of zircon concentrate at the end of separation shows low concentration of zircon grains, was hardly improved with a stronger magnetic separation. Zircon concentrate (density >3.3 g/cm^3) contains other diamagnetic minerals where grains of monazite were found commonly, making difficult to discriminate zircon grains when they show altered surface.

Morphology of zircon populations

In sample S8 the majority of zircons are rounded (85%), with many acicular prismatic grains, usually showing characteristic patterns of fluid inclusions as melt filled channels or stick shaped apatite crystals (Plate 12, 6.6a). Euhedral grains are the 15% of the total, where the 10% are the {101}-dominated associated with few number of {211}-dominated (5%) usually identified in sub-rounded grains shape (Plate 12, 6.6b). Colourless zircons are associated with yellow-brownish series.

SAMPLE S9

General

Sample S9 was collected along the Po River at Revello entering the Po Plain.

According to the granulometric distribution for sample S9, grain-size of zircon grains is between fine-to-medium sand. State of zircon concentrate at the end of separation show quite enough zircon grains not larger than 125 µm.

SAMPLE S10

General

Sample S10 was collected from the Varaita River.

According to the granulometric distribution for sample S10, grain-size of zircon grains is between medium-to-coarse sand. State of zircon concentrate at the end of separation show quite enough zircon grains not larger than 125 µm. Zircon concentrate (density >3.3 g/cm^3) contains a other diamagnetic heavy minerals which are given in table 2, where we commonly found diopside and kyanite.

Morphology of zircon populations

There are almost only rounded zircon grains in sample S9 (95%) while in sample S10 they represent the 85%, with scarce euhedral grains almost ranging between the 9 % for the {101}-dominated grains and a 6% for {211}-dominated zircons. Only colourless zircons have been observed.

SAMPLE S11

General

Sample S11 was collected along the Stura Demonte River draining the Argentera massif. According to the granulometric distribution for sample S11, grain-size of zircon grains is between medium-to-coarse sand. State of zircon concentrate at the end of separation show high concentration of large zircon grains between 63-200 µm, in spite of few apatite grains found in the concentrate, associated with other heavy minerals given in table 2 (appendix).

Morphology of zircon populations

In sample S11 rounded and sub-rounded zircons are widely diffuse representing the 79 % of the total zircon amount, represented more by the egg-shaped than acicular prismatic form. Euhedral grains are mainly represented by the {101}-dominated zircons (19 %), while the {211}-dominated zircons are the 9%. The former mostly includes P5/S25 types (plate 12, 6.9a), and some S19/S14 types, while the latter is recognized in sub-rounded grains by their shape (plate 12, 6.9c) with some S22/S12, S11/S2 types and S8 have been observed (plate 12, 6.9b,d).

Red series zircons are the most common (52%), with a wide range of colour from pale pink to hyacinth (plate 12, 6.8 c,d). Colourless zircons are the 40% ranging almost between 360-520 Ma. Majority of red series cluster around 200-300 Ma in age.

Northern Apennines

Length/width ratio and volume of zircon grains were plotted against U-Pb data. Resulting plots (fig.31) show that there is no linear correlation between zircon grain-age and grain size, thus minimizing the effect of hydraulic on the geochronological signature.

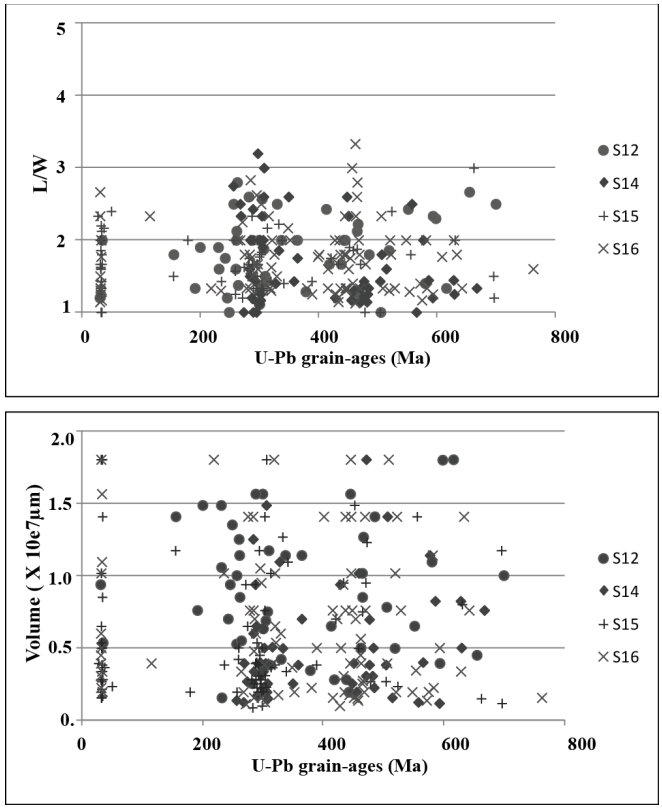

Fig. 31: First diagram shows no linear correlation between L/W vs. U-Pb grain-ages, as also demonstrated by the coefficient of linear correlation R^2, calculated for each sample: R^2S12=0.005; R^2S14=0.07; R^2S15=0.014; R^2S16= 0.02. Second diagram shows no linear correlation between average volume vs. U-Pb grain ages, as supported by the lower values of the coefficient of linear correlation R^2: R^2S12=0.011; R^2S14=0.022; R^2S15=0.024; R^2S16=0.015

SAMPLE S12

General

Sample S12 was collected along the Scrivia River draining the Ligurian Units and part of the TPB sedimentary sequences. According to the granulometric distribution for sample S12 calculated during zircon separation procedures, grain-size of zircon grains is between medium-to-coarse sand. State of zircon concentrate at the end of separation shows low concentration of zircon grains. Zircon concentrate (density >3.3 g/cm^3) contains other diamagnetic such as sphene and monazite (see table 2 in appendix).

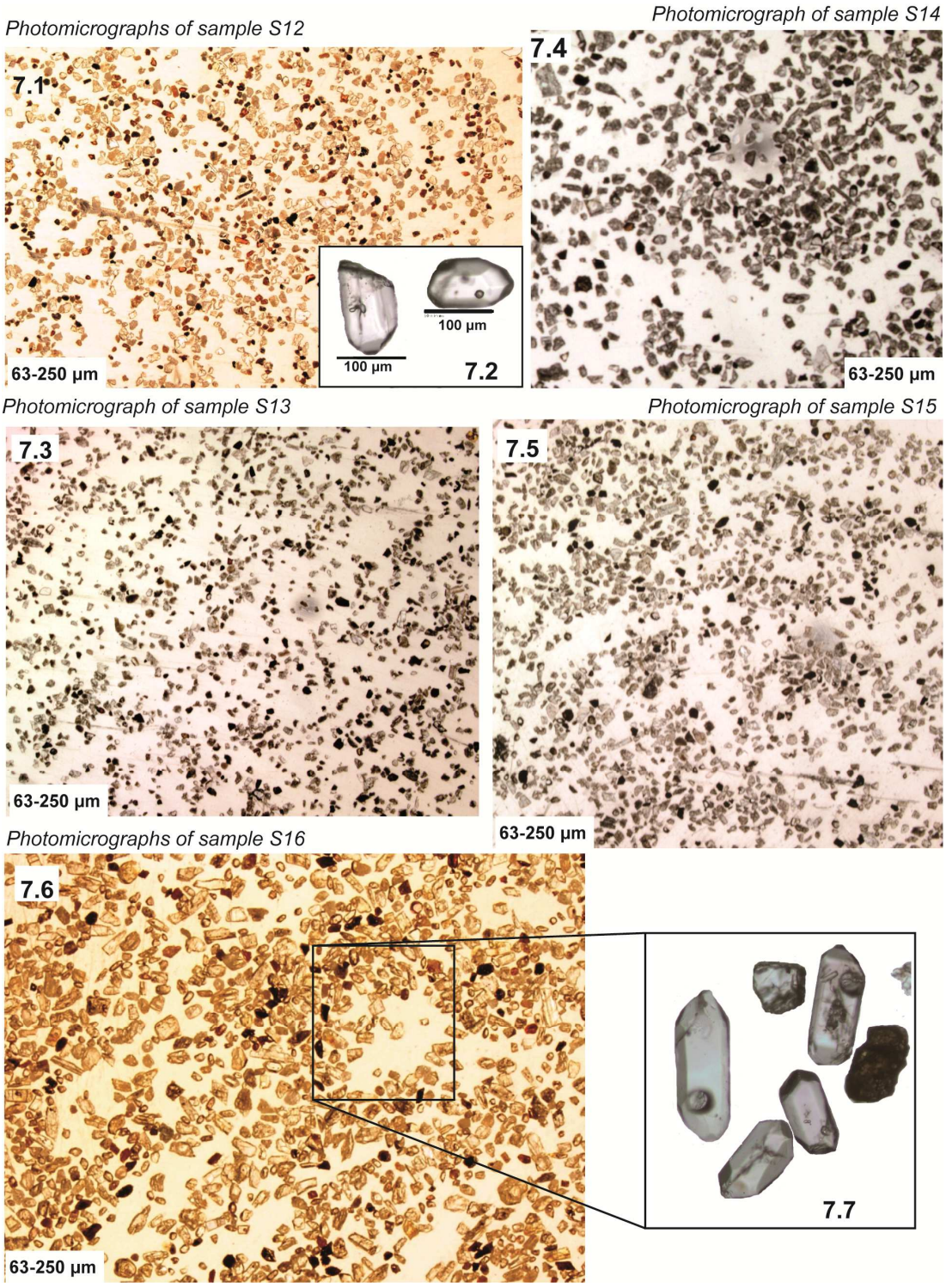

Fig. 32: Plate 14. Photomicrographs of samples from the Northern Apennines

Morphology of zircon populations

In sample S12 the majority of zircons are rounded (66%), with many egg-shaped grains. Euhedral grains are the 35% of the total, where the 21 % are the {211}-dominated zircons, hence the 14% are {101}-dominated zircons. The last are mostly represented by S19/S20, while the {211}-dominated zircons are characterised by morphologies related to the S13/S23 types. Colorless zircons are found frequently.

SAMPLE S13

General

Sample S13, collected along the Trebbia River, has grain-size between medium-to-coarse sand and state of zircon concentrate at the end of separation show the lower concentration of zircon grains than all other sample. Some problem during separation is possibly indicated by the occurrence of many crystals of Na-Metatungstate.

SAMPLE S14

General

Sample S14 was collected along the Taro river one of the most important drainage area of the northern Apennines for its large extension.

According to the granulometric distribution for sample S14 calculated during zircon separation procedures (see table 1) grain-size of zircon grains is between medium-to-coarse sand. State of zircon concentrate at the end of separation shows a modest concentration of zircon grains so that no further separations have been required.

Zircon concentrate (density >3.3 g/cm^3) contains other diamagnetic minerals where the occurrence of quite common grains of monazite makes sometimes difficult the identification of zircon grains when the latter present altered surface quite commonly in detrital samples (see table 2).

Morphology of zircon populations

In sample S14 zircon grains are almost all rounded (90%), where egg-shaped are abundant but also few acicular prismatic grains have been found. High rounding degree is regarded here as a criterion of polycyclic history.

SAMPLE S15

General

Sample S15 was collected along the Enza River.

According to the granulometric distribution for sample S15, grain-size of zircon grains is between fine-to very fine sand. State of zircon concentrate at the end of separation shows high concentration of zircon grains so that no further separation has been carried out. Zircon concentrate (density >3.3 g/cm^3) contains larger zircon grains as well as other diamagnetic minerals such as zoisite and rutile.

Morphology of zircon populations

In sample S15 the majority of zircons are rounded (67%), with many egg-shaped grains. Euhedral grains are the 33% of the total, where zircon typologies are quite equivalent with the 17% of {101}-dominated and the 16% of {211}-dominated zircons. {101}-dominated zircons are mostly represented by P5/P4 and P1 types as well as S19/S20 and few S4. {211}-dominated zircons, instead, are characterised by

a quite equivalent size between {101} and {211} pyramidal forms, where the most common typological combinations are represented by the couples S17-S18, S22-S23 and S13-S14 with also few S11 types.

SAMPLE S16

General

Sample S16 was collected along the Secchia River at Sassuolo.

According to the granulometric distribution for sample S16, grain-size of zircon grains is between very fine-to-fine sand. State of zircon concentrate at the end of separation show a very good concentration of zircon grains with size larger than 125 µm. Zircon concentrate (density >3.3 g/cm^3) contains other diamagnetic minerals such as zoisite, monazite and rutile already seen in other Apenninic samples (see table 2 in appendix for details).

Morphology of zircon populations

In sample S16, lots of zircon grains are rounded sub-rounded or fractured (82%). Between the euhedral grains (18%), where 10 % is represented by {101}-dominated and the 8 % by {211}-dominated zircons, as in plate 14, 7.7.

Po River trunk

Length/width ratio and average volume of zircon grains were plotted against dating results. Resulting plots show (fig.33) that any linear correlation occurs in none of the samples from the Po Plain making the geochronological signature robust with respect to hydraulic-sorting effects, making possible to assess the adequacy of

geochronological signature with respect to the hydraulic sorting effect on single grain age distribution.

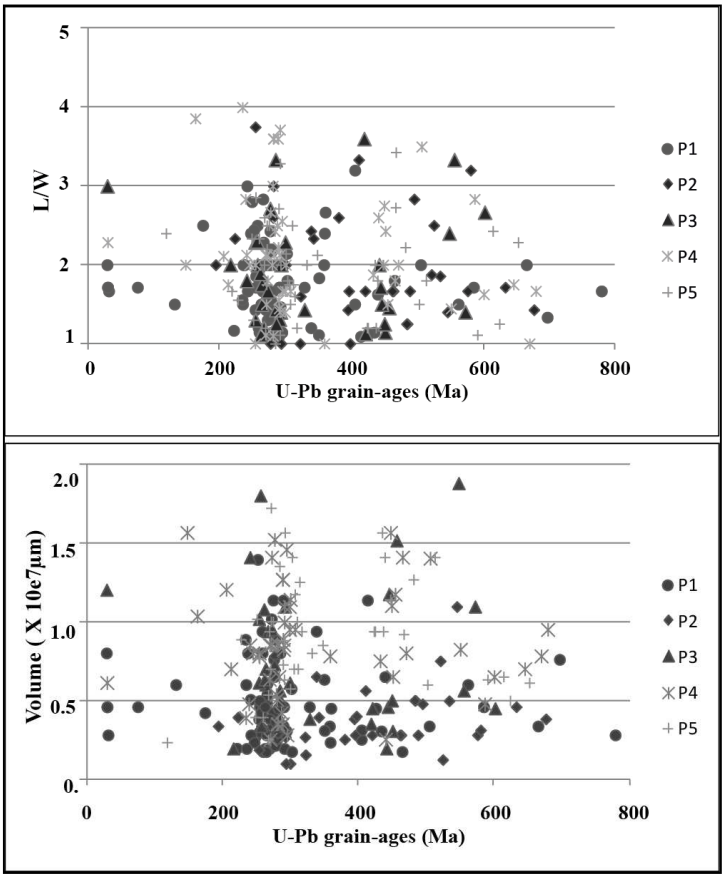

Fig. 33: First diagram shows no linear correlation between L/W vs. U-Pb grain-ages, as also suggested by low values of the coefficient of linear correlation R^2, calculated for each sample: R^2P1=0.001; R^2P2=0.023; R^2P3=0.001; R^2P4= 0.025; R^2P5= 0.009. The same situation is also observed in the plot of average volume vs. U-Pb grain ages, where the coefficient of linear correlation has the following values: R^2P1=0.0; R^2P2=0.07; R^2P3=0.008; R^2P4= 0.004; R^2P5= 0.002.

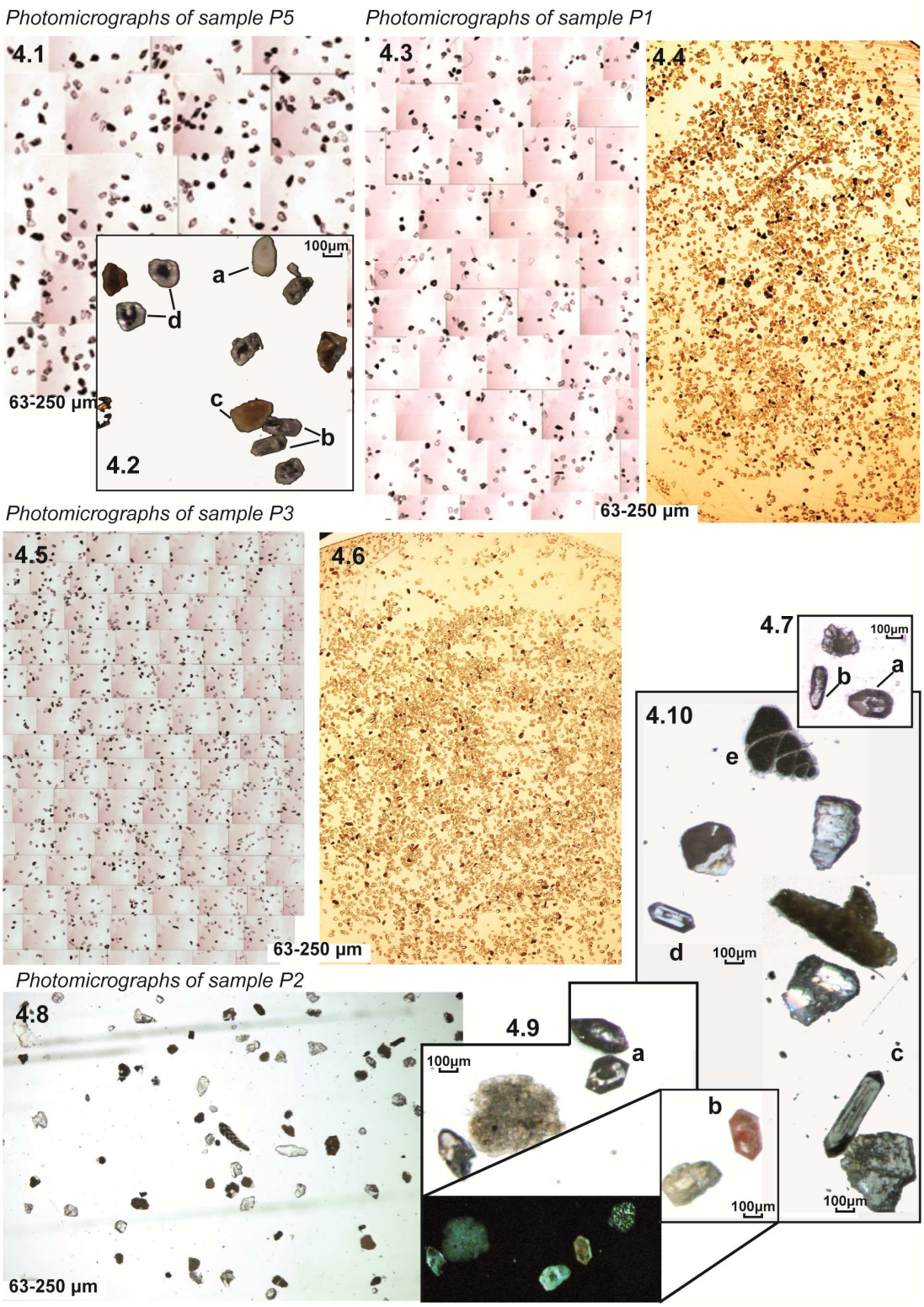

Fig. 34: Plate 15. Photomicrographs of samples from the Po River trunk

SAMPLE P1

General

Sample P1 was collected in locality Torreberetti along the Po river trunk after the confluence of major tributaries of Western Alps.

According to the granulometric distribution for sample P1, grain-size of zircon grains is between very-fine-to-fine sand with few silt grains. State of zircon concentrate at the end of separation shows few zircon grains ranging in size between (63-125 µm), so that refining of zircon concentrate by means of further separation was necessary. The refined concentrate seems much improved after sieving with a finer mesh. In Plate 15, photomicrographs 4.3, 4.4 extracted from P1 sample map, show the difference observed in zircon concentrate before and after further separations.

Zircon concentrate (density >3.3 g/cm^3) contains other diamagnetic minerals where the kyanite was the most abundant with grain-size considerably larger than zircon (see table 2 for details).

Morphology of zircon populations

In sample P1 the majority of zircons show rounded and sub-rounded morphologies (77%), where the 56 % is represented by sub-rounded grains, where the grains shape is often recognizable, while the 21% of rounded shaped includes the acicular prismatic, egg-shaped and spherical grains. Euhedral types represent only the 14%, with a slightly difference between the {101}-dominated (15%) and {211}-dominated (7%) zircons. {101}-dominated morphologies are represented by P3/P4 types and S10/S15, but S25 type was also observed. {211}-dominated zircons instead, are represented, by a dominance of S23/S8 types where {101} pyramidal faces is almost

comparable with {211} pyramid, but S11/S12 types have been also observed, assessing the occurrence of strong {211}-dominated crystals.

Common colourless series of zircon grains are associated with a less common series show milky zircons is often associated to zircons with different degree of metamictization.

SAMPLE P2

General

Sample P2 was collected in locality Rivarone along the Tanaro River main trunk a Po tributary which drains the Argentera massif and the Ligurian Alps.

According to the granulometric distribution for sample P2, grain-size of zircon grains is very fine sand with many grains just smaller than 63 µm close to the silt-grain-size. State of zircon concentrate at the end of separation procedures shows a good concentration of zircon grains. Heavy minerals observed in the zircon concentrate are described in detail in table 2.

Morphology of Zircon populations

In sample P2 the majority of zircons shows rounded and sub-rounded morphologies (72%), with the 18 % represented by sub-rounded grains, with a dominance of acicular prismatic form, while the 54% are rounded shaped. Euhedral types are the 24%, where the {101}-dominated zircons represent the 15%. In Sample P2 we observed the following features:

- {211}-dominated types are represented by types where the {101} pyramidal faces are well recognizable, as S23/S13 or S8 types, as in Plate 15, 4.9a

- {101}-dominated zircons show acicular prismatic habit, usually referred to D/P5 and P4 types, as shown in Plate 15, 4.9c and 4.10d, respectively
- There are many shells (probably fitting with some foraminifera species as suggested in different works (Ricci Lucchi et al., 1982; Barbieri and Panieri, 2004) probably from the TPB source area showing a complete refilling of some oxides (e.g. pyrite or limonite), which have recrystallized replacing the organic material, details in Plate 15, 4.8 and 4.10e

Colourless zircons are the most common, however there are also few grains showing different shades between pink and hyacinth, their particularity need a specific discussion:

- Euhedral {101}-dominated zircon is characterized by almost opaque core surrounding by as opaque rim, emphasized by a strong shining red colour. There are only few grains showing these features and they all range between 290-320 Ma. We are likely to name this zircon population as “series 56”, from the number of the most representative grain shown in Plate 15, 4.9b. Morphological features of "series 56" could be used as a marker of a proper source area located upstream sample P2.

SAMPLE P3

General

Sample P3 was collected along the Po River trunk in locality Cornale before the confluence of the Ticino River, downstream the Tanaro and the Scrivia rivers confluences.

According to the granulometric distribution for sample P3 calculated during zircon separation procedures (see table 1 in appendix for details), grain-size of zircon grains is very fine-to-fine sand.

State of zircon concentrate at the end of separation procedures shows few zircon grains, and high amount of other heavy minerals such as of large crystals of kyanite (see table 2), so that refining of zircon concentrate by means of further separation has been required. We apply a stronger magnetic separation (see ch.2 for details), but the concentrate were much improved only after sieving with finer mesh.

Plate 15, 4.5 and 4.6 try to show the state of zircon concentrate respectively before and after refining. Then zircon concentrate was observed on a polished slide for morphological analysis prior to geochronological dating.

Morphology of zircon populations

In sample P3 the majority of zircons show rounded and sub-rounded morphologies (77%), where the 19 % is represented by sub-rounded grains, where the grains shape is often recognizable (plate 15, 4.7b), while the 60% of rounded shaped includes the acicular prismatic, egg-shaped and spherical grains. Euhedral types represent only the 21%, with a slightly difference between the {101}-dominated (15%) and the {211}-dominated (6%) zircons. Types P3/P4 and S10/S15 are commonly represented between the {101}-dominated zircons, S3/S2 and S12 types (Plate 15, 4.7a), instead are more common in the other group. Dominant colourless series of zircon grains are associated with less common milky zircons, showing different degree of metamictization.

SAMPLE P4

General

Sample P4 was collected along the Ticino River main trunk, upstream Pavia in locality Bereguardo. According to the granulometric distribution for sample P4 calculated during zircon separation procedures (see table 1), grain-size of zircon grains is very fine-to-fine sand. State of zircon concentrate at the end of separation procedures show a good concentration of zircon grains, so that no further separation was required. Then zircon concentrate was observed on a polished slide for morphological analysis prior to geochronological dating. Zircon concentrate (density >3.3 g/cm^3) contains other diamagnetic minerals where the kyanite was the most abundant with grain-size considerably larger than zircon (see table 2).

Morphology of zircon populations

In sample P4 the majority of zircons show rounded and sub-rounded morphologies (64%), where the 38 % is represented by sub-rounded grains, while the 27% of rounded shaped includes mainly the acicular prismatic shaped grains. A significant amount of euhedral grains with the 35% of the total, where the {101}-dominated zircons (21%) are represented mainly by S19 type and S15/S5 types some P2 are observed. Morphology {211}-dominated represents the 14%, including S21/S6 and S17/S22 types. Dominant colourless series of zircon grains are associated with less common milky zircons.

SAMPLE P5

General

Sample P5 was collected along the Po River trunk at Zerbo, after the confluence of the Ticino River. According to the granulometric distribution for sample P5, grain-size of zircon grains is very fine-to-fine sand. State of zircon concentrate at the end of separation procedures show few zircon grains much smaller than other heavy minerals, and high amount of large crystals of kyanite, so that refining of zircon concentrate by means of further separation was required, by a finer sieving according to procedures described in chapter 2. Then zircon concentrate were observed on a polished slide for morphological analysis prior to geochronological dating. Zircon concentrate (density >3.3 g/cm^3) contains other diamagnetic minerals where the kyanite was the most abundant with grain-size considerably larger than zircon (see table 2).

Morphology of zircon populations

In sample P5 the majority of zircons show rounded and sub-rounded morphologies (75%), where the 19 % is represented by sub-rounded grains, while the 56% of rounded shaped includes mainly the acicular prismatic shaped grains. Few euhedral grains are the 21% of the total, where the {101}-dominated zircons are the 14% mainly represented by P5/P3 types. Few {211}-dominated morphologies (7 %) usually show equivalent size of both pyramidal shapes so that the main types observed are S18/S13. Dominant colourless series of zircon grains (plate 15, 4.1b,c,d) are associated with less common milky zircons (plate 15, 4.1a).

CHAPTER 7

U-Pb signals

Introduction

The U-Pb zircon grain-age distribution in the delta is a function of the U-Pb zircon grain-age distributions of upstream tributaries. Consequently the same peaks observed in the Po Delta samples can be traced within the distribution of the tributaries which drains the potential source areas. Starting from the delta, U-Pb zircon grain-age distributions were analyzed upstream up to their sources in order to recognize dominant and minor peaks which characterized the geochronological signal within the Po River drainage (fig.35). Major Po River's tributaries are characterized by a geochronological signature that reflects the source rocks providing a representative mirror of the bedrock U-Pb ages distribution in the drainage area (Bernet et al., 2001). This can be demonstrated by cross-checking the detrital zircon U-Pb ages against known values from the bedrock achieving a high level of confidence in detrital dating results. In this idea we compared detrital zircon ages with the bedrock U-Pb ages of zircon rims available from the large dataset published by Hunziker *et alii* (1992, in the Mémoires de Géologie, Lousanne) and from some recent data of geochronological studies in the Alps/Apennine belt.

Results discussed in these chapters demonstrate that provenance signals from source areas influence the U-Pb zircon grain-age distributions of samples from the Po River main trunk, as well as those from its delta.

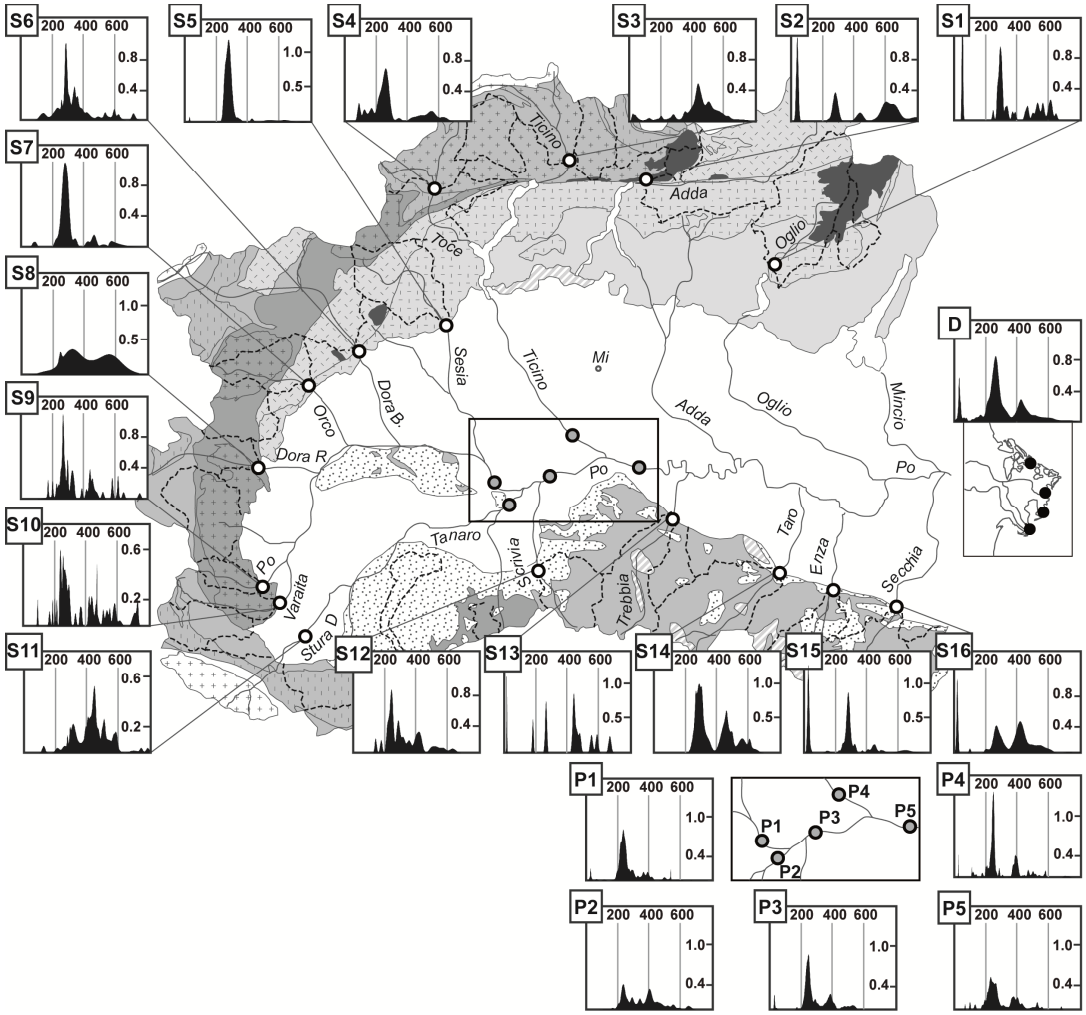

Fig. 35: Detrital U-Pb ages distribution of the Po River drainage. U-Pb signals of samples from the major Po river' tributaries draining potential source areas can be followed downstream the Po river trunk toward the delta. After major confluences probability density plots of samples P1, P2, P3 and P4, in fact, results from a mixture between dominant and minor peaks of the grain-ages distributions before the confluences.

U-Pb Signal in the Po River Basin

PO DELTA

The clusters in the distribution show distinct populations defined by discrete and well-defined peaks which are rather constant in each Po Delta samples (fig.36). The occurrence of very similar peaks in Po Delta samples attests that our quantitative approach has the advantage of preserving the relative proportions of age components. This allows to merging data from all four samples then out of 398 analyses, 357 yielded with concordant ages. The dominant population occurs in all samples, within a range from 280 Ma to 300 Ma. The younger population is represented by a single peak which comes at 30 Ma in each samples. The oldest prominent peaks within the distribution range between 420 Ma and 480 Ma. Minor grain-age populations ranging between 100-140 Ma, and 320-360 Ma not rule out the contribution of rocks of these ages as sources. Smaller peaks, not apparent in single samples, are shown at 150 Ma (2%) and 330 Ma (4%).

CENTRAL AND SOUTHERN ALPS

Probability density plot of sample S1 collected from the Oglio River (fig.37) shows a number of characteristic peaks which reflect the published U-Pb ages from zircon rims spreading from the 30-40 Ma of the Adamello pluton to older ages of 580-680 Ma (Liati et al., 2000; Schaltegger et al., 2009). The younger grain-ages yield a dominant peak at 31 Ma. After a lack of grain-ages from 50 to 230 Ma, the dominant peak which follows ranges between 240-340 Ma.

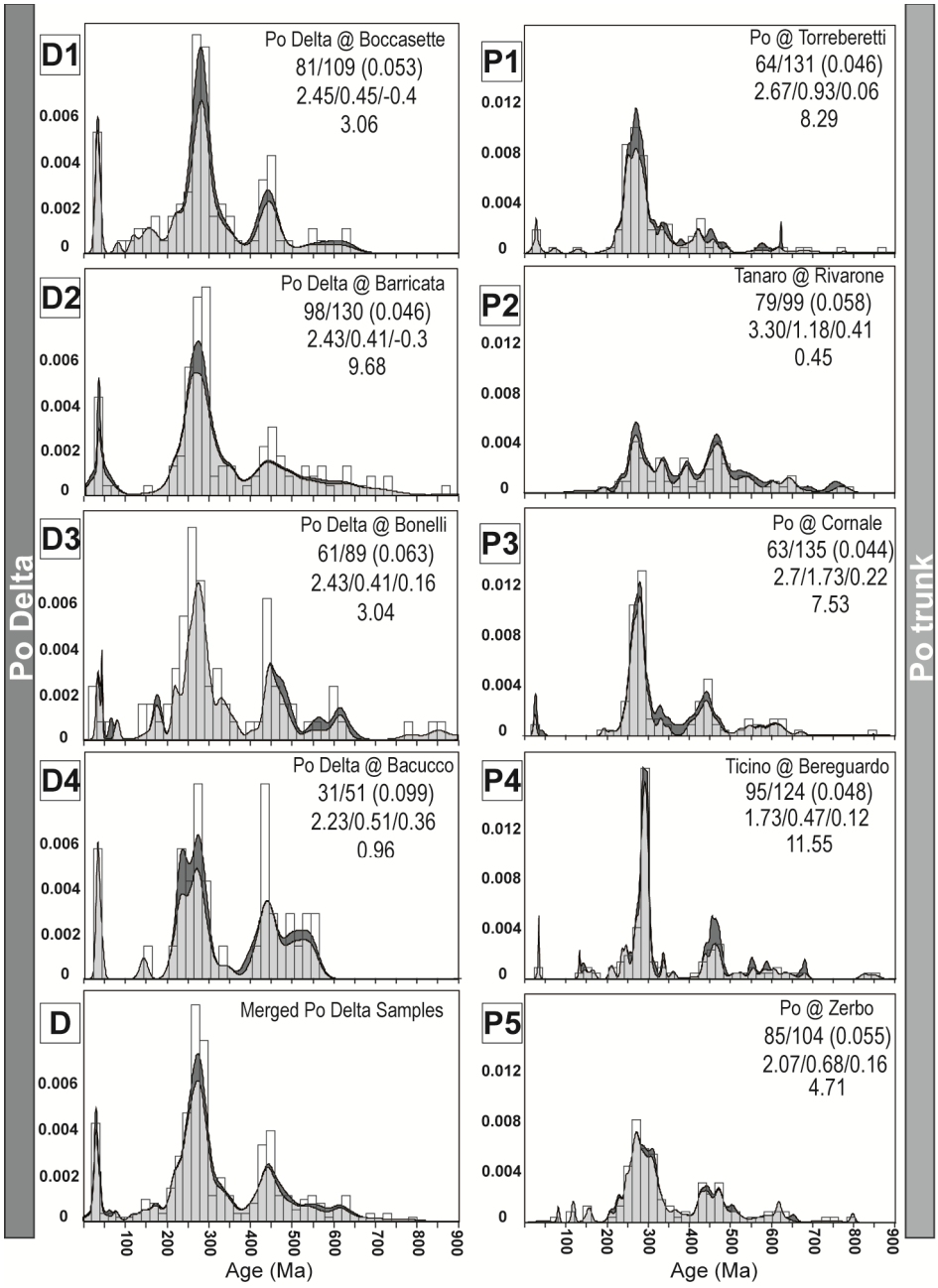

Fig. 36: U-Pb signal in the Po Delta (left) and in the Po trunk (right) samples. Keys top right in each plot are: first row, river's name and sampling locality; second row, number of concordant zircons vs. total number of analysed zircons, in parenthesis maximum probability of missing a fraction of the population with 95 % of confidence calculated according to Vermeesch (2004); third row, mean diameter (Dm), sigma (σ1), skewness (Sk); fourth row, HM concentration is given. Probability density plots obtained with Age Display (Sircombe et al., 2004), bin width (20 Ma) calculated according to Vermeesch (2004). Light grey area highlights grain-ages distributions of only concordant data. Dark grey area, instead, is referred to grain-ages distributions calculated considering both concordant and discordant data. Overlay of both distributions highlights that discordance does not affect particular grain-age populations.

Probability density plot of sample S2 from the Adda River (fig. 37) shows a number of characteristic peaks in agreement with the published U-Pb ages from zircon rims ranging between 30-40 Ma (John and Blundy, 1993). Younger grains ages define a dominant peak at 31 Ma. There is a lack of grain ages from 50 to 230 Ma, which is followed by a general spread of ages from 400 to 900 Ma, with a prominent peak ranging between 540 and 740 Ma. Grains older than 1Ga were also found.

The highest density of published zircon U-Pb ages is observed in the Lepontine Dome spreading from 100 to 700 Ma, with dominant populations ranging between 130 and 395 Ma and 450-500 Ma (Allegre et al., 1974; Hanny et al., 1974; Hunziker et al., 1989 and references therein). These ages are consistent with the probability density plot of detrital sample S3 and S4 (fig. 37). Characteristic peaks of sample S3 show a general spread from very young ages to ages older than 800 Ma. Examination of the younger ages (< 300 Ma) shows a significant number of ages with a peak at 38-40 Ma, and relatively abundant grains display age of 187 Ma, while a dominant peak is shown at 465 Ma. Probability density plot of sample S4 from the Toce River, instead, shows a dominant peak at 280 Ma. Significant peak is found at 100 Ma followed by a general spread since 200 Ma. Only few grains range between 440 Ma and 500 Ma.

NORTH-WESTERN ALPS

Published bedrock U-Pb ages in the Sesia River drainage show a strict range of ages between 280 and 339 Ma (Hurford et al., 1991; Paquette et al., 1989a; Koppel et al., 1974). Probability density plot for the detrital sample S5 (fig. 37) reflects this pattern with a marked dominant peak ranging between 220 and 380 Ma. Only few concordant grain display younger age than 30 Ma that may suggest the contribution

from the minor periadriatic bodies exposed along the Insubric line. Older grains are scarce, yielding small peaks spreading from 400 to 800 Ma. Published bedrock U-Pb ages in the Dora Baltea River drainage show a wide range between 466 and 157 Ma (Hunziker et al., 1989 and reference therein; Rubatto et al., 1998; Rubatto et al., 1999; Dalla Giovanna 2009; Paquette et al., 1989b). These components are clearly detected in the detrital sample S6 (fig. 37) where the probability density plot spread from 100 Ma to older ages at 800 Ma, with a dominant peak ranging between 260-313 Ma. Examination of the younger grains shows a small peak at 100 to 200 Ma.

High concentration of published bedrock U-Pb ages of zircons rims from the Orco river drainage displays a large range between 260 and older than 800 Ma (Guillot et al., 2002; Bertrand et al., 2005; Ring et al., 2005). Probability density plot of sample S7 reflects this pattern (fig.37), with ages spreading from 100 Ma to older than 800, with a dominant peak ranging between 240-320 Ma.

SOUTH-WESTERN ALPS

Bedrock U-Pb ages in the southern Western Alps spread in a narrow range from 150 and 168 Ma to older ages at 500 Ma, but their distribution is scarce and not homogeneous (Rubatto and Hermann, 2003; Tilton et al., 1989). Younger bedrock ages from zircon rims are shown at 61 Ma (Rubatto et al., 1998). The same pattern is detected in the detrital sample S8 (fig. 37) where the probability density plot show a general spread from 100 Ma to older ages, with two dominant peaks at 340-360 and 560-580 Ma.

Sample S9 represents the first geochronological signal detected in the Po River downstream its source (fig. 37). In the probability density plot of S9 significant peaks are found in the distribution ranging between 420-480 Ma, and other smaller peaks

at 180 Ma and 600 Ma. Dominant peak ranges between 220-320 Ma. A similar distribution is observed in sample S10 collected along the Varaita River. Probability density plot for the sample S10 shows a scattered pattern characterized by a dominant peak ranging between 220-320 Ma. Small other peaks are represented where examination of the younger grains shows a narrow peak at 100 to 200 Ma.

The probability density plot for the detrital sample S11 collected from the Stura Demonte River, reflects the clusters of published bedrock U-Pb ages ranging between 324 and 800 Ma (Paquette et al., 1989b; Dalla Giovanna, 2009). Significant peaks range from 250 Ma to older than 500 Ma. Dominant peak comes at 448 Ma, while a second larger peak comes at 322 Ma. Examination of the younger grains shows a small peak at 100 to 200 Ma.

LIGURIAN ALPS AND NORTHERN APENNINES

Bedrock U-Pb ages are scarce possibly because a lack of detailed studies in this sector of the belt. Probability density plot of detrital sample S12 from the Scrivia River (fig. 37) shows a general spread from 100 Ma to older ages, with a dominant peak ranging between 240 and 280. There are smaller peaks at 100 Ma and 200 Ma as well as older grains forming a peak ranging between 400 and 480 Ma.

Sample S13 from the Trebbia River is poor of zircons grains. Probability density plot shows small peaks scattered in the distribution at 100 Ma and at 200 Ma (fig.37). Dominant peak comes at 420-500 Ma. Examination of the younger grains shows a prominent peak at 30-40 Ma.

Published bedrock U-Pb ages are found in the Taro River drainage clustering between 150 and 165 Ma (Rubatto et al., 2003; Rampone et al., 1998). Probability density plot for the detrital sample S14 (fig.37) reflects this pattern in a small peak at

155 Ma, while dominant peak are found between 250 Ma and 300 Ma. A significant peak is also found at 448 Ma.

The Enza River has the smaller drainage area dominated by the foredeep turbidites units (Tuscan Units and Subligurian units) and the Epiligurian Units. Probability density plot of detrital sample S15 show a dominant peak ranging between 240 and 320 Ma (fig.37). Examination of the younger grains shows a significant peak at 30 Ma. There are other smaller peaks spreading to older ages from 340 to 700 Ma.

The Secchia River drains mostly the Oligocene-Miocene foredeep turbidites as well as the Epiligurian units. Published bedrock U-Pb zircon ages are not supplied for this area. Probability density plot for the sample S16 (fig.37) shows a dominant peak ranging between 280 and 340 Ma, followed by a significant peak between 400 and 500 Ma. Examination of the younger grains shows a significant peak at 30 Ma.

PO RIVER TRUNK

Sample P1 has been collected along the Po river main trunk, downstream the confluence of the main North-Western and South-Western Alps. Probability density plot shows a number of characteristic peaks (fig.36). Out of 109 analyses, 96 yielded zircons with concordant ages. Examination of the younger grains (<40 Ma) shows a small peak at 20-40 Ma. There is a general spreading, from the 100 Ma to 540 Ma with dominant peak ranging between 240-360 Ma followed by a small peak at 440 Ma. In addition sample P2 has been collected along the Tanaro River trunk after the confluence of the Stura Demonte River, downstream the small rivers draining the Ligurian Alps, before the confluence of the Scrivia River (fig.36).

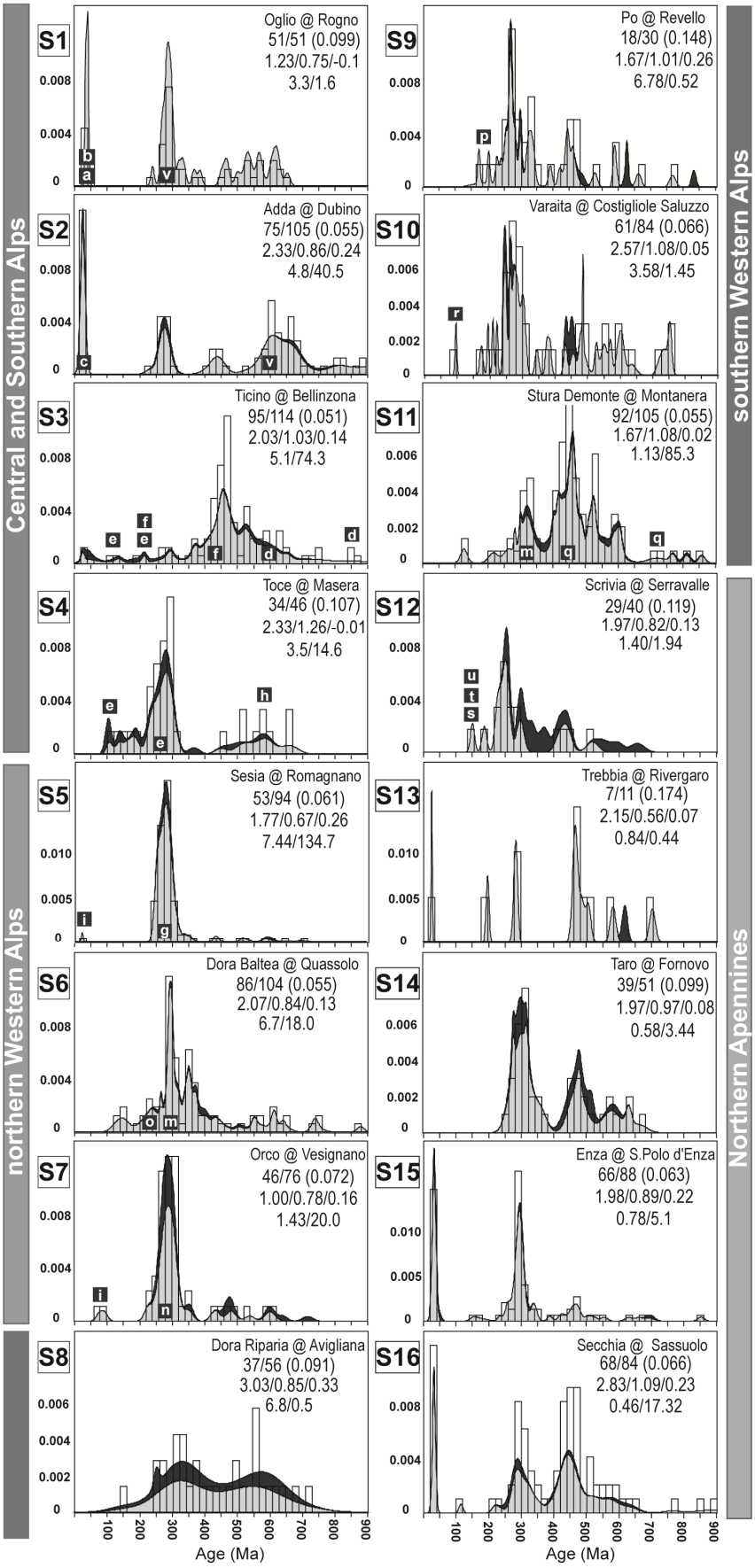
Central and Southern Alps
northern Western Alps
southern Western Alps
Northern Apennines
S1
Oglio @ Rogno
51/51 (0.099)
1.23/0.75/-0.1
3.3/1.6
S2
Adda @ Dubino
75/105 (0.055)
2.33/0.86/0.24
4.8/40.5
S3
Ticino @ Bellinzona
95/114 (0.051)
2.03/1.03/0.14
5.1/74.3
S4
Toce @ Masera
34/46 (0.107)
2.33/1.26/-0.01
3.5/14.6
S5
Sesia @ Romagnano
53/94 (0.061)
1.77/0.67/0.26
7.44/134.7
S6
Dora Baltea @ Quassolo
86/104 (0.055)
2.07/0.84/0.13
6.7/18.0
S7
Orco @ Vesignano
46/76 (0.072)
1.00/0.78/0.16
1.43/20.0
S8
Dora Riparia @ Avigliana
37/56 (0.091)
3.03/0.85/0.33
6.8/0.5
S9
Po @ Revello
18/30 (0.148)
1.67/1.01/0.26
6.78/0.52
S10
Varaita @ Costigliole Saluzzo
61/84 (0.066)
2.57/1.08/0.05
3.58/1.45
S11
Stura Demonte @ Montanera
92/105 (0.055)
1.67/1.08/0.02
1.13/85.3
S12
Scrivia @ Serravalle
29/40 (0.119)
1.97/0.82/0.13
1.40/1.94
S13
Trebbia @ Rivergaro
7/11 (0.174)
2.15/0.56/0.07
0.84/0.44
S14
Taro @ Fornovo
39/51 (0.099)
1.97/0.97/0.08
0.58/3.44
S15
Enza @ S.Polo d'Enza
66/88 (0.063)
1.98/0.89/0.22
0.78/5.1
S16
Secchia @ Sassuolo
68/84 (0.066)
2.83/1.09/0.23
0.46/17.32
Age (Ma)
Age (Ma)

Fig. 37: U-Pb signal of the major river Po tributaries. Keys top right in each plot are given in previous figure 36. In the fourth row HM concentration and calculated zircon fertility are given for each sample. Letters in square indicate published bedrock U-Pb ages of zircon rims widely distributed in the Po drainage. In the Central and Southern Alps (a) Liati et al., 2000; (b) Schaltegger et al., 2009; (c) John and Blundy, 1993, where the highest concentration of U-Pb ages is found in the Lepontine Dome (e) Allègre et al., 1974 and (f) Hanny et al., 1974. In the Sesia-Lanzo and Ceneri zones (g) Paquette et al., 1989a; (h) Koppel et al., 1974; (i) Rubatto et al., 1999; (l) Rubatto et al., 1998. High concentration of U-Pb ages is also found in the External massifs (m) Dalla Giovanna 2009; (q) Paquette et al., 1989b; (d) Hunziker et al., 1989, together with the Internal massifs (n) Guillot et al., 2002; (o) Ring et al., 2005, (p) Rubatto and Hermann, 2003 and (r) Tilton et al., 1989. U-Pb ages are also found in the Ligurian Units of the Northern Apennines (s) Borsi et al., 1996, (t) Rubatto et al., 2003 and (u) Rampone et al., 1998.

The geochronological signature of the P2 sample shows a relatively scattered distribution. Out of 75 analyses, 60 yielded concordant ages. Examination of the younger (<200 Ma) grains shows a small peak at 180 Ma, whereas a small peak at 100 Ma includes only discordant ages. Then there is a general spread from 200 Ma to 800 Ma, with two dominant peaks ranging between 260-320 Ma, and the latter at 460-500 Ma. Geochronological signal of sample P3 can be interpreted as the combination of signals of upstream samples P1 and P2 (fig.36). Out of 103 analyses, 96 yielded zircons with concordant ages. Examination of younger grains (<40 Ma) shows a significant peak at 30 Ma, probably due to the single input of the upstream sample P1, since the sample P2 does not show ages younger than 100 Ma. Dominant peak within the distribution are found between 220 and 320 Ma, followed by an older significant peak ranging between 380-500 Ma.

The Ticino River was sampled along its main trunk in order to detect the signature from the Central Alps before it reaches the Po River. Results from the probability density plot of sample P4 (fig.36) show a dominant peak between 200 and 340 Ma, followed by a minor peak between 380-500 Ma and few grains younger than 60 Ma, suggesting a Po River geochronological signature, but this idea needs to be carefully tested with statistical methods. After the Ticino river confluence, U-Pb signature of sample P5 (fig.36) displays dominant peak between 200 and 340 Ma, and a minor

peak at 400-500 Ma, but the absence of population younger than 40 Ma possibly suggest its progressive downstream dilution.

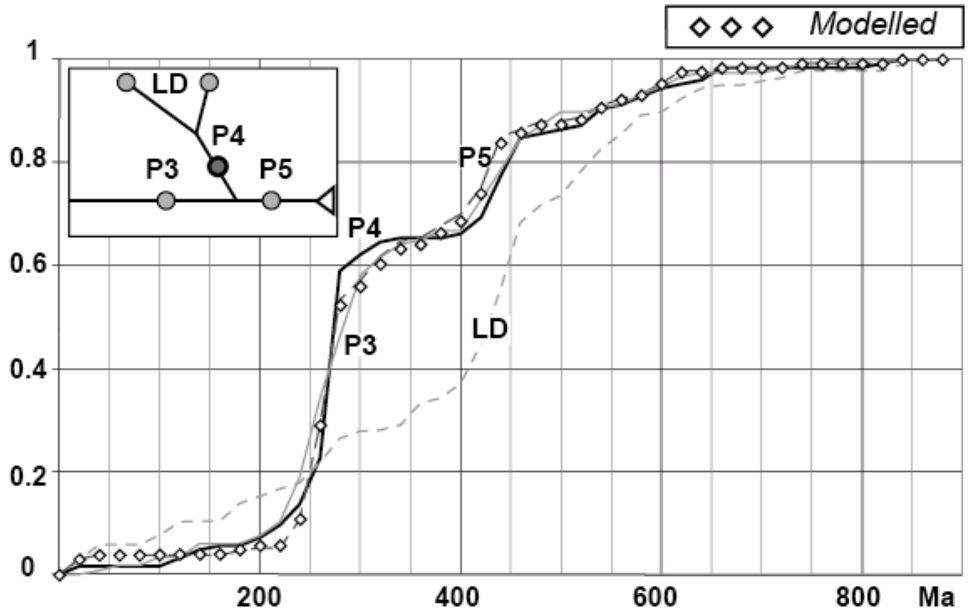

Fig. 38: Comparison between different distribution by using the K-S test is a useful tool to quantify the similarity of U-Pb signature of sample P4 with respect to a Po river or a Lepontine major contributions suggesting that sample P4 represents effectively a Po-like distribution.

Mixing of U-Pb signals

Calculating zircon budget

Zircon analysed along the Po River main trunk can be partitioned between the potential source areas in order to calculate the relative contribution of zircons derived from each portion of the basin.

The first step was to convert U-Pb probability density plots as cumulative probability plots. Each main-trunk sample along the Po river results by the combination of the upstream potential source areas in different proportion which can be determined by

combining the input cumulative distributions for any possible combination until the resulting modelled mixed distribution has the best fit with the observed distribution.

The best fit between modelled and observed cumulative distributions was assessed by the KS-test. The KS test measure the difference between distributions and could be proficiently employed also to cheek if mixing combination have been performed between different end members. Our analyses show that the modelled cumulative density plot of sample P4 is equivalent to observed distribution of sample P3 (fig.38). We can thus believe that the marked Po U-Pb signature in sample P4 can be related to the paleo-drainage of the Po River (e.g. Garzanti et al., 2011), so that modern rivers are possibly reworking the bed-load sediments carried by the Po River during last post-glacial.

Assessing zircon fertility of potential U-Pb source areas

Semiquantitative measures for estimating the zircon content in source rocks can be used to correct interpretations of relative contributions of detrital zircon populations and convert them in terms of sediment contribution. Establish zircon content in the source rock has been attempted in different studies by grain point counting in multiple thin sections (Silver et al., 1981) and by measuring zirconium concentrations determined by XRF analysis and coupled with grain counting (Amidon et al., 2005), or directly compared as a measure of zircon fertility (Dickinson, 2008) after assumption to unravel possible bias introduced by the high variability of zirconium contents in the source rocks (Moecher and Samson, 2006).

The relative proportion of ages defined by the detrital zircon grains are taken as representative of the relative proportion with which each source area contribute to sediment. However, if each source rock among the source area produces different

amounts of zircon, then each sub-basin within cannot be represented proportionally among the analysed zircons. Additionally the size of detrital zircon populations can be derived by the amount of zircons in proportion to the relative size of each sub-basin. Both assessments are important since the relative zircon contribution may be over (or under) estimated because of the different zircon content of drained source rocks, or because of the larger (or smaller) size of each sub-basin.

Because rivers provide statistic sampling of every source rocks exposed in the drainage area, hence measurements of zircon concentration in river sediments would represent with a high degree of accuracy the mean of zircon concentration in the source areas producing sediments.

Although the value of zircon content in sediment can be significantly modified during transport and deposition, we are able to evaluate this variability in terms of zircon concentration in each grain-size windows of bulk sediment. High-resolution petrography and heavy mineral analyses when coupled with sedimentological analyses can provide quantitative measurement of zircon concentrations in the studied as well as in the coarser and finer grain-size windows of the bulk sediment. High values of zircon content could be associated to higher values of HM concentration in samples from the Po Plain where hydrodynamic effects are more important than at the end of valleys. To unravel possible bias in the estimation of zircon content in the sediment, we have measured the grain density of sediment as a useful tool to evaluate any possible anomalous concentration of dense and ultradense minerals. Grain density resulting for all the analysed samples is in the range of the mean crustal rocks density (≈2.72 g/cm^3). The tabulated results (table 3 and 4 in appendix) allow an evaluation of the role of sedimentologic parameters and contrasting zircon content in sediments on shaping the detrital zircon population. For

this reason combination of U-Pb signature in recasting the potential source areas, have to be correct for the relative zircon content in river sediments.

Modelling U-Pb source areas

Potential source areas are defined by merging together each sub-basin of the main Po River tributaries divided into different source area. Hence the geochronological signature of such potential source areas will result from the combination of the U-Pb signatures measured in each sub-basin, corrected for the zircon fertility and the size of each sub-basin.

We are able to discriminate in the Po River basin six major sources, summarized in table 4 (see appendix):

- The Southern and Central Alps source area marked by strong zircon contribution of S2 sample, amplified by higher value of zircon fertility.
- The Lepontine Dome source dominated by the U-Pb signal of sample S3
- The North-Western Alps source area dominated by the zircon contribution of the S6 sample because of its drainage area is the largest
- The South-Western Alps source area recast on the basis of relative zircon contribution between sub-basins, where the contribution of the S8 sample results definitely higher than smaller sub-basins of S9 and S10 samples
- The Argentera source area represented by the only sample S11
- The Ligurian Alps and the Northern Apennines source areas include large size sub-basins where distributions were calculated on the basis of zircon fertility and the size of river 'sub-basin contributing to sediment.

Part IV
Discussion

CHAPTER 8

Downstream changes of detrital zircon morphology and U-Pb ages

Partitioning of U-Pb signal from potential sources to the Po Delta

The geochronological signature for the Po River samples results by continued downstream input of zircon from potential source rocks exposed in the belt. Mixture of dominant peaks within the distributions of the input samples will characterize the probability density plot of the downstream samples. The frequency of such populations will be amplified (or minimized) depending on the relative contributions from each source areas. Potential source areas are defined in terms of differential zircon fertility and extent of the drainage area according to the approach proposed by Malusà and Garzanti (2011). The relative contributions of zircon from each source area can be calculated by partitioning the geochronological signal downstream the Po River main trunk, from sources to the delta. Statistical techniques are used to evaluate the proportions in which the input age components should be combined to obtain the downstream mixed age distribution. Ages distribution are compared in terms of cumulative density plot since this allows better matches between the input source areas to finally obtain the downstream distribution. To quantify the best fit between two curves we perform the Kolmogorov-Smirnov (KS) test (Massey, 1951), which assesses the statistical significance of the difference between the distributions in terms of the maximum vertical deviation (i.e. distance) between distributions. Partitioning of the geochronological signal downstream the Po River trunk reveals a

stronger contribution from the north Western Alps achieved for the lowest values of the KS test between the observed and the modelled cumulative density plots of sample P1 (fig.39). This evidence is displayed also before the confluence of the Ticino River. Best fit between the observed and the modelled distribution of sample P3 support a stronger zircon contribution from the upstream sample P1.

The U-Pb signal which characterise the Po River Delta is essentially displayed already upstream the confluences with Apenninic rivers. This because zircon contributions from the Central and Southern Alps source areas as well as from the Northern Apennines are considerably less significant with respect to the Po River trunk. However zircon contributions from Southern Alps and Northern Apennine are not negligible because they provide to the younger age populations, since no young peaks are shown in sample P5.

Reproducibility of results from partitioning of U-Pb signal can be tested with a independent parameter. We opted to use quantitative measurements of zircon typology, applied to the same zircon grains sampled for U-Pb analysis, to check interpretations of relative contributions of detrital zircon populations.

Fig. 39: In the first diagram, geochronological signal C results from upstream input of both signal A and B. The former can give a zircon contribution between the 100% and the 75 %, while the contribution of the latter may reach a maximum value for the 25 %. In the second diagram C is turned into an input signal that together with D, combines in the downstream signal E. The best fit between the observed and the modelled distribution E is reached for a higher percentage of C ranging between 100-63% instead of the 37-0% for D. In the third diagram contribution from F is almost negligible, or quite low (0-20%), while the E provides with 100-80% to the G/G^{1} signal. The lowest values of the KS test are reached when contribution from E is higher. In the last diagram there are three components which provide to the signal of L. I and H/H^{1} can mutually contribute for a maximum of 20 %, or be negligible.

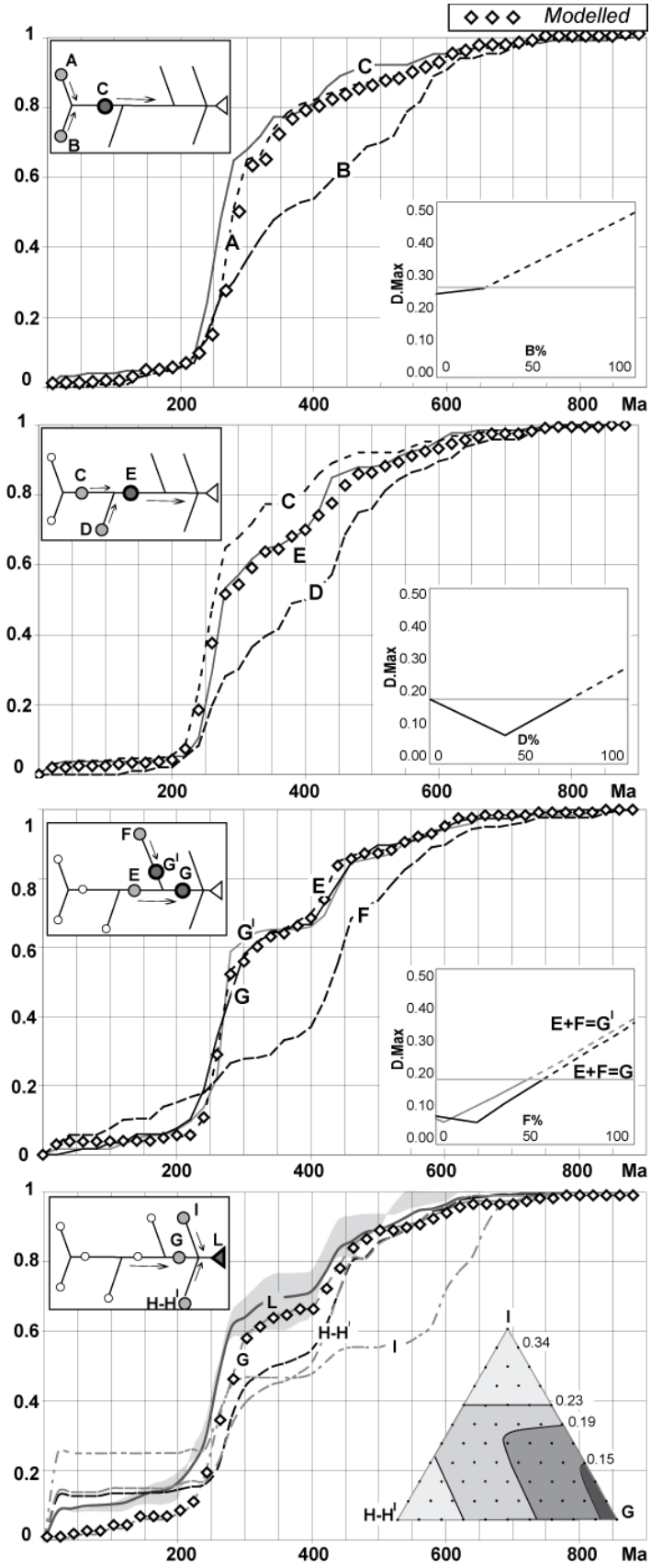
Modelled
A
B
C
D
E
F
G
G'
H-H'
I
L
D.Max
B%
D%
F%
E+F=G'
E+F=G
0.34
0.23
0.19
0.15
0
50
100
200
400
600
800
Ma

Constraint from zircon typology

Zircon morphology can provide an efficient tool to test our results, since typology of euhedral zircon can be identified all along the sediment pathway, helping to trace and fingerprint every source areas. The widely employed Pupin diagram has been simplified by dividing in two sides on the basis of dominant pyramidal faces.

Dominance of a (101) pyramidal face with respect to (211) describe the relation between different euhedral types for potential source areas (fig.40). Typological groups from the Central and Southern Alps show the lowest (101)/(211) ratio together with the Northern Apennine. The high values of (101)/(211) ratio recorded in the Po Delta can support a strong contribution from a potentially source characterized by a majority of (101)-dominated zircons. In particular the (101)/(211) ratio in the Po Delta avoid the Central Alps and the Northern Apennines as potentially sources, indicating, instead a more important contributions from the northern and southern Western Alps, the Argentera and the Ligurian Alps. Major zircon contribution supporting the (101)/(211) ratio measured in the delta should come from a potentially source characterized by higher (101)/(211) ratio that can be traced along the Po River trunk and likely referred to the northern Western Alps. Contributions from the other source areas have a secondary importance because the strong component of (211)-dominated zircons in the composition of the typological signal, as verified by the sample P2 from the Po plain.

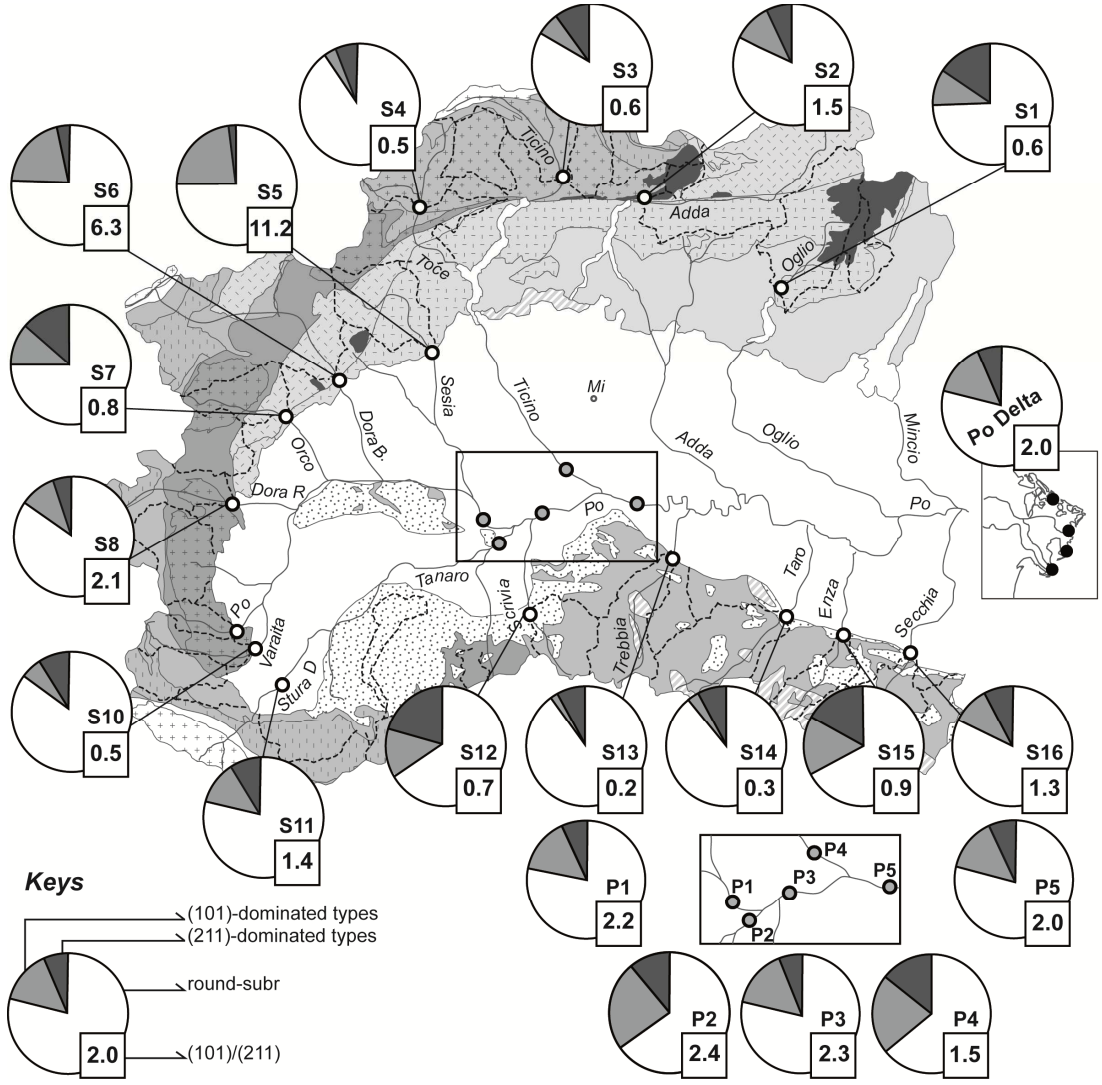

Fig. 40: Distributions of detrital zircon morphologies in the Po River drainage. (101)/(211) ratio of the delta requires major contribution from the northern Western Alps, showing (101)/(211) >>1, while all the other sources have (101)/(211)<2.

CHAPTER 9

Short term erosion pattern in the Alps-Apennines belt

Performing sediment budget from zircon budget

After partition of the U-Pb signal within the Po River basin, the resulting zircon contributions is a measure of the importance of each source areas contributing to the geochronological signal of the Po Delta. The variability of zircon concentration in analyzed sediments can largely influence the measurements of the relative sediment contribution shed from each source areas. This results is highlighted when performing sediment budget from the relative zircon budget, because zircon contribution estimated for a certain source area can become lesser or larger when converted into sediment contribution (fig.41). For this reason estimated zircon contributions are newly corrected for zircon fertility of each potentially source areas and for the size of each basin catchment. Although sediments show a wide range of zircon concentrations, applying the correction for the zircon fertility in partitioning of the U-Pb signal seems to not strongly influence the results. Given that, we expect neither the zircon concentration in sediments nor in their source rocks, determine the difference of zircon contributions between source areas in the composition of the U-Pb signal found in the Po Delta.

This result is important since the possible causes of differential zircon contribution should be not found in the diverse zircon concentrations in the source rocks, but it could depend on other factors as contrasting sediment contribution linked to a differential erosion rates between source areas.

Relative sediment contributions seem to be low-to-very-low from the Central and the Southern Alps source areas, possibly because zircons shed from the Adda and Ticino rivers may be trapped inside the pre-alpine lakes.

First order short-term erosion pattern

Integrated U-Pb geochronology an typological analysis of detrital zircons provide an erosion patterns on a short-term timescales (10^2–10^5 years) showing markedly different erosion rates between source areas of the Po River basin. The Western Alps are characterized by the highest sediment yield. These results deal with the suggestion that most of the sediment contribution delivered to the Po Delta is supplied by small parts of the Alps-Apennines orogen where short-term erosion rates are higher than in the surrounding areas (Malusà et al., 2009; Malusà and Resentini, 2011; Limoncelli et al., under preparation).

Although potential sediment storage in lakes is considered as a possible and inevitable source of bias in interpretation of relative sediment contributions, when viewed on a geologic time scale, this sediment storage is undoubtedly short lived because the sediment stored in the lakes during interglacial times will be scoured during the next glacial event (Trümpy, 1980; Jerz, 1993; Ehlers, 1996). For example interglacial periods last 30 ka to fill the Pre-Alpine lakes before they got scoured again during glaciations. Such short-term storage is insignificant given the Ma resolution of the detrital U-Pb dating method, and it might be minimized considering a large enough time window in detrital zircon U-Pb analyses.

Although the sediment storage in the pre-alpine lakes remains a problem that needs to be carefully evaluated, our results suggest that the most important sediment contribution shed from the Western Alps, and in particular from the North-Western

sector, is related to higher mass removal by erosion. Low values of relative sediment yield in the Northern Apennine could possibly result from the large amount of suspended-load produced by the widely exposed cover rocks (Ori, 1993).

Our dataset does not allow reliable estimates of erosion rates upstream the prealpine lakes in the Central and Southern Alps. Our interpretation is consistent with results from recent works showing that the highest erosion rates are found in the North-Western Alps and in particular in the Mont Blanc massif (e.g. Vernon et al., 2008; Bernet et al., 2001; Malusà and Resentini, 2011).

Such differences in the relative erosion rates could be promoted by local morphology because at the scale of the whole Po River catchment, each sub-basin show different mean slopes, local reliefs and distribution of glaciated areas, despite of the similar portion of exposed massive rocks (Argentera massif, Mont Blanc basement, Briançonnaise basement). However local morphology may explain only in part the differences in erosion patterns observed in the Po river basin. In this work we invoke as the dominant controlling factor on erosion, the complex interplay between tectonic and exogenic forces, supporting the primary role played by rock uplift triggered by indentation of Adria beneath the axial Alpine belt (e.g. Pfiffner et al., 2002; Rosenberg, 2004; Garzanti and Malusà, 2008).

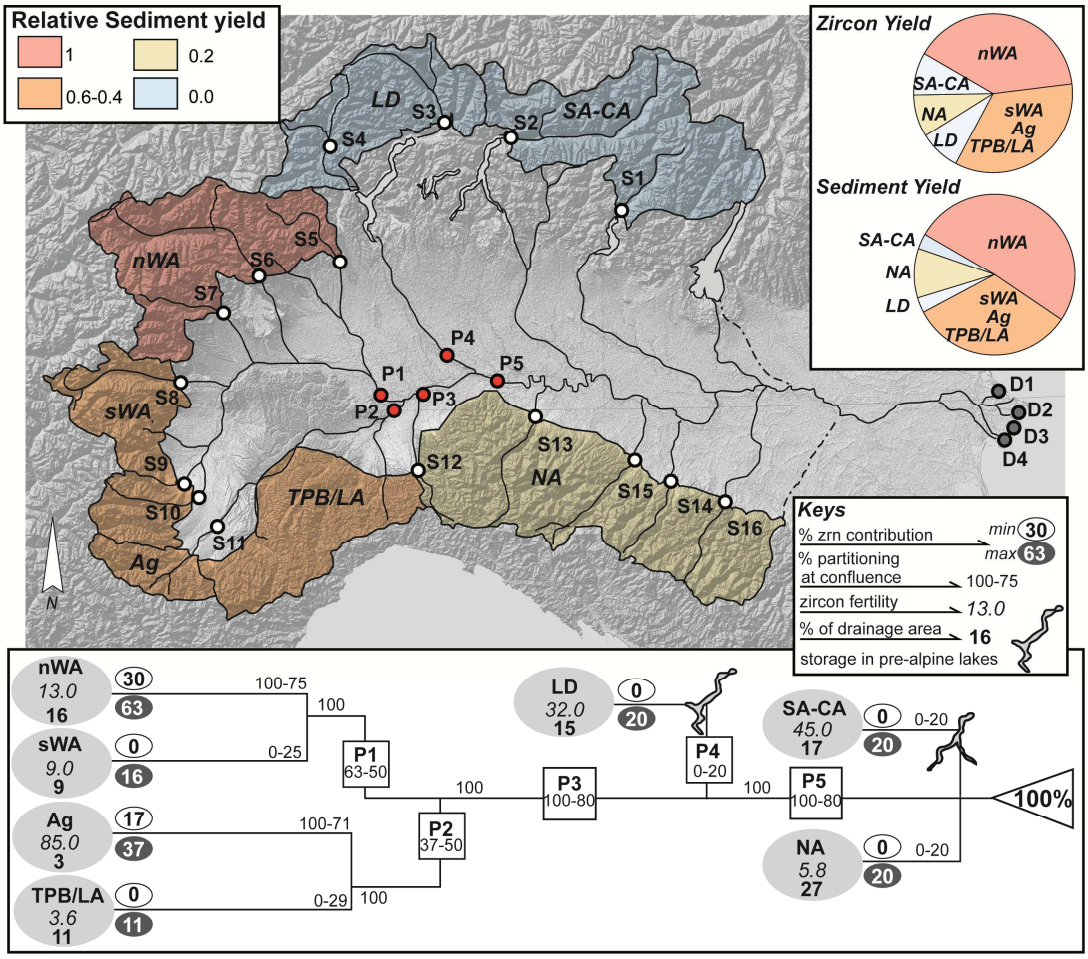

Fig. 41: First order erosion pattern in the Alps-Apennines belt. Relative proportions of sediments that each source area provides to the Po Delta, are calculated according to the flow diagram. High zircon contribution is associated to high sediment yield in the northern Western Alps. Sediment yield in the Southern-Central Alps and in the Northern Apennines instead is very low, suggesting low erosion rates in these areas.

CHAPTER 10

Conclusions

The study of the downstream changes of the geochronological signature of detrital zircons from modern sediments of Po River basin provides a proficient strategy to quantify the relative sediment yield produced by each source area of the Alps-Apennines orogen exposed in the Po River drainage.

LA-ICPMS U-Pb dating of detrital zircon grains can provide a quantitative control on grain-loss during separation procedures in order to assess a reliably characterization of every detrital zircon population contained in a sediment sample. This assessment is important when performing the sediment budget from the relative zircon budget shed from each source areas within the basin. We have focused on the characterization of the detrital zircon U-Pb signature in the Alps-Apennine belt, where we have analyzed 25 samples from recent sands collected along the main Po River's tributaries, and at specific sites along the Po river trunk, as well as at different location on its delta. The U-Pb signal reveals remarkable downstream changes in detrital zircon populations between the Po river trunk and its major tributaries.

When two detrital zircon populations of ages from different source areas are combined together to produce the downstream population, the relative contribution from each source can be estimated. We perform partitioning of the U-Pb signal from source areas to the Po Delta, in order to define the relative proportions in which the source areas contribute to the U-Pb signature of the Po Delta in terms of zircon and sediment contributions. The mixing proportions between the upstream samples can be established by comparing with the KS-test the observed and the modelled downstream distributions, the latter calculated for every combination of the upstream

mixing. Each potential source areas in the Po River basin have been defined on the basis of a proper U-Pb signature which results from the combination between the U-Pb distributions of detrital samples collected among the sub-basins of the Po River's tributaries. The U-Pb signature of each source area have been recast on the basis of the ppm zircon content measured in every sand samples and for the size of each sub-basins. The relative proportions of zircon contributions between source areas have been calculated from the U-Pb distribution of each potentially source coupled with correction for zircon content in sediment. This is because the contribution from a certain source area to the U-Pb detrital zircon signature can be under (or over) estimated depending on the zircon content in the sediment they produce.

Our approach to measure the zircon concentration gives results showing that the relative proportions of zircon contribution shed from each potentially source area are not influenced by the zircon content in the source rocks nor in sediments they produce. Hence, the relative zircon contribution calculated between source areas must be lead to other factors, as contrasting sediment contributions linked to a differential erosion pattern between source areas. When age signatures allow reliable discriminations of different sources, and the size of specific sub-basins is known, we can thus determine a short term erosion patterns on 10^2–10^5 timescales. Results from the Po River basin show that the higher proportion of sediment contribution comes from the North-Western Alps, while the other source areas could give a contribution in the order of the 20-10 % or be negligible. Despite some uncertainties, we can demonstrate the importance of the complex interplay between tectonic processes, climate and erosion, on the short-term erosion pattern on the light of the relative sediment load supplied in the last 10^2–10^5 years from the North-Western Alps or more precisely from a smaller portion of it, where erosion rates are one order of magnitude higher than in neighbour areas.

REFERENCES

Abbate E., Bortolotti V., Passerini P., Sagri M., 1970. Introduction to the geology of the Northern Apennines. Sedimentary Geology, 4, 207-249.

Abbate, E. & Sagri, M. 1984. Le unità torbiditiche cretacee dell'appennino settentrionale ed i margini continentali della Tetide. Memorie della Società Geologica Italiana, 24, 359–375.

Aleinikoff J.N., Moench R.H., Lyons J.B., 1985. Carboniferous U-Pb age of the Sebago batholith south-western Maine: metamorphic and tectonic implications. Geological Society American Bulletin, 96, 990-996.

Allègre C.J., Albarède F., Grünenfelder M. and Köppel V., 1974. $^{238}U/^{206}Pb$-$^{235}U/^{207}Pb$-$^{232}Th/^{208}Pb$ zircon chronology in alpine and non-alpine environment. Contributions to Mineralogy and Petrology , 43,163–194.

Allen, P.A. and Hovious, N., 1998. Sediment supply from landslide-dominated catchments: implications for basin reflect changes in tectonic boundary conditions, and thus margin fans. Basin Research., 10, 9–35.

Amidon, W.H., Burbank, D.W. and Gehrels, G.E., 2005. U-Pb zircon ages as a sediment mixing tracer in the Nepal Himalaya. Earth Planet Science Letters, 235, 244-260.

Andersen T., 2002. Correction of common lead in U–Pb analyses that do not report ^{204}Pb. Chemical Geology, 192, 59-79.

Barbier, R., 1948. Les Zones Ultra-Dauphinoise et Subbriançonnaise entre l'Arc et l'Isère. mémoire pour servir à l'explication de la carte géologique détaillée de la France ». Rapport technique, Ministère de la Production Industrielle.

Bearth, P., 1967. Die Ophiolite der Zone von Zermatt-Saas-Fee. Beitr. Geol. Karte Schweiz, 132, 1-130.

Beaumont C., Fullsack P., Hamilton J. 1992. Erosional control of active compressional orogens. edited by: K. McClay In Thrust Tectonic,. 1-18.

Benisek A., Finger F., 1993. Factors controlling the development of prism faces in granite zircons: a microprobe study. Contributions to Mineralogy and Petrology, 114, 441-451.

Bernet, M. and Spiegel, C., 2004. Detrital Thermochronology– Provenance Analysis, Exhumation, and Landscape Evolution of Mountain Belts. Geological Society of America, Special Paper, 378.

Bernet, M., Brandon, M.T., Garver, J.I., and Molitor, B., 2004a. Downstream changes of Alpine zircon fission-track ages in the Rhône and Rhine Rivers. Journal of Sedimentary Research, 74, 82-94.

Bernet, M., Brandon, M.T., Garver, J.I., and Molitor, B., 2004b. Fundamentals of detrital zircon fission-track analysis for provenance and exhumation studies with examples from the European Alps. in Bernet, M. and Spiegel, C. eds. Detrital thermochronology-Provenance analysis, exhumation, and landscape evolution of mountain belts. Boulder, Colorado. Geological Society of America Special Paper, 378, 25-36.

Bertrand, J.M., Guillot, F., Laterrier, J., Perruchot, M.P., Aillères, L., and Macaudière, J., 1998. Granitoids from the “Zone Houillère Briançonnaise” (Savoie and Valle d'Aosta, western Alps): geology and U-Pb geochronology. Geodinamica Acta, 11, p. 33-49.

Bigi G.,. Castellarin A, Coli M., Dal Piaz G. V., Sartori M., Scandone P., and Vai G. B., 1990. Structural Model of Italy, SELCA, Florence, Italy.

Black L.P, Williams I.S and Compston W., 1986. Four zircon ages from one rock: the history of a 3939 Ma-old granulite from Mt. Sones, Enderby Land, Antarctica. Contribution of Mineralogy Petrology, **94,** 427–437.

Bondesan, M., Favero, V., Viňals, M.J., 1995b. New evidence on the evolution of the Po-delta coastal plain during the Holocene. Quaternary International, 29/30, 105-110.

Bruguier O., Lancelot J.R., Malavieille J., 1997. U–Pb dating on single detrital zircon grains from the Triassic Songpan–Ganze flysch (Central China): provenance and tectonic correlations, Earth and Planetary Science Letters, 152, 217-231.

Burbank D.W, 2002. Rates of erosion and their implications for exhumation. Mineralogical Magazine, 66, 25-52.

Campbell I. H., Reiners P. W., Allen C. M., Nicolescu S., Upadhyay R., 2005. He–Pb double dating of detrital zircons from the Ganges and Indus Rivers: Implication for quantifying sediment recycling and provenance studies. Earth and Planetary Science Letters, 237, 402-432.

Carter, A. and Bristow C.S., 2000. Detrital zircon geochronology: enhancing the quality of sedimentary source information through improved methodology and combined U-Pb and fission-track techniques. Basin Research, 12, 47-57.

Carter, A. and Moss S.J., 1999. Combined detrital-zircon fission-track and U-Pb dating: a new approach to understanding hinterland evolution. Geology, 27, 235-238.

Castellarin, A. 2001. Alps-Apennines and Po Plain-Frontal Apennines Relationships. In: VAI, G. B. & MARTINI, I. P. (eds) Anatomy of an Orogen. Kluwer Academic Publishers, 177–196.

Cawood, P.A., Nemchin, A.A., Freemanc, M., Sircombe, K.N., 2003. Linking source and sedimentary basin: detrital zircon record of sediment flux along a modern river system and implications for provenance studies. Earth and Planetary Science Letters, 210, n.1-2, 259-268.

Chakoumakos B., C., Takashi M., Lumpkin G., R., Ewing R. C., 1987. Alpha-Decay—Induced Fracturing in Zircon: The Transition from the Crystalline to the Metamict State. Science, 236, 1556-1559.

Clari, P., Dela F., Novaretti, A., Timpanelli, M., 1995. Late Oligocene-Miocene sedimentary evolution of the critical Alps/Apennines junction: the Monferrato area. Northwestern Italy. Terra Nova, 7, 144-152.

Clift, P.D., Lee J.L., Hildebrand, P., Shimizu, N., Layne, G.D., Blusztajn, J., Blumc, J.D., Garzanti, E., Khane, A.A., 2002. Nd and Pb isotope variability in the Indus River System: implications for sediment provenance and crustal heterogeneity in the Western Himalaya. Earth and Planetary Science Letters, 200, n. 1-2, 91-106.

Compston W., Williams I.S., Meyer C., 1984. U-Pb geochronology of zircons from lunar breccia 73217 using a sensitive high mass-resolution ion microprobe. J Geophysical Research 89 Supp, p B525-B534.

Compston W.,1999. Geological age by instrumental analysis: the 29th Hallimond Lecture. Mineral Mag 63, 297-311.

Corfu, F., Hanchar, J.M., Hoskin, P.W.O., Kinny, P., 2003. Atlas of zircon textures. Reviews in Mineralogy and Geochemistry, 53, 1, 469-500.

Correggiari A., Cattaneo A., Trincardi F., 2005. The modern Po Delta system: Lobe switching and asymmetric pro-delta growth. Marine Geology, 222-223, 49-74.

Coward M.and Dietrich D.,1989. Alpine tectonics-an overview, *Geol. Soc. London Spec. Publ. 45*, ,in: M.P. Coward, D. Dietrich, R.G. Park, Editors , *Alpine Tectonics* 1–29;

Dal Cin, R., 1983. I litorali del delta del Po e alle foci dell'Adige e del Brenta: caratteri tessiturali e dispersione dei sedimenti, cause dell'arretramento e previsioni sull'evoluzione futura. Bollettino della Società Geologica Italiana, 102, 9- 56.

Dallagiovanna G, Gaggero L, Maino M, Seno S, Tiepolo M., 2009. U-Pb zircon ages for post-Variscan volcanism in the Ligurian Alps (Northern Italy). Journal of the Geological Society 166(1), 101–114.

Davis D.W., Williams I.S., and Krogh T.E., 2003. Zircon in geochronology: laser Ablation ICPMS. Reviews in Mineralogy & Geochemistry, 53, 244-275

Davis, D. W., 1982. Optimum linear regression and error estimation applied to U–Pb data. Canadian Journal of Earth Sciences, 19, 2141-2149.

Deer, W.A., Howie, R.S., and Zussman, J., 1982. Rock-Forming Minerals, 1A, Orthosilicates, second ed., London, Geological Society.

Devismes, P., 1978. Atlas photographique des minéraux d'alluvions. Mémoires du Bureau de Recherches Géologiques et Minières 95, 203 p.

Di Giulio A., 1999. Mass transfer from the Alps to the Apennines: volumetric constraints in the provenance study of the Macigno–Modino source–basin system, Chattian–Aquitanian, northwestern Italy, Sedimentary Geology, 124, 69-80.

Doglioni C.,Mongelli, F. and Pialli, G. 1998. Boudinage of the Alpine belt in the Apenninic back-arc. Memorie della Società Geologica Italiana, 52, 457–468.

Doglioni, C., Gueguen, E. Harabaglia, P., Mongelli, F., 1999. On the origin of west-directed subduction zones and applications to the western Mediterranean. Geological Society, London, Special Publications, 156, 541-561.

Dunkl I., Di Giulio A., and Kuhlemann J., 2001. Combination of single-grain fission-track chronology and morphological analysis of detrital zircon crystals in provenance studies-sources of the Macigno Formation (Apennines, Italy). Journal of Sedimentary Research, 71,516-525.

Ellenberger, F., 1958. Etude géologique du pays de Vanoise (Savoie). Mém. Service Carte Géol. France, 50, 561 p.

Elter, P. 1975. Introduction à la gèologie de l'Apennin septentrional. Bulletin de la Sociète Géologique de France, 7, 956–962.

Engi, M.. Bousquet, R.. and Berger, A. 2004. Explanatory notes to the map: metamorphic structure of the Alps. Central Alps. Mitt. Österr. Miner. Ges., 149, 157-173.

Enkelmann, Eva Weislogel, Amy Ratschbacher, Lothar Eide, Elizabeth Renno, Axel Wooden, Joseph, 2007. How was the Triassic Songpan-Ganzi basin filled? A provenance study. Tectonics, 26, TC4007, doi:10.1029/2006TC002078.

Ewing R., C., 1993. The metamict state: 1993- the centennial. Nuclear Instruments and Methods in Physics Research Section, 91, 22- 29.

Faccenna C., Becker T. W., Lucente, F. P., Jolivet, L. and Rossetti, F. 2001. History of subduction and back-arc extension in the Central Mediterranean. Geophysics Journal International, 145, 809–820.

Faure G., 1986. Principles of Isotope Geology, 2nd ed., John Wiley & Sons New York, Chichester, Brisbane, Toronto, Singapore, 589 pp.

Feng R., Machado N., Ludden J., 1993. Lead geochronology of zircon by LaserProbe-Inductively coupled plasma mass spectrometry (LP-ICPMS). Geochimica et Cosmochimica Acta 57, 3479-3486.

Fleischer M., Altschuler Z.S., 1969. The relationship of the rare-earth composition of minerals to geological environment. Geochimica et Cosmochimica Acta, 33, 725-732.

Fleischer R.L, Price P.B., Walker, R.M., 1975. Effects of temperature, pressure and ionization on the formation and stability of fission tracks in minerals and glasses. Journal of Geophysical Research 70, 1497-502.

Frey, M.. Desmons, J.. and Neubauer, F. 1999. The new metamorphic map of the Alps. Schweiz. Mineral. Petrogr. Mitt., 79, 1-209.

Fryer B.J., Jackson S.E., Longerich H.P., 1993. The application of laser ablation microprobe inductively coupled plasma mass spectrometry (LAM-ICPMS) to in situ (U)-Pb geochronology. Chemical Geology 109, 1-8.

Gandolfi G., Mordenti A., and L. Paganelli, 1982. Composition and longshore dispersal of sands from the Po and Adige rivers since the pre-Etruscan age, Journal of Sedimentary Petrology, 52, 797-805.

Garver J. I, 2003. Etching zircon age standards for fission-track analysis, Radiation Measurements, 37, 47-53.

Garver J., I., Kamp P., J.,J., 2002. Integration of zircon color and zircon fission-track zonation patterns in orogenic belts: application to the Southern Alps, New Zealand. Tectonophysics, 349, 203-219.

Garzanti E. and Malusà M.G., 2008. The Oligocene Alps: domal unroofing and drainage development during early orogenic growth. Earth and Planetary Science Letters, 268, 487-500.

Garzanti E., Canclini S., Moretti Foggia F., and Petrella N., 2002. Unraveling magmatic and orogenic provenance in modern sand; the back-arc side of the Apennine thrust belt, Italy. Journal of Sedimentary Research, 72, 2-17.

Garzanti, E., Andò, S., Vezzoli, G., 2008. Settling equivalence of detrital minerals and grain-size dependence of sediment composition. Earth and Planetary Science Letters, 273, 138–151.

Garzanti, E., Andò, S., Vezzoli, G., 2009. Grain-size dependence of sediment composition and environmental bias in provenance studies. Earth and Planetary Science Letters, 277, 422–432.

Garzanti, E., Vezzoli, G., Lombardo, B., Andò, S., Mauri, E., Monguzzi, S., 2004a. Collision-orogen provenance (western Alps).: detrital signatures and unroofing trends. Journal of Geology, 112, 145-164.

Gastil, G.R., De Lisle, M., Morgan, J.R., 1967. Some Effects of Progressive Metamorphism on Zircons. Geological Society of America Bulletin, 78, 879-906

Gebauer D. and Grünenfelder M., 1976. U-Pb zircon and Rb-Sr whole-rock dating of low-grade metasediments -Example: Montagne Noire (southern France). Contribution Mineralogy and Petrology, **59,** 13–32.

Gleadow A.J.W., Hurford A.J., Quaife R.D., 1976. Fission track dating of zircon: Improved etching techniques, Earth and Planetary Science Letters, 33, Issue 2, 273-276.

Guillot F., Schaltegger U., Bertrand J., Deloule E., Baudin T., 2002. Zircon U-Pb geochronology of Ordovician magmatism in the polycyclic Ruitor Massif (Internal W Alps). International Journal of Earth Sciences, 91, 964-978.

Guillot F., Schaltegger U., Bertrand J.M., Deloule E. and Baudin T., 2002. Zircon U-Pb geochronology of Ordovician magmatism in the polycyclic Ruitor Massif (Internal W Alps). International Journal of Earth Sciences, 91, 964–978.

Hanchar J.M and Miller C.F, 1993. Zircon zonation patterns as revealed by cathodo-luminescence and backscattered electron images: implications for interpretation of complex crustal histories. Chemical Geology, 110, 1-14.

Handy M.R., Streit J.E., 1999. Mechanics and mechanisms of magmatic underplating: inferences from mafic veins in deep crustal mylonite, Earth and Planetary Science Letters, 165, 3-4, 271-286.

Hänny R., Grauert B. and Soptrayanova G., 1975. Paleozoic migmatites affected by high-grade Tertiary metamorphism in the Central Alps (Valle Bodengo, Italy), Contributions to Mineralogy and Petrology , 51A, Geochronological Study (3rd ed.), 173–196.

Hansmann, W., and F. Oberli (1991), Zircon inheritance in an igneous rock suite from the southern Adamello Batholith (Italian Alps): Implications for petrogenesis, Contributions to Mineralogy and Petrology , 107, 501 – 518.

Hunziker J.C, Desmons J., and Hurford A.J. et al., 1989. Thirty-two years of geochronological work in the Central and Western Alps: a review on seven maps. Mémoires de Géologie (Lausanne), 13, pp 59.

Ireland T.,1999. New tools for isotopic analysis: Science 286, 2289-2290.

Jackson S.E., Longerich H.P., Horn I., Dunning R., 1996. The application of laser ablation microprobe (LAM)-ICP-MS to in situ U-Pb zircon geochronology. J Conf Abstr 1, 283.

Jackson, S.E., Pearsona, N.J., Griffina, W.L., and Belousovaa, E.A., 2004. The application of laser ablation-inductively coupled plasma-mass spectrometry to in situ U–Pb zircon geochronology. Chemical Geology, 211, 47-69.

Jeffries, T. E., Fernandez-Suarez, J., Corfu F., Gutierrez A. G. 2003. Advances in U-Pb geochronology using a frequency quintupled Nd:YAG based laser ablation system λ= 213 nm) and quadrupole based ICP-MS. Journal of Analytical Atomic Spectrometry, 18, 847- 855.

Jinying Q., 1982. Pethrochemestry of Mesozoic volcanic rocks in the Chu County, Anhui province and the characteristies of Plagioclases. Chinese Journal of Geology.

John, B. E., and Blundy J. D., 1993. Emplacement related deformation of granitoid magmas, southern Adamello Massif, Italy, Geological Society of America Bulletin, 105, 1517 – 1541.

Koeppel V., 1974. Isotopic U-Pb ages of monazites and zircons from the crust-mantle transition and adjacent units of the Ivrea and Ceneri zones (Southern Alps, Italy). Contributions to Mineralogy and Petrology , 43, 55–70.

Konstantinovskaia, E., and Malavieille, J., 2005. Erosion and exhumation in accretionary orogens: Experimental and geological approaches: Geochemistry Geophysics Geosystems, 6, Q02006, doi: 10.1029/2004GC000794.

Koscher, G., 1993. Origin and significance of the SEM cathodoluminescence from zircon. Journal of Microscopy, 171, 223-232.

Krogh T.,E, 1982. Improved accuracy of U-Pb zircon ages by the creation of more concordant systems using an air abrasion technique. Geochimica et Cosmochimica Acta. 46, 637- 649.

Kröner A., Jaeckel P., Williams I.S., 1994. Pb-loss patterns in zircons from a high-grade metamorphic terrain as revealed by different dating methods: U-Pb and Pb-Pb ages for igneous and metamorphic zircons from northern Sri Lanka. Precambrian Research, 66, 151-181.

Lanyon R., Black R. P., and Seitz H.-M., 1993. U-Pb zircon dating of mafic dykes and ist application to the Proterozoic geological history of the Vestfold Hills, East Antarctica. Contributions to Mineralogy and Petrology, 115, 184-203

Laubscher, H. P., 1983a. The late alpine (Periadriatic) intrusions and the Insubric Line, Memorie Società Geologica Italiana, 26, 21 – 30.

Lee J. K. W., Williams, I. S., Ellis, D. J., 1997. Pb, U and Th diffusion in natural zircon, Nature, 390, 159-162.

Lee J., K., W., Tromp, J., 1995. Self-induced fracture generation in zircon. Journal of Geophysical Research, 100, 17753-17770.

Liati A., Gebauer D., Fanning M., 2000. U-Pb SHRIMP dating of zircon from the Novate granite (Bergell, Central Alps): evidence for Oligocene-Miocene magmatism, Jurassic/Cretaceous continental rifting and opening of the Valais trough. Schweizerische mineralogische und petrographische Mitteilungen, 80, 305-316.

Ludwig K.R, 1980. Calculation of uncertainties of U-Pb isotope data. Earth and Planetary Science Letters, 46, 212–220.

Lustrino, M., Morra, V., Melluso, L., Fedele, L., Franciosi, L., 2009. The beginning of the Apennine subduction system in central-western Mediterranean: constraints from Cenozoic “orogenic” magmatic activity of Sardinia (Italy). Tectonics 28, TC5016.doi:10.1029/2008TC002419.

Malavieille J., 2010. Impact of Erosion, Sedimentation and Structural Heritage on the Structure and Kinematics of Orogenic Wedges: Analog Models and Case Studies. Geological Society America 20, 4-10.

Malusà M. G., Faccenna C., Garzanti E., Polino R., 2011. Divergence in subduction zones and exhumation of high pressure rocks (Eocene Western Alps), Earth and Planetary Science Letters, 310, 21-32.

Malusà, M.G. and Vezzoli, G., 2006. Interplay between erosion and tectonics in the Western Alps. Terra Nova, 18, 104-108.

Malusà, M.G., Zattin, M., Andò, S., Garzanti, E., and Vezzoli, G., 2009a. Focused erosion in the Alps constrained by fission-track ages on detrital apatites. Geological Society, London, Special Publications, 324, 141-152.

Mange M., A., and Maurer H., F., W., 1992. Heavy minerals in colour. Chapman & Hall (London and New york), 147 p.

Marroni, M., Della Croce, G. and Meccheri, M., 1988. Structural evolution of the M.Gottero Unit in the M.Zatta/M.Ghiffi sector. Ofioliti, 13, 29–42.

Marshall D.J., 1988. Cathodoluminescence of geological materials. Unwin Hyman, London.

Mattinson J., M., 1996. Zircon U–Pb chemical abrasion ("CA-TIMS") method: Combined annealing and multi-step partial dissolution analysis for improved precision and accuracy of zircon ages. Chemical Geology, 220, 47- 66.

Ménard and P. Molnar, 1988. Collapse of a Hercynian Tibetan plateau into a late Palaeozoic European basin and range province. Nature (London), 334,. 235–237.

Mezger K., Krogstad E. J., 1997. Interpretation of discordant U-Pb zircon ages: An evaluation. Journal of Metamorphic Geology, 15, 1, 127–140.

Miller B. V., Fetter A. H. and Stewart K. G., 2006. Appalachians Plutonism in three orogenic pulses, Eastern Blue Ridge Province, southern Geological Society of America Bulletin, 118, 1-2, 171-184.

Milliman, J.D., and Meade, R.H., 1983. World-wide delivery of river sediments to the oceans. Journal of Geology, 91, 1-21.

Molli G., 2008. Northern Apennine-Corsica orogenic system; an updated overview. Geological Society Special Publications, 298, 413-442.

Morton A.C., Claoué-Long J.C., Berge C., 1996. SHRIMP constraints on sediment provenance and transport history in the Mesozoic Statfjord Formation, North Sea. Journal Geological Society of London 153, 915-929.

Moser D.E., Heaman L.M., Krogh T.E., Hanes J., A., 1996. Intracrustal extension of an Archean orogen revealed using single-grain U-Pb zircon geochronology. Tectonics, 15, 1093-1109.

Müller B., Klötzli U., Flisch M., 1995. U-Pb and Pb-Pb zircon dating of the older orthogneiss suite in the Silvretta nappe, eastern Alps: Cadomian magmatism in the upper Austro-Alpine realm. Geology, 84, 457-465.

Murakami T., Chakoumakos B.C., Ewing R.C., Lumpkin G.R., Weber W.J., 1991. Alpha-decay event damage in zircon. American Mineralogist, 1510-1532.

Naeser, C.W., 1979. Fission track dating and geological annealing of fission tracks, E. Jager, J.C. Hunziker, Editors , Lectures in Isotope Geology, Springer-Verlag, New York ,154–169.

Nasdala L., Wenzel M., Vavra G., Irmer G., Wenzel T. and Kober B., 2001. Metamictization of natural zircon: accumulation versus thermal annealing of radioactivity-induced damage. Contribution of Mineralogy and Petrology, 141, 25–144.

Naylor, R.S., Steiger, R.H., Wasserburg, G.J., 1970. U-Th-Pb and Rb-Sr systematics in 2.7 b.y. old plutons from the southern Wind River Range, Wyoming. Geochimica et Cosmochimica Acta, 34, 1133-1159.

Nelson, B.W., 1970. Hydrography, sediment dispersal and recent historical development of the Po River Delta, Italy. In: Morgan, J.P. (Ed.), Deltaic Sedimentation, Modern and Ancient. SEPM Special Publications 15, 152–184.

Nemchin, A.A., and Cawood, P.A., 2005. Discordance of the U–Pb system in detrital zircons: Implication for provenance studies of sedimentary rocks. Sedimentary Geology, 182, 143-162.

Paquette J.-L., Chopin C. and Peucat J.-J., 1989. U-Pb zircon, Rb-Sr and Sm-Nd geochronology of high to very high pressure meta-acidic rocks from the Western Alps. Contributions to Mineralogy and Petrology , 101, 280–289.

Parfenoff, A., Pomerol, C., Tourenq, J., 1970. Les minéraux en grains, méthodes d'étude et détermination. Masson eds, Paris, 578 p.

Pfiffner, O. A., Schlunegger F., and Buiter S. J. H., 2002. The Swiss Alps and their peripheral foreland basin: Stratigraphic response to deep crustal processes, Tectonics, 21(2), 1009, doi:10.1029/2000TC900039.

Pin, C. Rodriguez, J., 2009. Comment on "Rheic Ocean ophiolitic remnants in southern Iberia questioned by SHRIMP U-Pb zircon ages on the Beja-Acebuches amphibolites" by A. Azor et al. Tectonics 28, 5 TC5013, doi:10.1029/2009TC002495.

Polino, R., Dal Piaz, G.V., and Gosso, G., 1990. An accretionary wedge model for the pre-collisional Cretaceous orogeny in the Alps. Mémoire Societé Géologique France, 156, 309-321.

Principi, G. and Treves, B. 1985. Il sistema corso-appenninico come prisma d’accrezione. Riflessi sul problema generale del limite Alpi-Appennini. Memorie della Società Geologica Italiana, 28, 549–576.

Pupin, J.P., 1980. Zircon and granite petrology. Contribution to Mineralogy and Petrology, 71, 207-220.

Rahaman W., Singh S. K., Sinha R. and Tandon S.K., 2009. Climate control on erosion distribution over the Himalaya during the past ~100 ka. Geology, Downloaded from geology.gsapubs.org on 5 June 2009.

Rahn M.K, Brandon M.T., Batt G.E., and Garver J.I., 2004. A zero-damage model for fission-track annealing in zircon. American Mineralogist, 89, 473-484.

Rampone E., Hoffman A.W. and Raczek I., 1998. Isotopic contrasts within the Internal Liguride ophiolite (N. Italy) the lack of a genetic mantle-crust link. Earth and Planetary Science Letters, 163, 175–189.

Reiners P. W. and Brandon M. T., 2006. Using Thermochronology to understand orogenic erosion. Annual Review of Earth and Planetary Sciences, 34, 419-466.

Resentini A.and Malusà M.G., 2011. Sediment budgets by detrital apatite fission rack dating (Rivers Dora Baltea and Arc, Western Alps). GSA special publication in press.

Ricci Lucchi F., 1986. The Oligocene to Recent Foreland Basins of the Northern Apennines. Foreland Basins, 103-139.

Ring U. and Collins A. S., 2005. U-Pb SIMS dating of synkinematic granites: timing of core-complex formation in the northern Anatolide belt of western Turkey. Journal of the Geological Society of London, 162, 289–298.

Roback R.C. and Walker N.W., 1995. Provenance, detrital zircon U-Pb geochronometry, and tectonic significance of Permian to Lower Triassic sandstone in south-eastern Quesnellia. British Columbia and Washington Geological Society of America Bulletin. 107, 665-675.

Rosenberg C.L., 2004. Shear zones and magma ascent: A model based on a review of the Tertiary magmatism in the Alps. Tectonics, 23, TC3002, 21 pp.

Roure F, Heitzmann P and Polino R, 1990. Deep structure of the Alps. Volume Speciale Società Geololica Italiana**,** 1**,** 1–367.

Roure, F., Bergerat, F., Damotte, B., Mugnier, J.L., Polino, R., 1996. The ECORS-CROP Alpine seismic traverse. Mémoire Societé Géologique France, 170,pp.113.

Rubatto D. and Hermann J., 2003. Zircon formation during fluid circulation in eclogites (Monviso, Western Alps): implications for Zr and Hf budget in subduction zones. Geochimica et Cosmochimica Acta, 67, 2173–2187.

Rubatto D., Gebauer D. and Compagnoni R., 1999. Dating of eclogite-facies zircons: the age of Alpine metamorphism in the Sesia–Lanzo Zone (Western Alps). Earth and Planetary Science Letters, 167, 141–158.

Rubatto D., Scambelluri M. 2003. U-Pb dating of magmatic zircon and metamorphic baddeleyite in the Ligurian eclogites (Voltri Massif, Western Alps). Contributions to Mineralogy and Petrology, 146, 341-355.

Rubatto, D., Gebauer, D., and Fanning, M., 1998. Jurassic formation and Eocene subduction of the Zermatt–Saas–Fee ophiolites: implications for the geodynamic evolution of the Central and Western Alps. Contributions to Mineralogy and Petrology , 132, 269-287.

Schaltegger U., Brack P., Ovtcharova M., Peytcheva I., Schoene B., Stracke A., Marocchi M. and Bargossi G.M., 2009. Zircon and titanite recording 1.5 million years of magma accretion, crystallization and initial cooling in a composite pluton (southern Adamello batholith, northern Italy). Earth and Planetary Science Letters, 286, 208–218.

Schaltegger, U., 1993. The evolution of the polymetamorphic basement in the Central Alps unravelled by precise U−Pb zircon dating. Contributions to Mineralogy and Petrology, 113, 466- 478.

Schmid, S.M., and Kissling, E., 2000. The arc of the western Alps in the light of geophysical data on deep crustal structure. Tectonics, 19, 62-85.

Silver L.T., Deutsch S., 1963. Uranium-Lead isotopic variations in zircons: a case study. The Journal of Geology, 71, 721-758.

Sircombe K.N., 2004. Age display: an EXCEL workbook to evaluate and display univariate geochronological data used binned frequency histograms and probability density distributions. Computer & Geosciences, 30, 21–31.

Sláma J., Košler J., Condon D.J., Crowley J.L., Gerdes A., Hanchar J.M., Horstwood M.S.A., Morris G.A., Nasdala L., Norberg N., Schaltegger U., Schoene B., Tubrett M.N., Whitehouse M. J., 2008. Plešovice zircon- A new natural reference material for U–Pb and Hf isotopic microanalysis. Chemical Geology, 249, 1-35.

Speer J.A., 1980. Zircon. in Orthosilicates, Ribbe, Reviews in Mineralogy, 5, 67-112.

Stampfli G.M., Mosar J., Marquer D., Marchant R., Baudin T., Borel G. 1998. Subduction and obduction processes in the Swiss Alps. Tectonophysics, 296, 159-204.

Stern R.A, Sanborn N. and Bleeker W., 1998. Exploiting the high spatial sensitivity of the ion micoprobe in studying Pb-loss mechanisms and U–Pb ages of metamict and altered zircon, . EOS Trans. AGU, 79, F951 Fall Mtg. Suppl.

Tilton G.R., Schreyer W. and. Schertl H.P., 1989.Pb-Sr-Nd isotopic behaviour of deeply subducted crustal rocks from the Dora Maira massif, Western Alps, Italy. Geochimica et Cosmochimica Acta, 53, 1391–1400.

Treves, B. 1984. Orogenic belts as accretionary prisms: the example of the Northern Apennines. Ofioliti, 9, 577–618.

Vavra, G., 1993. Systematics of internal zircon morphology in major Variscan granitoid types. Contributions to Mineralogy and Petrology, 117, 4, 331-344.

Vermeesch P., 2004. How many grains are needed for a provenance study?. Earth Planetary Science Letters, 224, 351–441.

Vernon A.J., van der Beek P.A., Sinclair H.D., Rahn M.K., 2008. Increase in late Neogene denudation of the European Alps confirmed by analysis of a fission-track thermochronology database. Earth and Planetary Science Letters, 270, 316–329.

Von Raumer, J.F., Ménot, R.P., Abrecht, J., and Biino, G. ,1993. The Pre-Alpine evolution of the External Massifs. in von Raumer, J. F., and Neubauer, F., eds. Pre-Mesozoic geology in the Alps. Berlin, Springer.

Wang X., Griffin W., L., O'Reilly S., Y., Zhou X., M., Xu X., S., Jackson S., E., and Pearson N., J., 2002. Morphology and geochemistry of zircons from late Mesozoic igneous complexes in coastal SE China; implications for petrogenesis. Mineralogical Magazine, 66, 235-251.

Wetherhill G.W., 1956a. Discordant uranium-lead ages, Transaction American Geophysical Union 37, 320-326.

Wetherhill G.W., 1956b. An interpretation of the Rhodesia and Witwatersrand age patterns. Geochimica et Cosmochimica Acta, 9, 290-292.

Willett S., Beaumont C., and Fullsack P., 1993. Mechanical model for the tectonics of doubly vergent compressional orogens. Geology, 21, 371-374.

Williams I.S, 1992. Some observations on the use of zircon U–Pb geochronology on the study of granitic rocks. Transaction of Royal Society. 83, 447-458.

Williams I.S.,1998. U-Th-Pb geochronology by ion microprobe. Rev Econ Geol 7, 1-35.

Yaoling QYZ, 1985. Mineralogy and trace element study of trachytic basalt, Gaoquiao destrict, Shandong. Journal of Mineralogy and Petrology.

Zeitler P.K., Meltzer A.S., Koons P.O., Craw D., Hallet B., Chamberlain C.P., Kidd W.S.F., Park S.K., Seeber L., Bishop M. and Shroder J., 2001. Erosion, Himalayan geodynamics, and the geomorphology of metamorphism, GSA Today, 11, 4-9.

ACKNOWLEDGMENTS

Marco Malusà, Eduardo Garzanti, Sergio Andò and Giovanni Vezzoli, are sincerely acknowledged for all their support and precious discussions through these years.

Andy Carter is kindly acknowledged for fruitful and formative period spent in the Laboratory of Thermochronology at the Birkbeck College of London,

François Guillot is heartily acknowledged for introducing me to the techniques of zircon typology and for his patient and careful reviews of this manuscript.

I would like to thank also Pio Norelli of the Pisa CNR for useful suggestions about fission tracks techniques, and Valeria Caironi of the University of Milano for helpful discussions about zircon typology. Andy Beard and Philippe Recourt are kindly acknowledged for allowing to improve analysis of detrital zircons with cathodoluminescence and BSE imaging presented in this work. Constructive discussions with Pieter Vermeesch and Igor Villa are also warmly acknowledged.

Marta Padoan, Alberto Resentini, Valentina Bracchi, Serena Lari, Paolo D'Adda and Stefano Basiricò are thanked for their help and friendship.

Then, I would like to thank my fellow PhD friends for helpful and passionate discussions on our present and future projects (Nikolaos Michail, Laura Gregory, Daniele Regis, Paola Manzotti, Deborah Donatio and Ajit Singh).

Thanks to all my friends Angela, Davide, Michele, Madda e Matti, Isadora, Rosa, Giuditta, Lorenza, Maggio, Sara, Claire, Josie Martha and Anna for sharing the lively experience in these years and for "joining the R-evolution" (cit.).

At least (but first in my thoughts) thanks to Angelino for his support and care.

Thanks to my parents, my sister and Teresa for having confidence in my projects, and thanks to my grandmothers and to the loving memory of my grandfathers for making these things happen.

Part V
Appendix

SAMPLE		SAMPLING		% CUMULATE						PERCENTILI					GRAIN-SIZE PARAMETERS				%AW/
cod	N°	River	Locality	**phi -1**	**phi 0**	**phi +1**	**phi +2**	**phi +3**	**phi +4**	**5**	**16**	**50**	**84**	**95**	**Dm**	**σφ**	**Sk1**	**AW**	tot>2
S3098	**D1**	Po	Boccasette	0	0.02	0.09	9.88	97.43	99.1	1.2	2	2.5	2.7	3	2.4	0.45	-0.44	63-250	89.22
S3403	**D2**	Po	Barricata	0	0	0.01	16.9	98.05	99.93	1.5	2	2.5	2.8	2.9	2.43	0.41	-0.34	63-250	83.02
S3097	**D3**	Po	Bonelli	0	0	0.08	18.68	99.17	99.93	2	2.2	2.4	2.7	2.9	2.43	0.26	0.16	63-250	81.25
S4073	**D4**	Po	Bacucco	0	0	0.02	46.32	99.94	99.99	1	1.9	2	2.8	2.9	2.23	0.51	0.36	63-250	53.67
S3926	**P1**	Po	Torre Beretti	0	0.18	2.59	20.87	72.16	93.43	1	1.8	2.6	3.6	4.2	2.67	0.93	0.06	63-250	72.56
S3927	**P2**	Tanaro	Rivarone	0	0.43	1.09	4.74	43.29	74.42	1.7	2.4	3	4.5	6	3.3	1.18	0.41	63-250	69.68
S3505	**P3**	Po pre Ticino	Casei Gerola	0	2.62	5.46	24.28	24.28	88.91	1	1.8	2.5	3.8	4.5	2.7	1.03	0.22	63-250	64.63
S4208	**P4**	Ticino	bereguardo		0.03	6.89	87.45	99.41	99.9	1	1.3	1.7	2.2	2.6	1.733	0.47	0.118	63-250	12.44
S4057	**P5**	Po	Zerbo	0	0.04	0.22	50.56	96.9	99.09	1.1	1.4	2	2.8	3.3	2.07	0.68	0.16	63-250	48.53
S3513	**S1**	Oglio	Rogno	0	5.75	35.59	88.1	97.23	98.6	0	0.45	1.3	1.95	2.5	1.23	0.75	-0.09	63-250	10.5
S3506	**S2**	Adda	Dubino	0	0.14	0.98	42.38	42.38	97.46	1.2	1.5	2.2	3.3	3.9	2.33	0.86	0.24	63-250	55.09
S3510	**S3**	Ticino	Bellinzona	0	1.69	14.02	61.38	61.38	98.08	0.3	1.1	1.9	3.1	3.8	2.03	1.03	0.14	63-250	36.7
S3554	**S4**	Toce	Masera	0	2.41	16.87	40.33	40.33	89.72	0.5	1	2.4	3.6	4.5	2.33	1.26	-0.01	63-250	49.39
S3553	**S5**	Sesia	Romagnano	0	0.27	8.75	74.12	99.28	99.94	0.6	1.2	1.6	2.5	2.9	1.77	0.67	0.26	250-500	65.37
S3603	**S6**	Dora Baltea	Quassolo	0	0.38	6.18	51.39	51.39	97.54	0.9	1.2	2	3	3.5	2.07	0.84	0.13	63-250	46.15
S3556	**S7**	Orco	Cuorgnè	0	8.64	58.27	93.48	98.37	99.76	-0.3	0.3	0.9	1.8	2.4	1	0.78	0.16	250-500	35.21
S3520	**S8**	Dora Riparia	Avigliana	0	0.04	0.17	6.65	64.73	88.74	2	2.3	2.9	3.9	5	3.03	0.85	0.33	63-250	82.09
S3518	**S9**	Po	Revello	0	1.18	20.38	72.37	92.48	97.76	0.2	0.8	1.5	2.7	3.7	1.67	1.01	0.26	63-250	25.39
S3517	**S10**	Varaita	Costigliole S.	0	1.6	8.81	31.57	76.32	92.78	0.6	1.6	2.5	3.6	4.4	2.57	1.08	0.05	63-250	61.21
S3515	**S11**	Stura Demonte	Montanera	0	4.91	32.61	61.92	88.57	97.62	0.2	0.5	1.7	2.8	3.5	1.67	1.08	0.02	63-250	35.7
S3503	**S12**	Scrivia	Serravalle	0	0.52	7.52	57.9	90.2	97.26	0.7	1.2	1.9	2.8	3.5	1.97	0.82	0.13	63-250	39.36
S4014	**S13**	Trebbia	Rivergaro	0	0	1.1	42.6	95.03	98.34	1.2	1.6	2.1	2.75	3	2.15	0.56	0.07	63-250	55.74
S3719	**S14**	Taro	Fornovo	0	2.37	14.04	51.89	86.59	98.42	0.3	1.1	1.9	2.9	3.7	1.97	0.97	0.08	63-250	46.53
S4016	**S15**	Enza	S. Polo d'Enza	0	1.01	7.43	51.93	87.25	95.96	0.7	1.25	1.9	2.8	4	1.98	0.89	0.22	63-250	44.04
S4017	**S16**	Secchia	Sassuolo	0	1.73	5.42	17.77	60.78	83.75	1	1.9	2.6	4	4.7	2.83	1.09	0.23	63-250	65.98

Table 1. Grain-size parameters calculated after separation procedures. Dm-mean diameter, σφ-sigma φ; Sk1-skewness; AW-analysed window, %AW/tot>2- % analysed window/ bulk sediment> 2mm

	HEAVY MINERALS D 1.2> 3.3			SOURCE AREAS																								
	Observed Minerals	Description		Po Delta				Po Trunk					Central Alps				Western Alps							Northern Apennines				
		N//	NX	D1	D2	D3	D4	P1	P2	P3	P4	P5	S1	S2	S3	S4	S5	S6	S7	S8	S9	S10	S11	S12	S13	S14	S15	S16
most common heavy minerals	Garnet	High relief, colourless; pitted surface and conchoidal breakage patterns	isotropic character												few					few							
	Kyanite	Habit characteristic, elongated on Caxis combination of perfect cleavage and parting	moderate birefringence, large extinction angle PAO oblique between 27-32 °C	ab	few	ab	ab	ab	ab	com	ab	com		few	ab	ab	few			few	com	com	few			com		
	Monazite phosphates	High relief, rounded, egg-shaped or spherical morphology, colourless-to-pale amber, frequent surface pitting	Strong birefringence, strong absorption line in the yellow with pocket spectroscope		rr					rr			com	com						com			few	com		com		com
	Rutile	very high relief, yellow or red colour both N// and NX	striation or twinning		com					few				few	few		com								com		com	com
	Sphene	High lustre; extreme relief outline suorrounded by a dark rim	Strong birefringence, characteristic sky blue close to extinction point	com	com	com	com	ab	ab	com	ab	com		ab	com	com	com			ab	ab	ab	com	com	ab			
	Zircon	Extreme relief, characteristic morphology, colourless to pink/ yellow shade, possible inclusions	Strong birefringence; parallel extinction in elongated grains; uniaxial (+)	com	com	few	few	com	com	ab	com	com	few	com	com	com	ab	com	ab	com	few	few	ab	com	rr	few	ab	ab
	Zoisite	High relief; short prismotic habit	Moderate to low birefringence through the edges, anomalous interference colours slightly sky blue close to extinction, well-defined isogyres separate the field into blue and yellow sectors	few	ab	few	few	com	com		com	ab	ab	com		few				ab	ab	ab	few				few	few

Table 2. Observed heavy minerals in analysed samples and their optical properties. Occurrence of mineral grains ab- abundant ; com- common ; few- few ; rr- rare

	HEAVY MINERALS D 1.2> 3.3			SOURCE AREAS																								
	Observed Minerals	Description		Po Delta				Po Trunk					Central Alps				Western Alps							Northern Apennines				
		N//	NX	D1	D2	D3	D4	P1	P2	P3	P4	P5	S1	S2	S3	S4	S5	S6	S7	S8	S9	S10	S11	S12	S13	S14	S15	S16
others heavy minerals	Augite	high relief corrosion features eacth pits on C	Extinction is large 35°-40°, moderate birefringence																									
	Carbonate	extreme birefringence relief changes rotating microscope's stage	very high-order interference colours										com															
	Clinozoisite	High relief, prismatic habit, pale colours	anomalous interference tints PAO orthogonal to elongation of crystal										ab															
	Diopside	Prismatic morphology cleveages moderate to strong birefringence	High birefringence with concentric colour bands, extinction between 38°-48° biaxial (+) PAO // C																		few	com						
	Oxidized shells	well defined frame filled with pyrite or other oxides	isometric						ab																			com

Table 2. Observed heavy minerals in analysed samples and their optical properties. Occurrence of mineral grains ab- abundant ; com- common ; few- few ; rr- rare

Sample cod	Sample N°	River	Locality	ppm D>3.3 su tot<2	%Zr in mount	ppm Zr su tot<2	Zrn >GSW	**Zrn GSW**	Zrn <GSW	Corrected ppm Zrn
S3098	D1	Po	Boccasette	119	6.0	7.1	1.00	**97.00**	1.00	7.33
S3403	D2	Po	Barricata	925	3.0	27.7	1.00	**98.00**	1.00	28.31
S3097	D3	Po	Bonelli	908	4.0	36.3	0.00	**100.00**	0.00	36.34
S4073	D4	Po	Bacucco	91	2.0	1.8	-	-	-	-
S3926	P1	Po	Torre Beretti	3468	15.2	527.1	10.00	**71.00**	19.00	742.36
S3927	P2	Tanaro	Rivarone	127	40.8	51.7	6.00	**53.00**	40.00	97.60
S3505	P3	Po pre Ticino	Casei Gerola	1585	1.0	15.8	11.00	**66.00**	22.00	24.01
S4208	P4	ticino	bereguardo	626	4	25.0	-	-	-	-
S4057	P5	Po	Zerbo	734	1.0	7.3	-	-	-	-
S3513	S1	Oglio	Rogno	74	3.7	2.8	54.00	**46.00**	0.00	6.03
S3506	S2	Adda	Dubino	337	9.0	30.3	15.00	**75.00**	10.00	40.47
S3510	S3	Ticino	Bellinzona	528	9.0	47.5	27.00	**64.00**	9.00	74.26
S3554	S4	Toce	Masera	216	4.0	8.6	24.00	**59.00**	18.00	14.64
S3553	S5	Sesia	Romagnano	347	0.5	1.7	2.00	**28.00**	70.00	6.19
S3603	S6	Dora Baltea	Quassolo	680	1.9	13.0	23.00	**72.00**	5.00	17.99
S3556	S7	Orco	Cuorgnè	719	0.5	3.6	19.00	**46.00**	35.00	7.81
S3520	S8	Dora Riparia	Avigliana	146	9.0	13.2	3.00	**66.00**	31.00	19.97
S3518	S9	Po	Revello	36	0.8	0.3	40.00	**56.00**	4.00	0.52
S3517	S10	Varaita	Costigliole S.	104	0.9	0.9	15.00	**65.00**	20.00	1.45
S3515	S11	Stura Demonte	Montanera	109	43.7	47.8	38.00	**56.00**	6.00	85.37
S3503	S12	Scrivia	Serravalle	13	11.0	1.4	23.00	**73.00**	5.00	1.94
S4014	S13	Trebbia	Rivergaro	41	1.0	0.4	-	**90.00**	-	0.44
S3719	S14	Taro	Fornovo	70	3.3	2.3	-	**66.00**	-	3.44
S4016	S15	Enza	S. Polo d'Enza	132	2.7	3.5	-	**70.00**	-	5.01
S4017	S16	Secchia	Sassuolo	215	5.0	10.7	-	**62.00**	-	17.32

Table 3. Calculations for assessing zircon fertility in source rocks; ppm D>3.3 su tot>2- ppm no-magnetic minerals concentrate/ bulk sediment >2 mm; GSW- grain-size window; Zrn >GSW: percentage of zircon grains in the coarser analysed window; Zrn GSA: percentage of zircon grains in the analysed window; Zrn<GSA: percentage of zircon grains in the finer analysed window

River's Sub-basin	Sample	Sample's U-Pb Signal	mean basin area	correct Zrn ppm tot<2	contribution %	Potential Source Area
Oglio	**S1**	S1	26	1.6	2	
Adda	**S2**	S2	56	40.5	91	***Southern Alps***
Moesa	-	S2	8	75	5	
Mera	-	S2	10	11	2	
Ticino	**S3**	S3	30	74.3	70	***Lepontine Dome (Central Alps)***
Maggia	-	S3	17	12.3	6	
Toce	**S4**	S4	53	14.6	24	
Sesia	**S5**	S5	21	6.2	10	
Dora Baltea	**S6**	S6	58	18	78	***North-Western Alps***
Orco	**S7**	S7	11	7.8	6	
Stura di Lanzo	-	S7	10	7.5	6	
Dora Riparia	**S8**	S8	36	20	79	
Pellice	-	S8	4	0.5	0	
Maira	-	S8	25	5.7	16	***South-Western Alps***
Po Revello	**S9**	S9	10	0.5	4	
Varaita	**S10**	S10	20	1.4	1	
Isasca	-	S10	5	0.3	0	
Stura Demonte	**S11**	S11	100	85.4	100	***Argentera***
Scrivia	**S12**	S12	29	1.9	21	
Belbo	-	S8	11	3.6	17	***Ligurian Alps***
Orba	-	S8	4	9.7	16	
Bormida	-	S12	55	2.1	46	
Trebbia	**S13**	S13	7	0.4	1	
Taro	**S14**	S14	12	3.4	14	
Nure	-	S14	7	1.9	5	***Northern Apennine***
Enza	**S15**	S15	6	5	10	
Secchia	**S16**	S16	11	17.3	64	
Panaro	-	S16	8	2.3	6	

Table 4. Relative zircon contributions from each source area.

The complete database of

- Detrital zircon morphologies (table 5) and

- Detrital zircon U-Pb ages (table 6)

is not available on-line,

People interested can send a request by e-mail to:

marta.limoncelli@gmail.com

or

m.limoncelli@campus.unimib.it